

Relativity: Introducing relativity and quantum theory by ruler & compass geometry of phase

William G. Harter and Tyle C. Reimer

Department of Physics
University of Arkansas
Fayetteville, AR 72701

A quantitatively precise and logically compelling Occam's Razor¹ introduction to special relativity and quantum theory can be done with a few simple steps aided by ruler and compass. A number of concepts that students invariably find arbitrary, mysterious, or quasi-paradoxical are elegantly resolved.

This development models pairs of laser beams or cavity modes that produce a Minkowski coordinate lattice geometry in space-time and a reciprocal lattice geometry in per-space-time (Fourier space). This leads to a revealing roadmap for classical mechanical and quantum variables that derives and clarifies their differential relations yet requires little more than high-school trigonometry.

This geometric approach improves both conceptual visualization and the computational techniques for these subjects while showing they are really two sides of a single subject. Such a unified approach could allow these pillars of modern physics to be introduced earlier and in greater depth in the growing range of physics curricula. It also reveals heretofore hidden insight and provides new avenues for research.

(First draft as of Jan. 10, 2017)

1. Introduction to relawavity	3	
2. A novel review of trigonometry and previews of its applications		5
<i>Complex algebra and calculus</i>	8	
<i>Phasors and complex wave functions</i>	8	
<i>A phasor clock has only one hand!</i>	10	
<i>At c the phasor clocks freeze!</i>	10	
<i>What's waving? (...and what's not?)</i>	11	
3. Space-time vs Per-space-time: Fourier's keyboard of the Gods		12
<i>c-Scaled wave graphs and Doppler shifts</i>	13	
<i>Evenson's axiom and Doppler shifts</i>	14	
<i>Rapidity and its Doppler shift arithmetic</i>	16	
4. Wave-zero 2-CW coordinate grids	18	
<i>Geometry of Minkowski phase and group wave-lattices</i>		20
<i>Understanding relawavity parameters and Lorentz transformations</i>		22
<i>Invariance of phase to Lorentz transformation</i>		23
<i>Thales-Euclid means and geometry of hyperbolic invariants</i>		24
<i>PW Sums of multiple CW harmonics and Doppler effects</i>		26
5. Properties and applications of relawavity geometry	28	
<i>Space-proper-time plots and the stellar-aberration angle</i>		28
<i>TE-Waveguide geometry</i>	30	
<i>Wave parameter variation with group velocity</i>	31	
<i>Table 2. Relawavity ratios versus rapidity-ρ, guide angle-σ, and $\beta=u/c$</i>	33	
6. Relativity gives basic wave mechanics of matter	34	
<i>What is energy?</i>	35	
<i>What's the matter with energy?</i>	36	
<i>How light is light?</i>	38	
7. Relawavity geometry of Hamiltonian and Lagrangian functions		39
<i>Phase, action, and Lagrangian functions</i>	39	
<i>Hamiltonian functions, Poincare invariants, and Legendre contact transformation</i>		41
<i>Hamilton-Jacobi quantization</i>	43	
8. Relawavity geometry of quantum transitions	46	
<i>Symmetry and conservation principles</i>	46	
<i>Single-photon transitions and Feynman diagram geometry</i>		47
<i>Photon transitions obey rocket-science formula</i>	47	
<i>Geometric level and transition sequences</i>	48	
<i>Half-sum-and-difference transition web</i>	50	
9. Accelerated frames and optical Einstein-elevator	51	
<i>Metrology in accelerated frames</i>	56	
<i>Mechanics in accelerated frames</i>	57	
The Purest Light and a Wave-Resonance Hero – Ken Evenson (1932-2002)		59

1. Introduction to relativity

For well over a century the introductory teaching of special relativity (SR) and quantum mechanics (QM) has been problematic for critically thinking students who seek conceptual comprehension. A paraphrasing of many such student comments might be, “*I didn’t understand all that, but I don’t think our professor did, either!*”

In spite of such doubts, many thousands of students of physics, chemistry, engineering, and now even biological sciences have soldiered through SR and QM to create a vast technology based on them with new sciences still arising from these pillars of modern physics. Beginnings of QM by Planck² (1900), of QM and SR by Einstein^{3,4,5} (1905), and QM matter waves by DeBroglie⁶ (1923) were great advances in a theory related to electromagnetic (EM) wave phenomena that still yields new applications and theory.

Yet, doubts about establishing basic SR or QM axioms may cause enough discomfort for an SR or QM professor to exclaim, “*Just trust me! This all works out in the end!*” Such painful beginnings cannot be healthy for the science or for the society that supports it. Evidence of this is seen in the plethora of painful popular attempts to describe either SR or QM. All this begs us to apply Occam’s Razor¹.

The following article describes the result of decades long search⁷ at the University of Arkansas for a technically sweet front-end to modern SR and QM physics education as well as improved ways to develop classical mechanics (CM). The upshot is that SR and QM merge into a single subject and need not, indeed *should not*, continue to be taught separately. Space-time SR aberrations and related QM Lagrangian and Hamiltonian variables are constructed by a single elegant logic involving a few ruler and compass strokes derived from geometry of laser wave cavity interference.

Such a simple development allows younger students to begin acquiring understanding of modern physics theory while relating it to classical geometry and mechanics going back to Thales (600 BCE), Euclid (300BCE), and Galileo (1500ACE). This effort extends work by the Feynman, Leighton, and Sands projects of 1964 at CalTech that gave *The Feynman Lectures in Physics*⁸.

Full Disclosure: One of the authors (WGH) was a grad student of Richard P. Feynman and William G. Wagner (a co-author of Feynman’s text on Gravitation⁹) at CalTech and UCI between 1964 and 1968. The current project began at Georgia Tech¹⁰ in 1985 and continued at UAF from 2001 to the present¹¹.

In order to be self-contained, this exposition begins with a novel and refreshing geometric review of trigonometry of the six circular and six hyperbolic sine-tangent-secant and complimentary cosine-cotangent-cosecant functions. The circular six are functions of unit-circle sector area σ while the hyperbolic six depend on unit-hyperbola sector area ρ and all reveal some little known relations.

A “trigonometric road-map” (TRM) relates twelve trig functions and shows that hyperbolic sine and cosine sum and difference give the \pm exponentials: $e^{\pm\rho} = \cosh\rho \pm \sinh\rho$. Hyperbolic functions with real exponential power series derived from interest-rate formulae are simpler than circular functions that involve the mysterious $i = \sqrt{-1}$ in complex exponentials $e^{\pm i\sigma} = \cos\sigma \pm i\sin\sigma$. So the former serve to derive the latter in a first step to show the role of complex wave functions $Ae^{\pm i(kx - \omega t)}$ in QM and SR theory and how real exponentials $e^{\pm\rho}$ rescale wavevector k , wave angular frequency ω , and wave amplitude A .

Later e^{+p} and e^{-p} are seen to be blue and red Relativistic Doppler shifts while σ is the stellar-aberration or waveguide-beam-entry angle¹². Both measure first order relativistic effects that are well known like police Doppler radar. Second-order effects like Lorentz contraction are immeasurably tiny at terrestrial speeds and much more mysterious. Yet second-comes-first in standard¹³ SR texts. Here a first-things-first approach based on Doppler shifts turns out to be clearer and quicker and a lot more revealing.

This involves matching a “trigonometric road-map” (TRM) with a diagram of wave interference geometry for colliding laser plane waves that is named the “Relativity Baseball-Diamond” (RBD). The RBD is constructed from real-wave zeros that trace space-time Minkowski grids. So the logic of this development involves comparing TRM geometry based on unassailable mathematical axioms with a RBD geometry of SR and QM wave mechanics based on potentially assailable physical axioms having several challenging issues including uncertainty, non-locality, and space-time aberration.

The physical axioms for SR are picked with Occam’s razor¹ in mind¹⁴. Beside the time reversal symmetry axiom there is one axiom that is (or should be) a classroom show-stopper. That axiom demands that the speed of light *en vacuo* be the same constant for all observers. We prefer to name this *Evenson’s Axiom: All colors go the same speed $c=299,792,458m\cdot s^{-1}$* after Kenneth Evenson¹⁵ who measured c using overtones in a laser frequency chain in 1972. Later he worked to establish c as the definition of the meter, thus setting the stage for a precision revolution that included, among other things, ultra-high resolution laser spectroscopy, the Global Positioning System, and the LIGO projects.

It is important to emphasize how counter-intuitive a super-constant c would be to Galileo and should be to anyone first dealing with SR. (It has been called the *Roadrunner Axiom* after Chuck Jones’ cartoons.) Galileo could be excused if he assumed c was infinite ($c=\infty$) so then all would see the same c . But, how can a *finite* c be so regarded the same by all? A demystifying answer to this and other apparent paradoxes is based primarily on Doppler shifts.

A prerequisite to deriving SR and QM fundamentals involves thought experiments with Evenson’s axiom that show why *en vacuo* c has to be constant. An ideal blue-green $600THz$ laser beam may be seen to lack a “birth certificate” in the sense that it might be made by an approaching laser operating below $600THz$ as well as a receding laser with output above $600THz$. One needs to explain clearly why all $v=600THz$ beams share the same $\lambda=0.5\ \mu m$ wavelength of a co-moving $600THz$ laser and how this implies the same *en vacuo* speed $c=\lambda\cdot v$.

Full understanding of Doppler effects requires a review of wave mechanics that follows the introduction of the geometry of the TRM and RBD. This involves two complimentary four-dimensional theaters, space-time (\mathbf{x}, ct) and per-space-time ($c\mathbf{k}, \omega$). The first examples are limited to two-dimensional graphs of space-time (x, ct) and per-space-time (ck, ω). In later sections it will be shown that TRM plots occupy both (x, ct) and (ck, ω) as well as space-space (x, y) plots and per-space-per-space (ck_x, ck_y) plots.

Michelson and Morely¹⁶ showed wave interference is a fine way to measure relativity of space-time. Now *relativity* shows wave interference is also a fine way to *think* about relative motion. By ruler & compass it derives and clarifies Lorentz-Einstein formulae, Lagrangians, Hamiltonians, Feynman diagrams, and Compton effects including wave frame dynamics for “Einstein elevator” acceleration.

2. A novel review of trigonometry and previews of its applications

Every scientific calculator has an SIN button and, as we tell our home-churched students, this is not such a bad thing. In fact it stands for Slope of INcline and (multiplied by 100) gives the percent of grade or ratio of altitude gained over road distance traveled along the freeway bypass around their town. Next to SIN is a COS or COmplimentary Slope giving ratio of level distance over road distance. Fig. 1a is a plot of sine ($\sin\sigma=\frac{3}{5}$) and cosine ($\cos\sigma=\frac{4}{5}$) of angle $\angle\sigma=36.87^\circ$ that makes 3:4:5 triangles. Angle in radians $\sigma=0.6435=\pi\frac{36.87^\circ}{180^\circ}$ is also total sector area for a unit ($B=1$) circle. (That is π for $\sigma=\pi$.) Fig. 1 use a non-standard convention to plot complimentary $\cos\sigma$ as a vertical projection while $\sin\sigma$ is horizontal. This is done to match Minkowski plots later on where space x is plotted on horizontal axis and time t on the vertical axis. It is complimentary to a standard Newtonian plot of x (vertical) versus time (horizontal).

The result of pressing a calculator TAN button for angle $\angle\sigma=36.87^\circ$ is the TANgent or $\tan\sigma=\frac{3}{4}$ (the ratio $\tan\sigma=\frac{\sin\sigma}{\cos\sigma}$) labeling the hypotenuse of a smaller 3:4:5 triangle on top of Fig. 1a. That tangent line is also the altitude of the largest 3:4:5 triangle in Fig. 1a, and it encloses the upper σ -sector. The three circular functions $\sin\sigma$, $\cos\sigma$, and $\tan\sigma$ are sufficient for elementary physics but it helps to have three more that are inverses of the primary three. The secant ($\sec\sigma=\frac{1}{\cos\sigma}=\frac{5}{4}$), cosecant ($\csc\sigma=\frac{1}{\sin\sigma}=\frac{5}{3}$), and cotangent ($\cot\sigma=\frac{1}{\tan\sigma}=\frac{4}{3}$) as plotted in Fig. 1b to show *two* additional (and larger) 3:4:5 triangles. (Study carefully the mid and lower right hand side of Fig. 1b.)

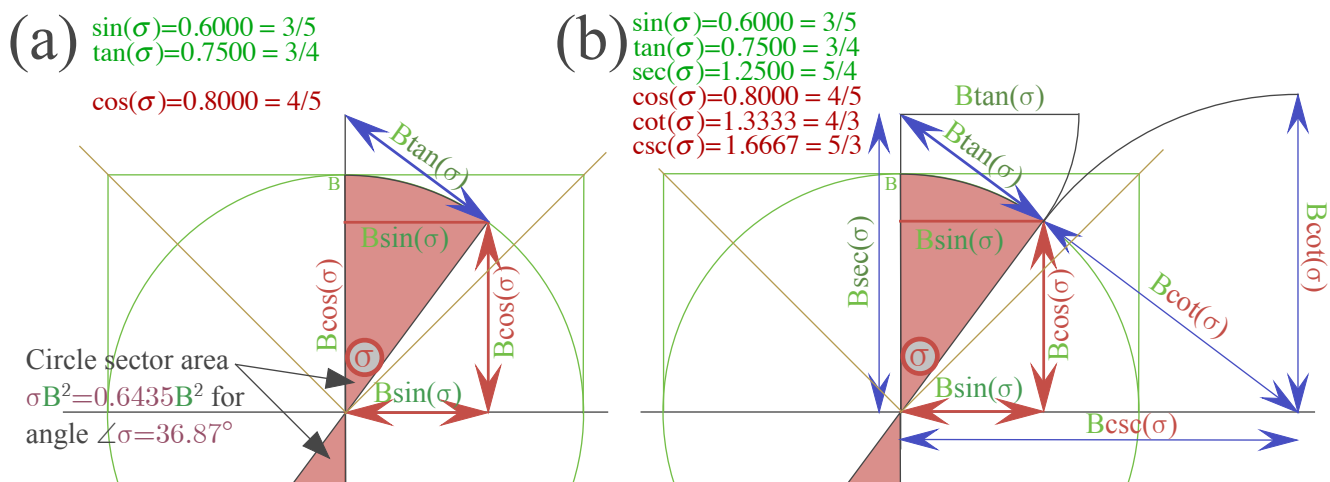


Fig. 1. Circular TRM's (a) Primary circular function triplet. (b) Full TRM sextet of circular functions.

A TRM suitable for SR and QM functions and theory involves replacing six circular functions in Fig. 1b with six hyperbolic functions as shown in Fig. 2 and Fig. 3 that play similar roles in labeling coordinates, tangents, and their intercepts around an equilateral hyperbola. Each circular function (such as $\sin\sigma=\frac{3}{5}$) is like an “urban dweller” that has a “country cousin” (for $\sin\sigma=\frac{3}{5}=\tanh\rho=\frac{3}{5}$) with same numerical value ($\frac{3}{5}$ here) that is a function of hyperbolic sector area ($\rho=0.6931$ with angle $\angle\nu=30.96^\circ$ in this example) as listed on top of Fig. 2 and plotted nearby. For each country-urban pair there is a flipped pair (here: $\tan\sigma=\frac{3}{4}=\sinh\rho$) that shares a value ($\frac{3}{4}$ in that example) for the same hyper sector ($\rho=0.6931$ or angle $\angle\nu=30.96^\circ$) and corresponding circle sector ($\sigma=0.6435$ or angle $\angle\sigma=36.87^\circ$). A circle-hyperbolic (“urban-country”) pair $\sin\sigma=\frac{3}{5}=\tanh\rho$ and $\tan\sigma=\frac{3}{4}=\sinh\rho$ is listed on top left of Fig. 2 and plotted to the right below. (Fig.2 plots hyperbolic ρ -labels. Fig.1b plots circular σ -labels.)

Total area ρ of sector pairs connecting opposite sides of a hyperbola is derived by an integral similar to one giving total sector area σ connecting sides of a circle. See (69) in Sec. 9.

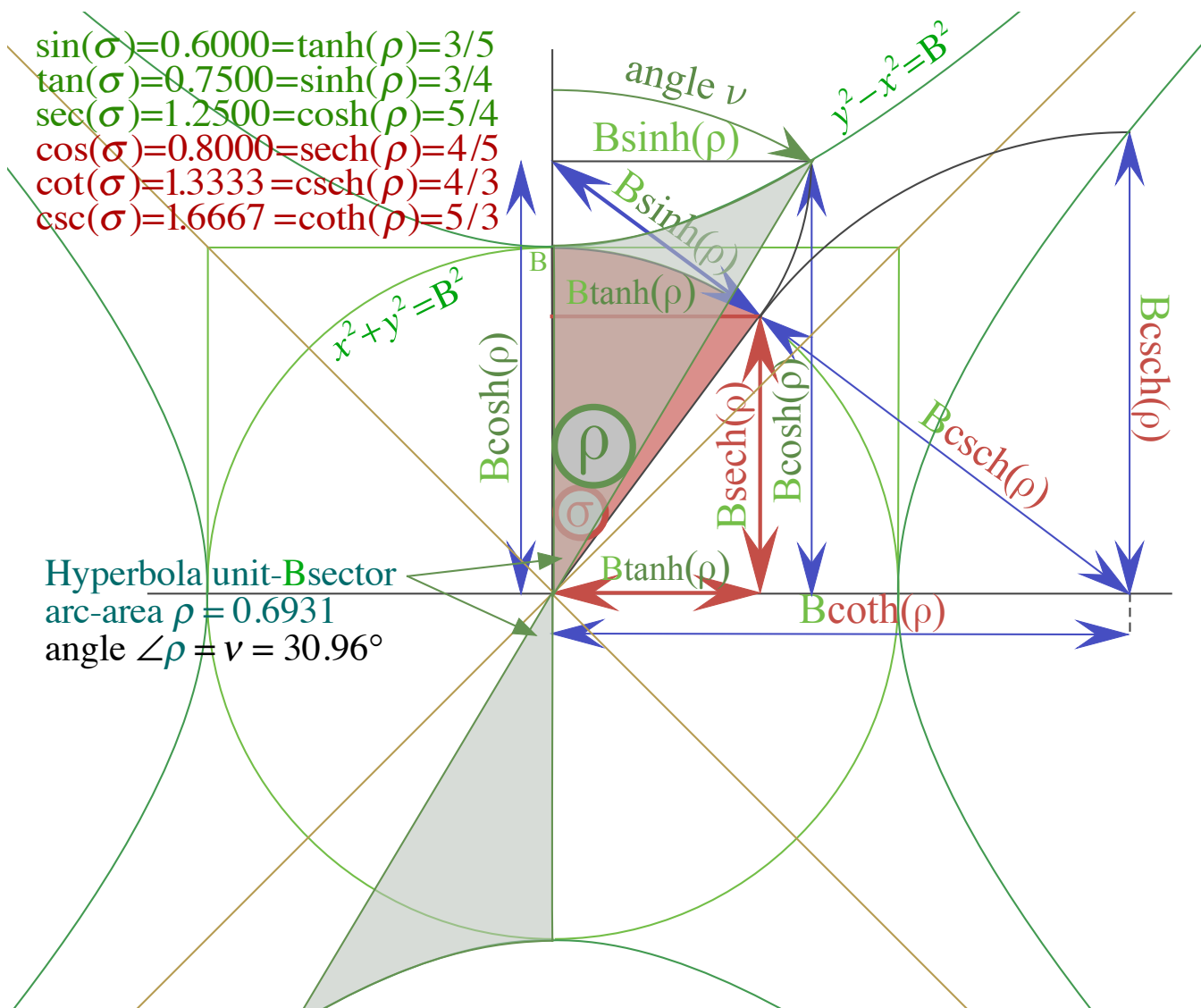


Fig. 2 TRM Hyperbolic labeling of Fig. 1b.

Preparing TRM Fig.2 for SR and QM theory requires several more lines, circles, tangents, and intercepts that will label wave coordinates for SR and physical quantities for QM. The resulting TRM is Fig. 3. Most of the figure lies within a square with 45° diagonal **OR**. Sides of **OR** have length equal to base B times sum of hyperbolic sine and cosine that is a rising (+) exponential.

$$Be^{+\rho} = B(\cosh \rho + \sinh \rho) = B\left(\frac{5}{4} + \frac{3}{4}\right) = 2B \quad (1)$$

To the left of **OR**'s base is a small square with 45° diagonal **OL** normal to **OR**. Sides of **OL** have length equal to base B times the difference of hyperbolic cosine and sine that is a decaying (-) exponential.

$$Be^{-\rho} = B(\cosh \rho - \sinh \rho) = B\left(\frac{5}{4} - \frac{3}{4}\right) = \frac{1}{2}B \quad (2)$$

In Fig. 3 a circle through point **P** of radius $B\sinh \rho$ bisects hyperbola baseline **OB** where square **OL** ends.

Complex algebra and calculus

Slopes, tangent points, and axis intercepts are the important geometric concepts for relativity interference analysis that leads to SR and QM wave properties. The slope at **P** is derived in two distinct ways, first as a finite slope ratio $\frac{\Delta y}{\Delta x}$, and second as an infinitesimal derivative $\frac{dy}{dx}$. The first $\frac{\Delta y}{\Delta x}$ is the ratio $\frac{\text{altitude}}{\text{base}}$ for the triangle with $|\mathbf{IP}\mathbf{O}|$ base $B\text{sch}\rho$ and altitude $B\text{sech}\rho$ supporting slope $\frac{\text{sech}\rho}{\text{csch}\rho} = \frac{\sinh\rho}{\cosh\rho} = \tanh\rho$. The second $\frac{dy}{dx}$ analysis involves the algebra and calculus of Fig. 3 promised in the introduction. Before doing that, notice that the slope of the line **OG** is also $\frac{\sinh\rho}{\cosh\rho} = \tanh\rho$, but line **OP** has inverse slope $\frac{\cosh\rho}{\sinh\rho} = \text{coth}\rho$ as does the vertical hyperbolic tangent line through point **G**.

Calculus of Fig. 3 geometry uses an infinite- n -compounding limit of the interest rate- r formula.

$$e^{rt} = \lim_{n \rightarrow \infty} \left(1 + \frac{rt}{n} \right)^n \quad (3)$$

Infinite- n limit of binomial series is an exponential power- p series of $(rt)^p$ with $1/p!$ coefficients.

$$e^{+rt} = 1 + rt + \frac{(rt)^2}{2} + \frac{(rt)^3}{2 \cdot 3} + \frac{(rt)^4}{2 \cdot 3 \cdot 4} + \frac{(rt)^5}{2 \cdot 3 \cdot 4 \cdot 5} + \frac{(rt)^6}{2 \cdot 3 \cdot 4 \cdot 5 \cdot 6} + \dots \quad (4a)$$

$$e^{-rt} = 1 - rt + \frac{(rt)^2}{2} - \frac{(rt)^3}{2 \cdot 3} + \frac{(rt)^4}{2 \cdot 3 \cdot 4} - \frac{(rt)^5}{2 \cdot 3 \cdot 4 \cdot 5} + \frac{(rt)^6}{2 \cdot 3 \cdot 4 \cdot 5 \cdot 6} - \dots \quad (4b)$$

Half-sum and half difference of $e^{\pm rt}$ series define the hyperbolic cosine ($\cosh(rt)$) and sine ($\sinh(rt)$).

$$\frac{e^{+rt} + e^{-rt}}{2} = 1 + \frac{(rt)^2}{2} + \frac{(rt)^4}{2 \cdot 3 \cdot 4} + \frac{(rt)^6}{2 \cdot 3 \cdot 4 \cdot 5 \cdot 6} - \dots = \cosh(rt) \quad (5a)$$

$$\frac{e^{+rt} - e^{-rt}}{2} = rt + \frac{(rt)^3}{2 \cdot 3} + \frac{(rt)^5}{2 \cdot 3 \cdot 4 \cdot 5} + \dots = \sinh(rt) \quad (5b)$$

Sum and difference gives equation (1) and (2) consistent with figures 2 and 3. Replacing rate r with imaginary rate ir where $i = \sqrt{-1}$ gives powers $i^0=1, i^1=i, i^2=-1, i^3=-i, i^4=1, i^5=i, i^6=-1, i^7=-i, \dots$ that repeat sequence- $(1, i, -1, -i)$ every 4th-power. Then hyper-sine-cosine becomes the circular-sine-cosine.

$$\frac{e^{+irt} + e^{-irt}}{2} = 1 - \frac{(rt)^2}{2} + \frac{(rt)^4}{2 \cdot 3 \cdot 4} - \frac{(rt)^6}{2 \cdot 3 \cdot 4 \cdot 5 \cdot 6} - \dots = \cos rt \quad (6a)$$

$$\frac{e^{+irt} - e^{-irt}}{2} = i rt - i \frac{(rt)^3}{2 \cdot 3} + i \frac{(rt)^5}{2 \cdot 3 \cdot 4 \cdot 5} - \dots = i \sin rt \quad (6b)$$

Sum and difference of this pair gives the Euler-DeMoivre formulae.

$$e^{+i\sigma} = \cos(\sigma) + i \sin(\sigma), \quad e^{-i\sigma} = \cos(\sigma) - i \sin(\sigma). \quad (7)$$

This is used to make wave functions and phasors that help to visualize wave mechanics.

Phasors and complex wave functions

A single continuous wave or 1-CW is plotted as a complex phasor array in a space-time plot of Fig. 4. Einstein's math teacher, Herman Minkowski¹⁷, chose the space-time (x, ct) convention plotting $space=x$ in horizontal direction and $c \cdot time=ct$ along vertical axis. Lightspeed factor c makes the temporal ct -axis have the same spatial units as the x -axis and so the 1-CW moves along 45° lines of constant phase. Each phasor is like a clock sitting in a 300THz laser beam defined by wave function $\psi_{k,\omega}(x,t) = A e^{i(kx - \omega t)}$ and its space and time derivatives. (General exponential derivative: $\frac{d}{dt} e^{rt} = r e^{rt}$ follows from Eq.(4a).)

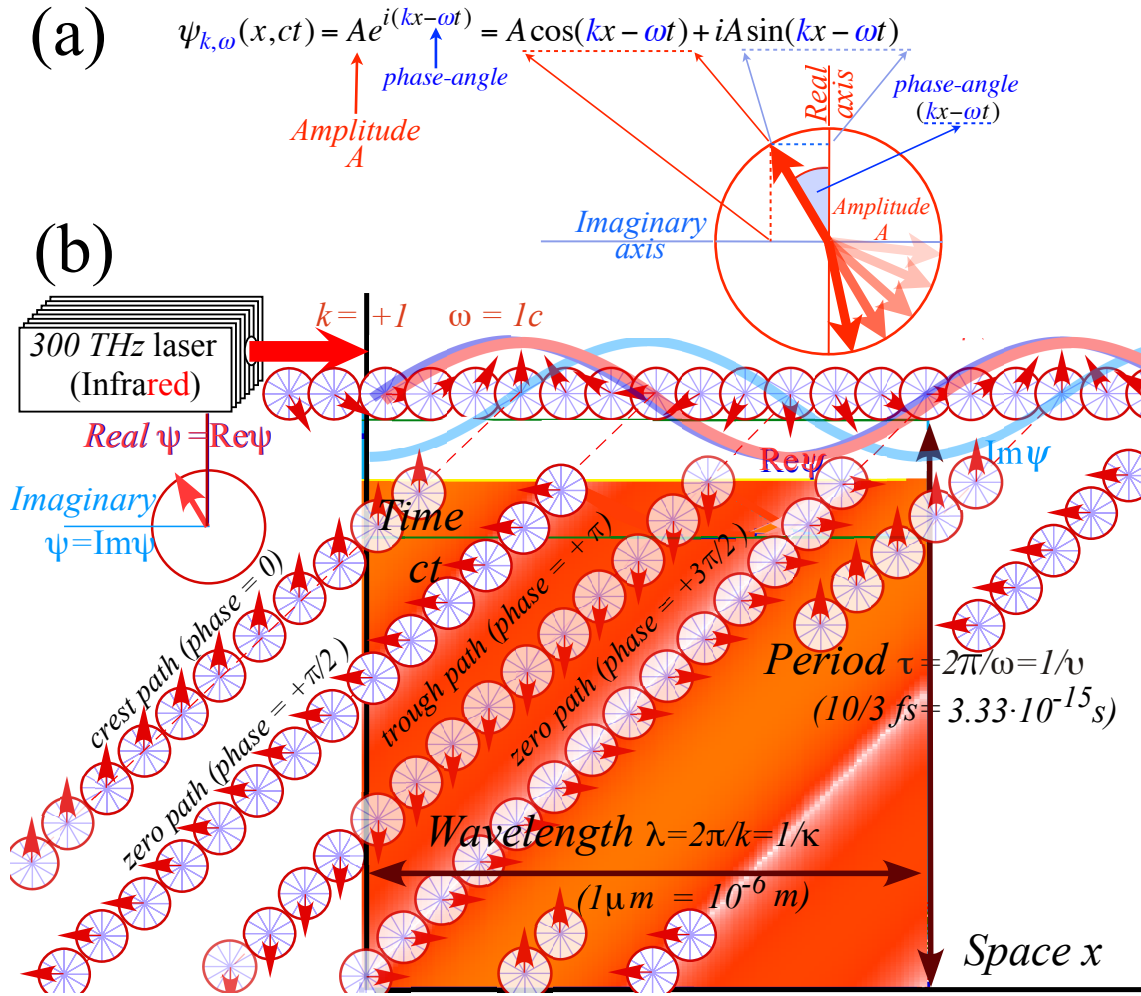


Fig. 4 Single Continuous Wave (1-CW) (a) A phasor clock wavefunction $\psi_{k,\omega}(x,ct)$. (b) Spacetime array of $\psi_{k,\omega}$ -phasors.

Phasor plots in Fig. 4 are re-oriented by 90° in a non-conventional way so the real axis points upward and the imaginary axis points to the left along beam-line. A $\psi_{k,\omega}$ pointing up corresponds to a $\text{Re}\psi$ -wave crest with phase angle $kx-\omega t=0$, and where $\psi_{k,\omega}$ points down corresponds to a $\text{Re}\psi$ -wave trough with phase angle $kx-\omega t=\pi$. In between is $\text{Im}\psi$ -crest with phase $kx-\omega t=\pi/2$ or $\text{Im}\psi$ -trough with phase angle $kx-\omega t=3\pi/2$. These half- π tracks locate $(\text{Re}\psi_{k,\omega}=0)$ -lines such as the white line in lower right of Fig. 4b. $(\text{Re}\psi_{k,\omega}=0)$ -lines mark (x,ct) grids in Sec. 4 and help visualize relativity effects.

Space and time derivatives of any phasor $\psi_{k,\omega}(x,t)=Ae^{i(kx-\omega t)}$ sheds some light on their behavior.

$$\frac{\partial}{\partial x} \psi_{k,\omega}(x,t) = \frac{\partial}{\partial x} Ae^{i(kx-\omega t)} = ikAe^{i(kx-\omega t)} = -kA \sin(kx-\omega t) + ikA \cos(kx-\omega t) \quad (8a)$$

$$\frac{\partial}{\partial t} \psi_{k,\omega}(x,t) = \frac{\partial}{\partial t} Ae^{i(kx-\omega t)} = -i\omega Ae^{i(kx-\omega t)} = \omega A \sin(kx-\omega t) - i\omega A \cos(kx-\omega t) \quad (8b)$$

(8b) shows imaginary part $\text{Im}\psi_{k,\omega} = A \sin(kx-\omega t)$ multiplied by ω is real part of t -derivative $\frac{\partial}{\partial t} \psi_{k,\omega}$. Note that wave imaginary part $\text{Im}\psi$ in top of Fig. 4(b) is a quarter wavelength ahead of the real wave $\text{Re}\psi$.

This quite well matches an unfortunate mantra for US Stockholder-Driven corporations:

Imagination precedes Reality by exactly one Quarter!

Needless to say, this rule does not always favor corporate research quality in the 21st century.

Nevertheless, the concept of wave phase, indeed, *relative* phase, is an important key to understanding relativity, quantum mechanics, and dynamics of any oscillating or “wavy” system. If the relative phase between a pair of k_{AB} -coupled neighboring phasors is $\Delta\Phi = \Phi_A - \Phi_B$ then the rate of A -to- B energy or action transfer is proportional to the product of amplitudes $A \cdot B$ with coupling k_{AB} constant and $\sin\Delta\Phi$.

$$\text{Transfer } A\text{-to-}B \approx k_{AB} A \cdot B \cdot \sin\Delta\Phi$$

So if phasor A is *ahead* (that is *clockwise*) relative to phasor B , then A is feeding energy (or action) to B , and *vice versa*, if B is ahead of A then B is feeding A .

In the beam phasor line of Fig. 4b each clock is ahead of the one to its right by $\Delta\Phi$ but behind the one to its left by the same amount $\Delta\Phi$. So as the clocks turn clockwise the wave will move left-to-right and with it, presumably, its energy or action. No phasor grows or shrinks as it passes on all that it gets.

The actual speed of the wave is found by more elementary considerations of phase. Simply setting the phase equal to a constant (like 0 or $\pi/2$...in Fig. 4b) gives the equation for its path.

$$kx - \omega t = \text{const.} \quad \Rightarrow \quad x = \frac{\omega}{k} t + \frac{\text{const.}}{k}$$

The time coefficient $\frac{\omega}{k}$ is the 1-CW phase velocity that, in this case is that of light $\frac{\omega}{k} = c$. In the (x, ct) plot of Fig. 4b this makes 45° paths. Definitions of wave parameters like $\omega = 2\pi\nu$ and $k = 2\pi\kappa$ follows in Sec. 3.

The concept of a 1-CW (that is a *Single-Continuous-Wave*) is greatly simplified here and in what follows. A CW-laser is standard jargon since the invention of the He-Ne laser in 1962. For our purposes of developing thought experiments we assume a perfect plane wave inside the beam such as is imagined in Fig. 4. The acronym CW can also mean *Coherent Wave* (elementary lasers are described by coherent states of photons) or *Colored Wave* (lasers are known for frequency or, if visible, *color* purity) or just plain *Cosine Wave* (that is the real part of the *Complex Wave* function $Ae^{i(kx - \omega t)}$.)

This is to distinguish from a PW (that is a *Pulse-Wave* or *Packet-(of)-Waves* or *Particle-(like)-Wave*) that are made of many frequencies or colors combined to form localized “spikes” or pulses that act more like particles. Newton might have liked this kind of “corpuscles” if they had been available in 18th century laboratories, but laser a CW would have given him “fits” as discussed in Sec. 6.

A phasor clock has only one hand!

While 1-CW phasors can have great spectral purity and precision, the value of phase is only given modulo 2π . After each revolution by 2π the recoding of time just starts over again. It is just a second-hand with no minute-hand or hour-hand (or week-hand, or-year-hand, etc.) to extend the range of a temporal record that space-time plots like Fig. 4 can provide.

Evenson had to solve this in order to count 500-TeraHertz light waves and did so by producing harmonics and sub-harmonics using non-linearity of metal-insulator-metal diodes. Later work by Theodore Hensch and others involved PW lasers with enormous “frequency-combs” of precisely spaced coherent Fourier components, essentially a clock with a thousand hands.

At c the phasor clocks freeze!

Fig. 4 can be viewed in some mind-bending ways. It is intended as a line of 20 phasor clocks attached to a CW laser with each turning at its $\omega = 2\pi \cdot 300\text{THz}$ infrared frequency. Then each phase marches at the speed c of light through this line. Alternative extreme view has 20 frozen clocks being dragged past the laser at the speed c of light. (Actually we would need about 20-thousand clocks so every pixel has a clock reading the correct value of phase $kx - \omega t$ assigned to the (x, ct) pixel.)

Between the above two extremes are slower-moving-than- c clock-trains turning at a slower-than- ω angular frequency yet always leaving the same phase $kx - \omega t$ on each (x, ct) pixel! This bizarre property is due to *phase invariance*. [By the time you reach (23) in Sec. 4 all this should be clearer.]

What's waving? (...and what's not?)

The most tenuous questions of light wave analysis lie in their axiomatic underpinnings. More simply, what is it that is waving up and down in the “Real part” $\text{Re}\psi$ and/or in its t -derivative (scaled by angular frequency ω) that is the “Imaginary part” $\text{Im}\psi$ plotted as sine-curves on the laser beam in Fig. 4?

The short answer is that $\text{Re}\psi$ represents the electric field or \mathbf{E} -field, and $\text{Im}\psi$ represents $\dot{\mathbf{E}}/\omega$, the time derivative $\dot{\mathbf{E}}$ of \mathbf{E} scaled down by ω so the two form a quadrant of a rotating circular phasor ψ . That conforms to Maxwell's physics of **vector** fields transverse to the beam direction \mathbf{k} of wave propagation. Since it is impractical to draw \mathbf{E} -vectors waving in and out of the page, we lay them onto the page going up and down in the direction of the time axis, and not where they should be.

This kind of plot does not spoil accuracy of later figures (Fig.9 and Fig. 10) since they will be tracing the *zeros* or *nodes* of $\text{Re}\psi$ waves at precisely the time instants that they occur. But, it does limit the display to the most elementary linear/plane polarized light wave, but this simplified stand-in for a real laser is enough to derive a wave-based formulation of elementary relativity and quantum theory.

Perhaps, it would be nice if light could be a 3-dimensional scalar wave such as the $\Psi(x,y,z,t)$ that appear in many textbooks, but those are not the optical cards that Nature has dealt us. Indeed, that is also an oversimplified stand-in, as well.

Real IR-to-UV laser beams have less than micron wavelengths traveling through beams that have more than a millimeter-wide Gaussian profile. That provides an ample region that is well described by a plane wave function $\psi_{\omega,k}(x,t)=Ae^{i(kx-\omega t)}$ if we avoid considering the complexity of possible polarization vector states normal to the beam axis \mathbf{k} .

So the wave complex amplitude “waves” (that is, oscillates sinusoidally) as a function of space-time independent variables (x,t) . This happens while inverse-space and inverse-time wave parameters, such as ω and k described in following Sect. 3, do *not* “wave” at all. Instead they vary or “Doppler-shift” according to the velocity of source and observer but stay precisely fixed if that velocity is constant.

Understanding Doppler shift is an important key to understanding relativity and quantum theory, and this is where that begins.

3. Space-time vs Per-space-time: Fourier's keyboard of the Gods

Physics students have to learn proper names for most physical units such as a *Joule* of energy, a *Newton* of force, or a *Watt* of power. Surprisingly there are no such names attached to most fundamental units, those of time (second) and space (meter). (One might argue for renaming the meter an *Evenson* after he helped redefine it. Or one could apply the name *Trump* to the 4.1-light year distance to the star α -Proxima, our nearest possibly habitable refuge from the former.)

Still, there are some more or less well established proper names for units of *per-space-time*. Most well known is the *Hertz* unit ($1 \text{ per second} = 1s^{-1}$) named after Heinrich *Hertz* (1857-1894), an inventor of radio transmission. Less well known among atomic and molecular spectroscopists is the *Kayser* unit of ($1 \text{ per centimeter} = 1cm^{-1}$) named after Heinrich *Kayser* (1853-1940) known for analyzing solar spectra. They were born only four years apart, but Hertz only lived 37 years while Kayser lived to 87.

These pioneers deserve a coordinate frame to compliment the Einstein-Minkowski (x, ct)-frame. (Herman Minkowski¹⁸ (1864-1909) also died young at 45 shortly after failing to interest Einstein in his space-time plot. This may be due to Prof. Herman's calling Albert a "lazy dog" or another pejorative.) Fig. 5 relates a Kayser-Hertz (per-space κ , per-time ν) plot (on the left) to the usual (space x , time t) plot (on the right) that might be used to track water waves or sound waves. The primary objective of Fig. 5 is to review standard wave terms, notation, and velocity formulae.

A single Kayser-Hertz point or vector ($\kappa \frac{\text{(waves)}}{\text{meter}}$, $\nu \frac{\text{(waves)}}{\text{second}}$) produces one continuous wave (1-CW) that fills space-time with a wave having (wavelength $\lambda \frac{\text{meters}}{\text{(wave)}}$, wave-period $\tau \frac{\text{seconds}}{\text{(wave)}}$). Fig. 5 has wavenumber $\kappa = \frac{3}{2}$ waves *per meter* and wave-frequency $\nu = \frac{4}{5}$ waves *per second* in per-space-time. That is wavelength $\lambda = \frac{2}{3}$ meters *per wave* as well as wave-period $\tau = \frac{5}{4}$ seconds *per wave* in space-time. Kayser-Hertz space is better known as Fourier space where one imagines as a "control-panel" or "keyboard" to produce waves in space-time. The name "Keyboard of the Gods" is coined to suggest that mortal musicians cannot control *both* frequency $\nu = 1/\tau$ and wavelength λ or wavenumber $\kappa = 1/\lambda$.

The idea of mapping an entire space-time wave like the 300THz wave in Fig. 4 from a single Kaiser-Hertz point ($\kappa \frac{\text{(waves)}}{\text{meter}}$, $\nu \frac{\text{(waves)}}{\text{second}}$) of Fourier space requires a stretch of imagination. A wavelength or period in Fig. 4 involves a 2π phasor revolution as defined by wavefunction $\psi_{k,\omega}(x,t) = Ae^{i(kx-\omega t)}$ whose parameters are *angular frequency* $\omega = 2\pi \nu$ and *angular wavenumber* $k = 2\pi \kappa$ or *wavevector* $\mathbf{k} = 2\pi \kappa$.

The letter k (or greek "kappa" κ) honors Kaiser, but Hertz is not so noticed. Instead the greek "nu" ν for number is used. Since ν is easily confused with velocity "v" we will use "omicron" (ν) for number ν of waves per second (frequency). Conventional Greek-L or "lambda" λ denotes wave-Length and Greek-T or "tau" stands for wave-Time period τ , again without a proper name.

Ideal Fourier models fix the $(k, \omega) = 2\pi(\kappa, \nu)$ points in per-space-per-time. That determines wave velocity ν in space-time. Fig. 5 lower right corner has a space/time formula for ν as slope of wave paths.

$$\frac{\text{distance}}{\text{time}} = \frac{\text{wavelength}}{\text{wave period}} = \frac{\lambda}{\tau} = \frac{1/\kappa}{1/\nu} = \lambda \nu = \frac{\nu}{\kappa} = \frac{\omega}{k} = \frac{2/3}{5/4} = \frac{8}{15} = \nu \quad (9)$$

This often called *phase velocity* since it is the velocity of any particular phase, say zero phase: $0 = kx - \omega t$. Solving this gives velocity or slope equation $x = \frac{\omega}{k} t \equiv \nu t$ that agrees with (9) and has space-time slope relative to the vertical (time t or period τ) axis in Fig. 5. (It is a less familiar kind of slope.)

A vertical velocity vector \mathbf{v} in space-time (x, t) indicates a zero wave speed while a horizontal vector \mathbf{v} indicates infinite speed $\nu = \infty$. This inverts in per-space-per-time (k, ω) of Fig. 5 (left) where velocity is indicated by slope of \mathbf{v} relative to the horizontal (wavenumber $k = 2\pi \kappa$) axis. This is a more familiar kind of slope. A horizontal \mathbf{v} has zero slope and indicates zero speed while vertical \mathbf{v} is ∞ . Soon there will be shown light wave examples of both these extremes!

□ The “Keyboard of the gods” : per-space-per-time plot versus space-time Minkowski plot

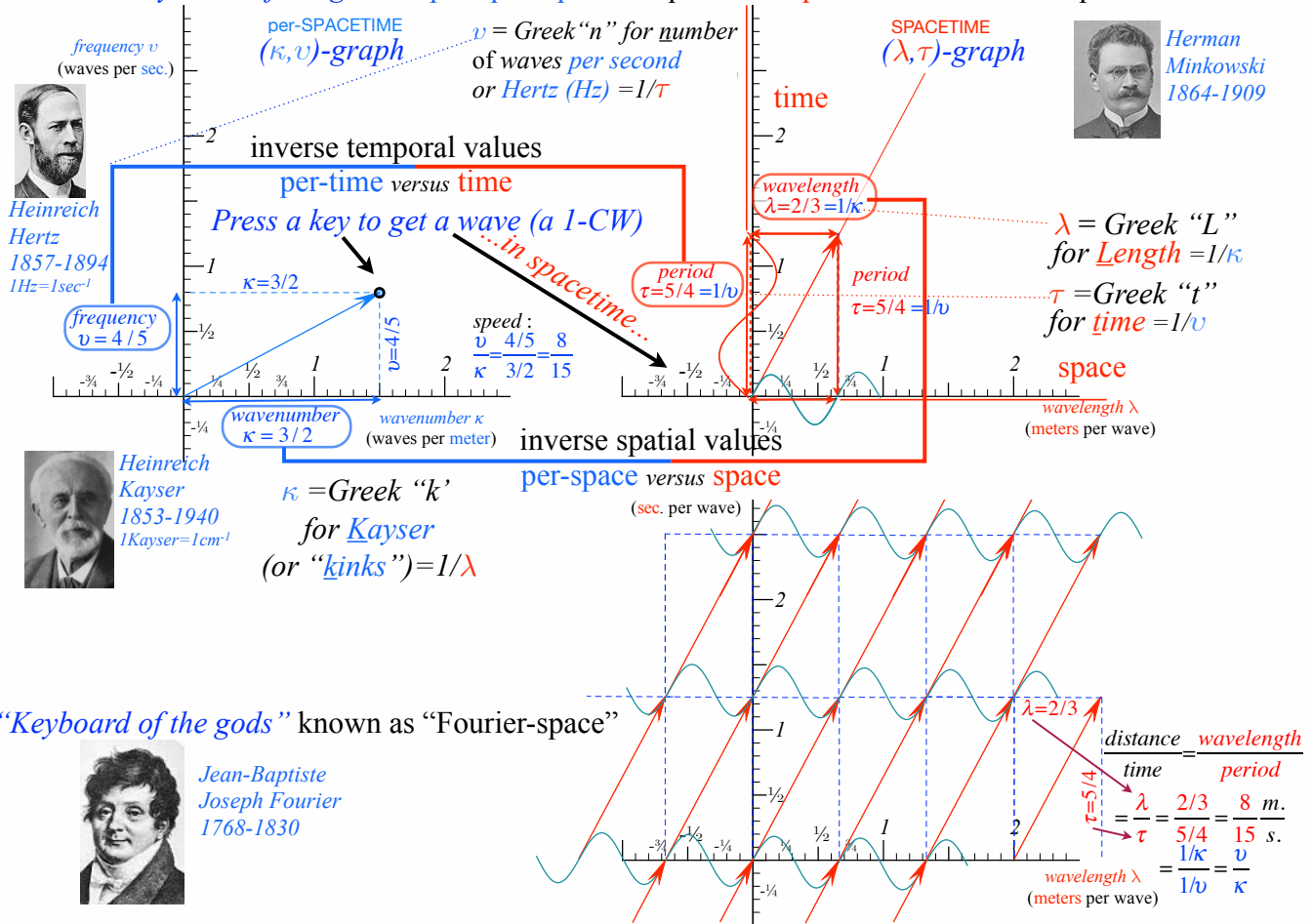


Fig. 5 Comparing a wave point in Kaiser-Hertz per-space-time to its Minkowski space-time view of resulting wave.

c-Scaled wave graphs and Doppler shifts

Wave velocity $v = \frac{8}{15}$ is plotted with slope $\frac{8}{15}$ in per-space-per-time on lefthand side of Fig. 5 but the space-time slope on the righthand side has inverse $\frac{15}{8}$ slope relative to horizontal. If light speed is a super constant $c = 2.99792458 \cdot 10^8 \text{ms}^{-1}$ it is convenient to rescale (9) to make c be *unit slope* in either plot.

$$c = \frac{\lambda}{\tau} = \frac{v}{\kappa} = \frac{\omega}{k} \quad \text{rescaled by } c \text{ to: } 1 = \frac{\lambda}{c\tau} = \frac{v}{c\kappa} = \frac{\omega}{ck} \tag{10}$$

This was done in space-time (x, ct) -plot of Fig. 4 and now for per-space-time plot $(ck, \omega) = 2\pi(c\kappa, \nu)$ on the lefthand side of Fig. 6 with its corresponding (x, ct) -space-time plot on the righthand side. Frequency units of both per-space-time axes are the same $\nu_A = 600\text{THz}$ units. The vertical ν -axis is directly so, but the horizontal $c\kappa$ -axis is indirectly so and without the c -factor, the κ unit is $\kappa_A = 2 \cdot 10^6$ waves per meter.

The vertical time ct_A axis of the $(x, ct) = (\lambda, c\tau)$ graph has the same $\frac{1}{2}$ -micron units of length that the horizontal space x_A -axis has. Without the c -scale factor the unit of time is $\tau_A = \frac{5}{3} \text{fs} = 1.667 \cdot 10^{-15} \text{sec}$. The units are assigned to a full blue-green 600THz wave made of two half waves, 1-peak and 1-trough separated by two real wave zeros $\sin 0$ and $\sin \pi$. When $\sin 0$ paths hit the vertical time axis a “hit” is recorded on the time axis in Fig.6 at time units $\dots, -2, -1, 0, +1, +2, \dots$ each due to a period $\tau_A = \frac{5}{3} \text{fs}$.

Now consider the more rapid succession of “hits” for a line sloping into the negative direction so it has head-on collisions with the $\sin\theta$ paths at time units $\dots-\frac{9}{4}, -\frac{6}{4}, -\frac{3}{4}, 0, \frac{3}{4}, \frac{6}{4}, \frac{9}{4}, \dots$ corresponding to a Doppler *blue-shift factor* of $\frac{4}{3}$. Then 600THz shifts to $\frac{4}{3}600 = 800\text{THz}$. A less rapid frequency of “hits” occurs along the path moving to the right and having rear-end collisions at $\dots-\frac{9}{2}, -\frac{6}{2}, -\frac{3}{2}, 0, \frac{3}{2}, \frac{6}{2}, \frac{9}{2}, \dots$ corresponding to a Doppler *red-shift factor* of $\frac{2}{3}$. Then 600THz shifts to $\frac{2}{3}600 = 400\text{THz}$.

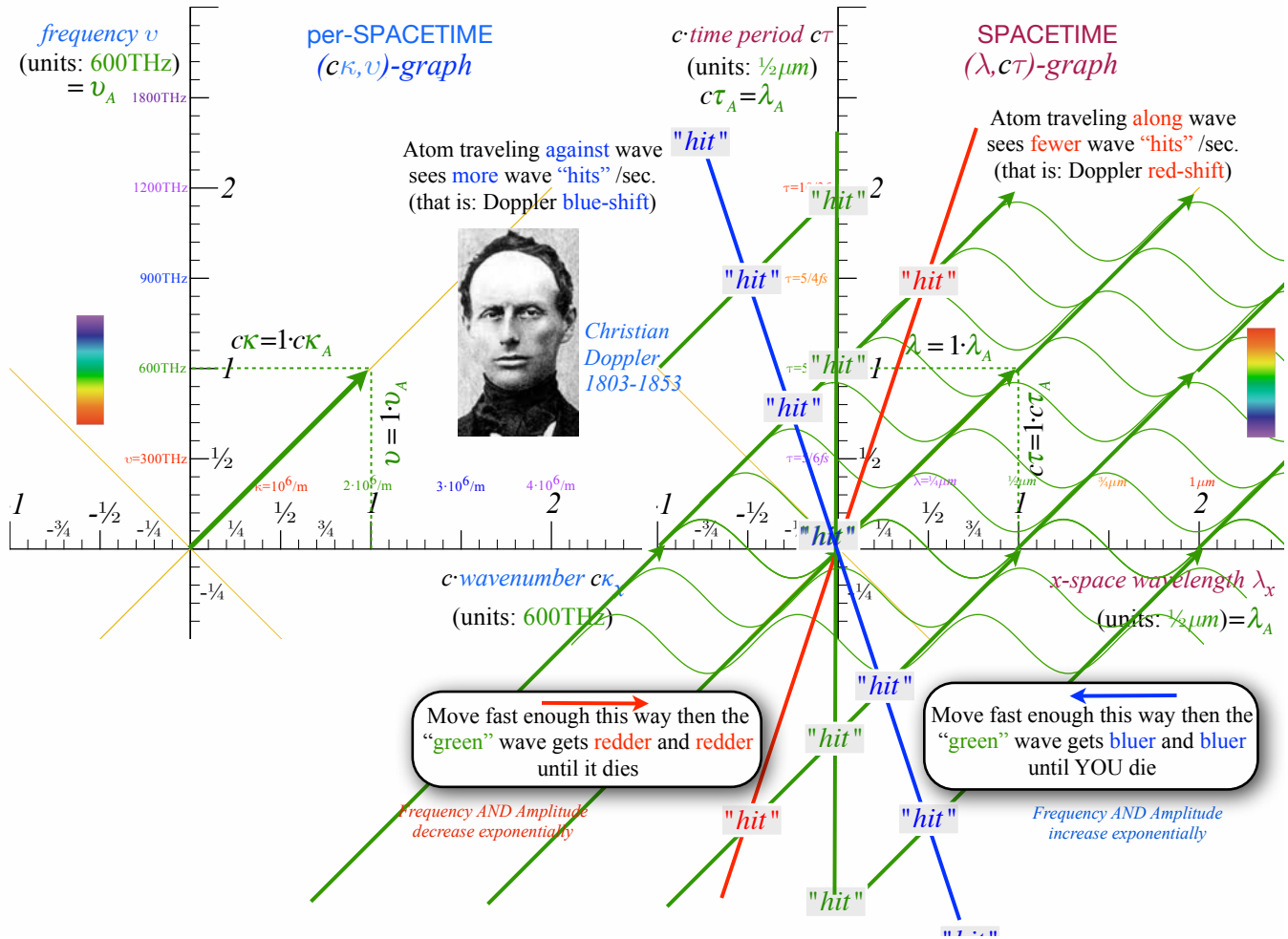


Fig. 6. Laser 600THz wave plots c -scaled (a) Per-space-per-time plot ($c\kappa, \nu$) (b) Space-time plot (x, ct).

As will be shown, Doppler blue shift is limited only by infinite ν and a red shift only by zero ν in spite of the speed limit c for all hapless mortal travelers. If you go faster to the right (along light beam flow) the light becomes redder and weaker until it disappears. If you go faster to the left (against light beam flow) the light becomes bluer and stronger until *you* disappear! (Or die of γ -ray poisoning.)

Evenson's axiom and Doppler shifts

It has become traditional in quantum optics to imagine beams between a point B and a point A to be manned (or woman-ed) by live characters named Bob and Alice, respectively. Our Doppler thought experiment begins with Bob sitting stationary relative to Alice but millions of kilometers to the East of her (far right of Fig.7) with Alice's laser shining on Bob. Unbeknownst to Bob, Alice is able to tune the laser on her spaceship and plans to do so as she accelerates toward Bob. Alice has cleverly programmed the laser to tune its frequency down with each increase of her velocity so Bob continues to see an

unchanged 600 THz reading on his receiver-spectrometer. If Alice and Bob have a communication channel like a cell phone, Alice will also have to detune her end of that channel appropriately in order to not make Bob suspicious. (Bob assumes Alice is maintaining her stay-at-home role.)

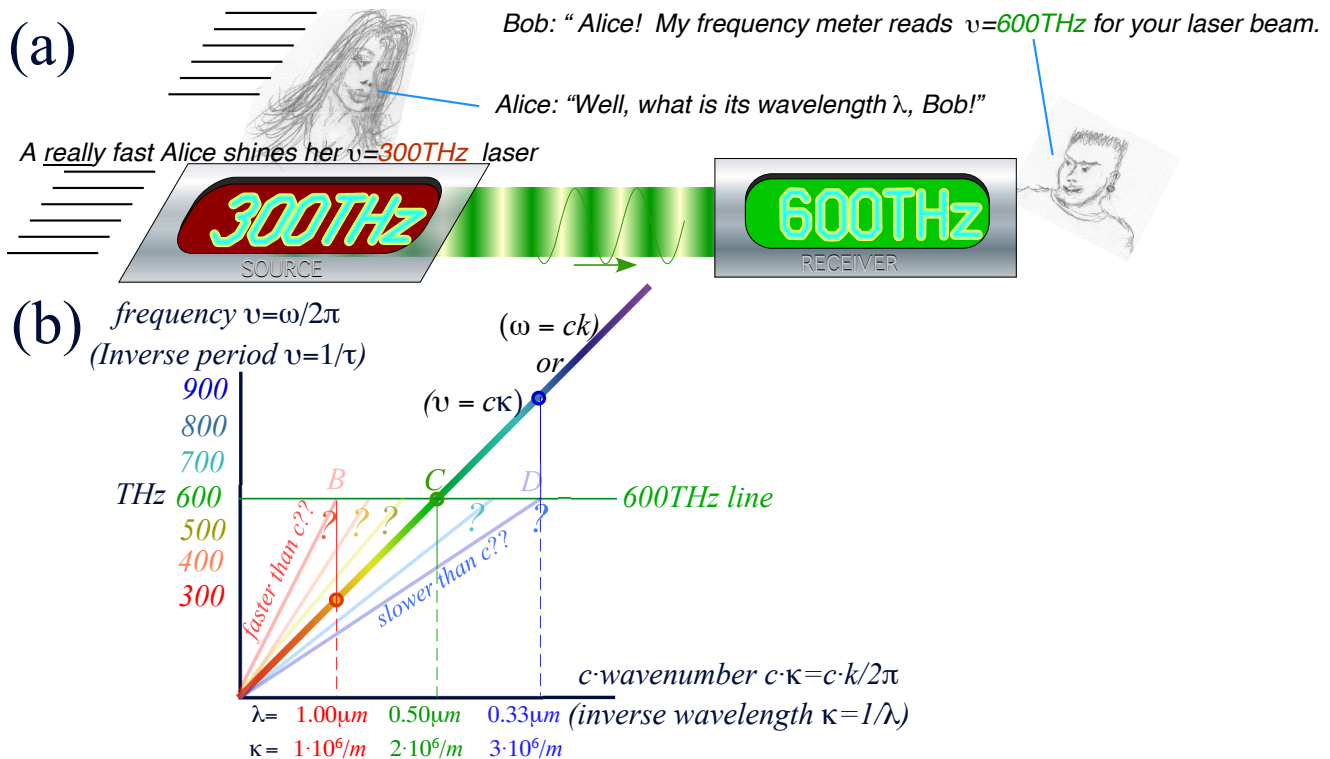


Fig. 7 Alice's 300THz laser approaches Bob. (a) Bob sees $\nu=600\text{THz}$. (b) What $\lambda=1/\kappa$ does Bob measure?

Now suppose Alice pauses her acceleration at a velocity corresponding to an octave Doppler blue factor of $b=2$, that is, while Bob thinks he is still receiving her steady blue-green 600 THz laser beam, she has actually down-tuned her laser to an infrared 300 THz as in Fig. 7a. To check in with Bob, Alice must tune her phone receiver up by factor of 2 and her phone transmitter down by a factor of 2, just like her laser. (Tune-up-or-down by 2 is due to time reversal symmetry as explained below.)

Always the trickster, Alice asks Bob if he notices anything different about her laser beam. Bob replies, "It's still your beautiful blue-green and reads 600 THz to 18 digits." Alice says, "Okay, you've checked your frequency (ν)-meter, but what is your wavelength (λ)-measurement?"

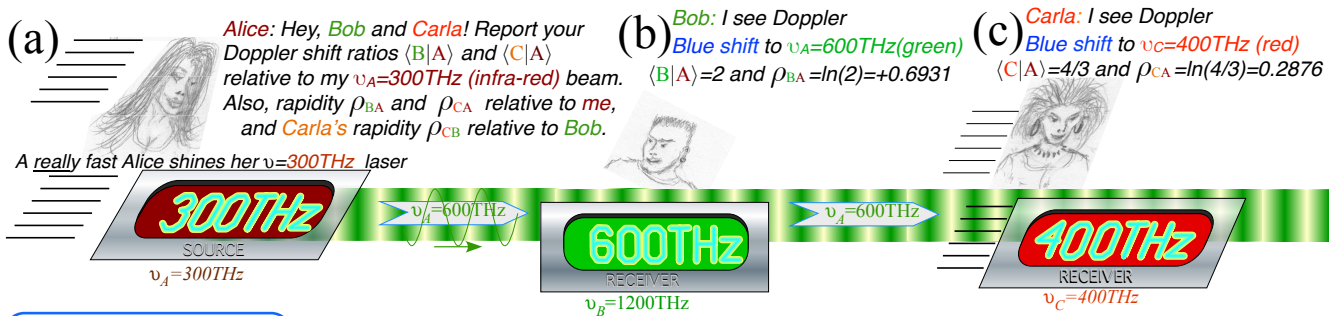
Alice's leading question is a crucial one for relativity and quantum theory. She is asking if Bob is receiving some 'phony' kind of blue-green 600 THz, in this case, one that was produced by an infrared 300 THz laser moving very rapidly toward Bob. And, more generally, one may ask, "How many kinds of 'phony' blue-green, or of any other color or frequency, are possible in the vacuum of the universe?" One set of possibilities lies on the 600THz line of per-space-time $(c\kappa, \nu)$ plot in center of Fig. 7b and includes B ($\lambda=1\text{micron}$ or $\kappa=1 \cdot 10^6\text{m}^{-1}$) thru C ($\lambda=\frac{1}{2}\text{micron}$ or $\kappa=2 \cdot 10^6\text{m}^{-1}$) to D ($\lambda=\frac{1}{3}\text{micron}$ or $\kappa=3 \cdot 10^6\text{m}^{-1}$). But, years of spectroscopy rule out 'phony' 600THz blue-green that do not have wavelength $\lambda=\frac{1}{2}\text{micron}$. The only choice in Fig. 7b is C and only possible 600THz light speed is $c = \frac{\nu}{\kappa} = \frac{600 \cdot 10^{12}}{2 \cdot 10^6} = 3 \cdot 10^8 \text{m} \cdot \text{s}^{-1}$.

Alice could adjust her ship-and-laser to give any frequency to Bob's frequency meter. So any light Bob sees must fall on the 45° line of the $(c\kappa, \nu)$ plot in Fig. 7b. This verifies Evenson's Axiom requiring all 1-CW colors to march in lock-step at speed c .

A $(c\kappa, v)$ plot is also called a *dispersion* plot. Points lying below the 45° line ($v=c\kappa$) belong to waves *slower* than vacuo light ($v/\kappa < c$). Those above the line are faster than c ($v/\kappa > c$). A waveform composed of sub or super luminal speeds would *disperse*, that is, super luminal components would outrun the sub luminal ones and thereby garble its initial waveform and information therein. Even a tiny frequency variation of speed c would give totally garbled light from galaxies millions (or billions!) of light-years away. (Goodbye Hubble images!)

Rapidity and its Doppler shift arithmetic

Thought experiments involving Doppler effects of relativistic quantum optics begs for a third member, Carla, on the SR optics team of Bob and Alice. Fig. 8 expands the Fig. 7 view in Bob’s frame with Alice approaching so Bob sees her infrared 300Thz source Doppler blue-shifted to green 600Thz. Carla is moving to the right more slowly than Alice so she also sees Alice’s 300Thz Doppler blue-shifted but only to red 400THz. A cartoon notation for speed shows v -meter&reader leaning into their direction of motion and trailing “contrail” lines. The speeds imagined here a truly enormous. It is later shown that Bob’s Doppler shift of Alice’s 300THz to his 600THz means she is approaching him at $\frac{2}{3}c$. (At that speed she could circumnavigate the Earth more than 4 times per second!)



Doppler ratio:

$$\langle R|S \rangle = \frac{v_{RECEIVER}}{v_{SOURCE}}$$

$$\rho_{RS} = \ln \langle R|S \rangle$$

or:

$$\langle R|S \rangle = e^{\rho_{RS}} = e^{-\rho_{SR}}$$

Definition of Rapidity ρ_{RS}

Bob-Alice Doppler ratio:

$$\langle B|A \rangle = \frac{v_B}{v_A} = \frac{600}{300} = \frac{2}{1}$$

Carla-Alice Doppler ratio:

$$\langle C|A \rangle = \frac{v_C}{v_A} = \frac{400}{300} = \frac{4}{3}$$

Bob-Alice rapidity:

$$\rho_{BA} = \ln \langle B|A \rangle = \ln \frac{2}{1} = 0.6931$$

Carla-Alice rapidity:

$$\rho_{CA} = \ln \langle C|A \rangle = \ln \frac{4}{3} = 0.2876$$

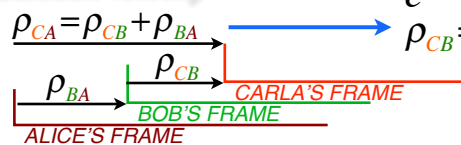
$$\rho_{AB} = \ln \langle A|B \rangle = \ln \frac{1}{2} = -0.6931 = -\rho_{BA}$$

Galileo Galilei



1564-1642

Galileo’s Revenge (part 1)
Rapidity adds just like Galilean velocity



Carla-Bob Doppler ratio:

$$\langle C|B \rangle = \frac{v_C}{v_B} = \frac{v_C}{v_A} \frac{v_A}{v_B} = \langle C|A \rangle \langle A|B \rangle = \frac{4}{3} \frac{1}{2} = \frac{2}{3}$$

Carla-Bob rapidity:

$$e^{\rho_{CB}} = e^{\rho_{CA}} e^{\rho_{AB}} = e^{\rho_{CA} + \rho_{AB}}$$

$$\rho_{CB} = \rho_{CA} + \rho_{AB} = 0.2876 - 0.6931 = -0.4055$$

$$= \ln \frac{4}{3} + \ln \frac{1}{2} = \ln \frac{2}{3}$$

Fig. 8 Doppler $\langle R|S \rangle$ and Rapidity ρ_{RS} (a) Alice’s source and basic definitions. (b-c) Example of rapidity addition

In Fig. 8a Doppler shift ratio is defined by $\langle R|S \rangle = v_{RECEIVER}/v_{SOURCE}$. (Think R over S : $\langle R/S \rangle$.) Also given is a definition of *rapidity* ρ_{RS} as the natural logarithm of Doppler ratio ($\rho_{RS} = \ln \langle R|S \rangle$). The ρ_{RS} definition simplifies arithmetic of high-speed velocity addition where, as shown later, velocity u_{RS} of R relative to S (in units of c) is hyper-tangent $\tanh \rho_{RS}$ of their relative rapidity ρ_{RS} . (Here: $\tanh(\ln 2) = \frac{3}{5}$.)

Fig. 8(b-c) shows how rapidity ρ_{CB} of Carla relative to Bob is the sum of rapidity ρ_{CA} of Carla relative to Alice and the rapidity ρ_{AB} of Alice relative to Bob. Graph of equivalent sum $\rho_{CA} = \rho_{CB} + \rho_{BA}$ is in lower left of Fig. 8 and resembles Galilean velocity addition. However, ρ -sums are exact while Galileo's v -sums are approximate and fail badly at high speeds. ρ -sums have \pm sign rules: a (+)-sign for approach rapidity (blue shift) and (-)-sign for withdrawal rapidity (red shift). (Think of a friend's arrival as positive ρ while departure is negative ρ .) Note v -rule: $\langle A|B \rangle = 1/\langle B|A \rangle$ and ρ -rule: $\rho_{AB} = -\rho_{BA}$ in Fig.8.

4. Wave-zero 2-CW coordinate grids

Optical single-Continuous Waves (1-CW) obey Evenson's Axiom and march lockstep en-vacuo at speed c with any and all other 1-CW going in a given direction $\hat{\mathbf{k}}$. Observer's motion along $\hat{\mathbf{k}}$ cannot alter 1-CW speed c , but will affect a 1st-order Doppler shift $e^{\pm\rho}$ for both frequency $\omega=2\pi\nu$ and wave-vector $\mathbf{k}=2\pi\boldsymbol{\kappa}$ in each 1-CW per-space-time vector $K=(c\mathbf{k},\omega)$. Following Fig. 8, observer motion along $\hat{\mathbf{k}}$ will shorten K by red-shift factor $e^{-\rho}$ while motion against $\hat{\mathbf{k}}$ will lengthen K by blue-shift factor $e^{+\rho}$.

$$K \xrightarrow{\text{red-shift}} K'=e^{-\rho}K=(c\mathbf{k}e^{-\rho},\omega e^{-\rho}) \quad (11a) \quad K \xrightarrow{\text{blue-shift}} K'=e^{+\rho}K=(c\mathbf{k}e^{+\rho},\omega e^{+\rho}) \quad (11b)$$

Fig. 9 has (x,ct) -plots of a head-on collision between wave e^{iR} moving right from Alice in Fig. 9a and wave e^{iL} moving left from Carla in Fig. 9c. It makes a wave-sum $e^{iR}+e^{iL}$ for Bob shown in Fig. 9b. Alice's wave has phase $R=kx-\omega t$ of a 1-CW moving rightward according to $x=\frac{\omega}{k}t+\frac{\text{phase}}{\text{constant}}$ at speed $\frac{\omega}{k}=c$. Carla's wave has phase $L=-kx-\omega t$ of a 1-CW moving leftward according to $x=-\frac{\omega}{k}t+\frac{\text{phase}}{\text{constant}}$. (It has a $(-k)$.)

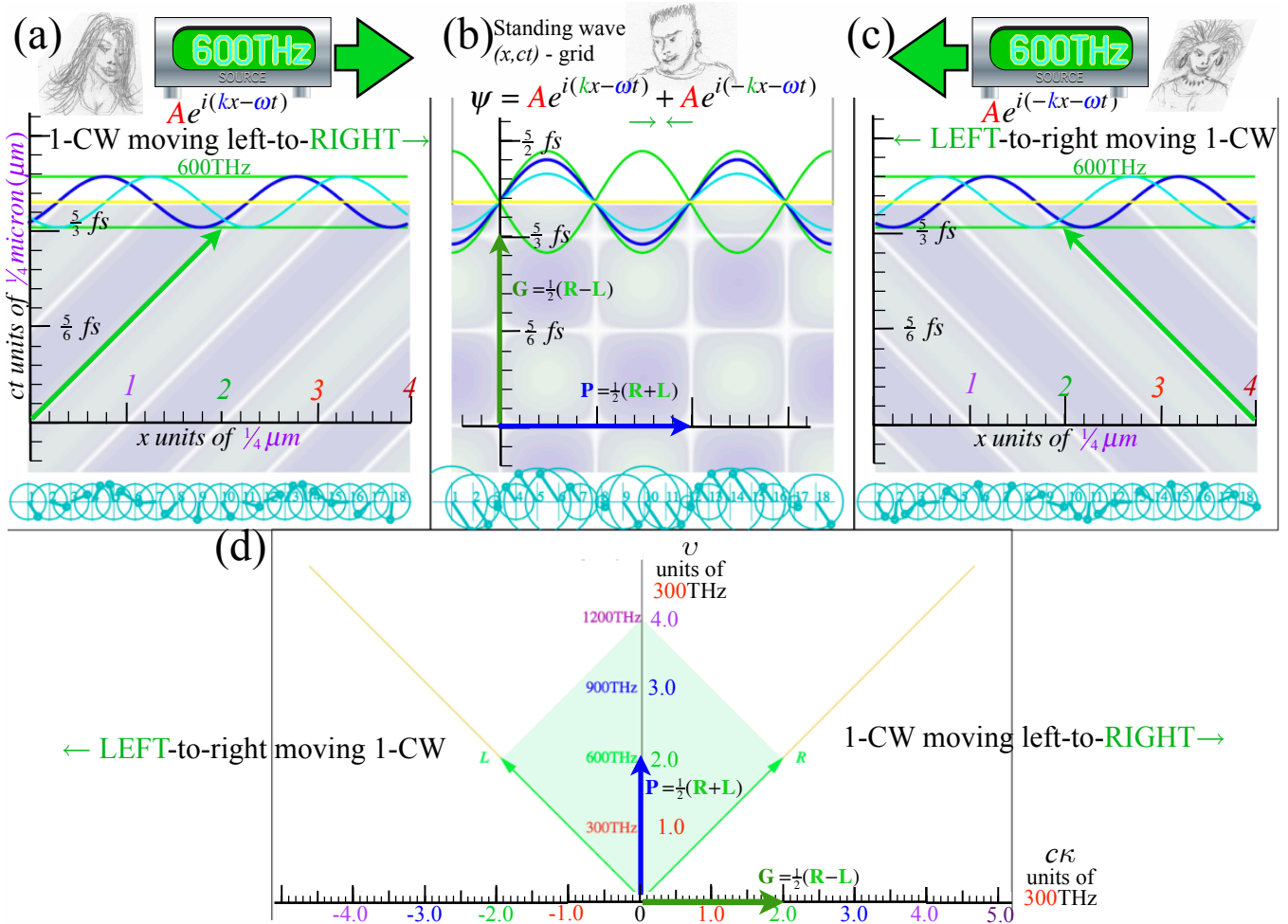


Fig. 9 (x,ct) wave plots (a) Alice's R-CW (b) Bob's Group G over Phase P (c) Carla's L-CW (d) $(c\kappa, \nu)$ plots of P over G

Zeros of the real part of the 2-CW seen in Fig. 9b trace a space-time coordinate grid of white lines. In elementary algebra, zeros are found by factoring. Plane wave-sum $e^{iR}+e^{iL}$ is factored as follows.

$$e^{iR}+e^{iL} = e^{\frac{i(R+L)}{2}} \left(e^{\frac{i(R-L)}{2}} + e^{-\frac{i(R-L)}{2}} \right) = 2e^{\frac{i(R+L)}{2}} \cos \frac{R-L}{2} = 2e^{-i\omega t} \cos kx \quad \text{where: } R=kx-\omega t \text{ and: } L=-kx-\omega t \quad (12)$$

Fig. 9b plots Real part of phase factor $e^{-i\omega t} = \cos\omega t - i\sin\omega t$ in dark blue and the Imaginary part in cyan. $e^{-i\omega t}$ is x -independent but is amplitude-modulated by Group factor $2\cos kx$, a time-independent 2-sided envelope. Group envelope zeros trace vertical coordinate lines in Fig. 9b and have zero x -velocity. This corresponds to a Group **G**-vector with zero slope in per-space-time plot of Fig. 9d. The Phase **P**-vector in Fig. 9d has infinite slope. This indicates an infinite velocity for phase zeros¹⁹. They exhibit this every $\frac{1}{2}$ -period in (x, ct) plot Fig. 9b. Bob sees two “instantons” zip by in each period of $\tau_{phase} = \frac{5}{3} \cdot 10^{-15} s = \frac{5}{3} fs$.

Bob’s $(c\kappa, v)$ plot in Fig. 9b is what we call a “Relativity Baseball-Diamond” (RBD). Origin is *home-plate*, the **R**-vector is the *1st-baseline*, the **L**-vector is the *3rd-baseline*, **R+L** points to *2nd-base*, and Phase **P** = $\frac{1}{2}(\mathbf{R}+\mathbf{L})$ points to *Pitcher’s mound*, and Group **G** = $\frac{1}{2}(\mathbf{R}-\mathbf{L})$ points to center of a *Grandstand*.

A sheared RBD is in Fig. 10d. It has a Doppler blue-shift $e^{\rho_{BA}}=2$ of Alice’s light to 1200THz (now *1st-baseline* is twice as long) combined with a Doppler red-shift $e^{-\rho_{BA}}=\frac{1}{2}$ of Carla’s light to 300THz (now *3rd-baseline* is half as long). $(c\kappa, v)$ -plot geometry in Fig. 9d or Fig. 10d is reflected (literally, thru the diagonal) in the (x, ct) -plot in Fig. 9b or Fig. 10b, respectively. This is powerful! It’s a ruler&compass derivation of Alice and Carla space-time (x', ct') and per-space-time $(c\kappa', v')$ coordinates as seen by Bob speeding toward Alice (her beam blue-shifted to 1200Hz) and away from Carla (red shifted to 300THz).

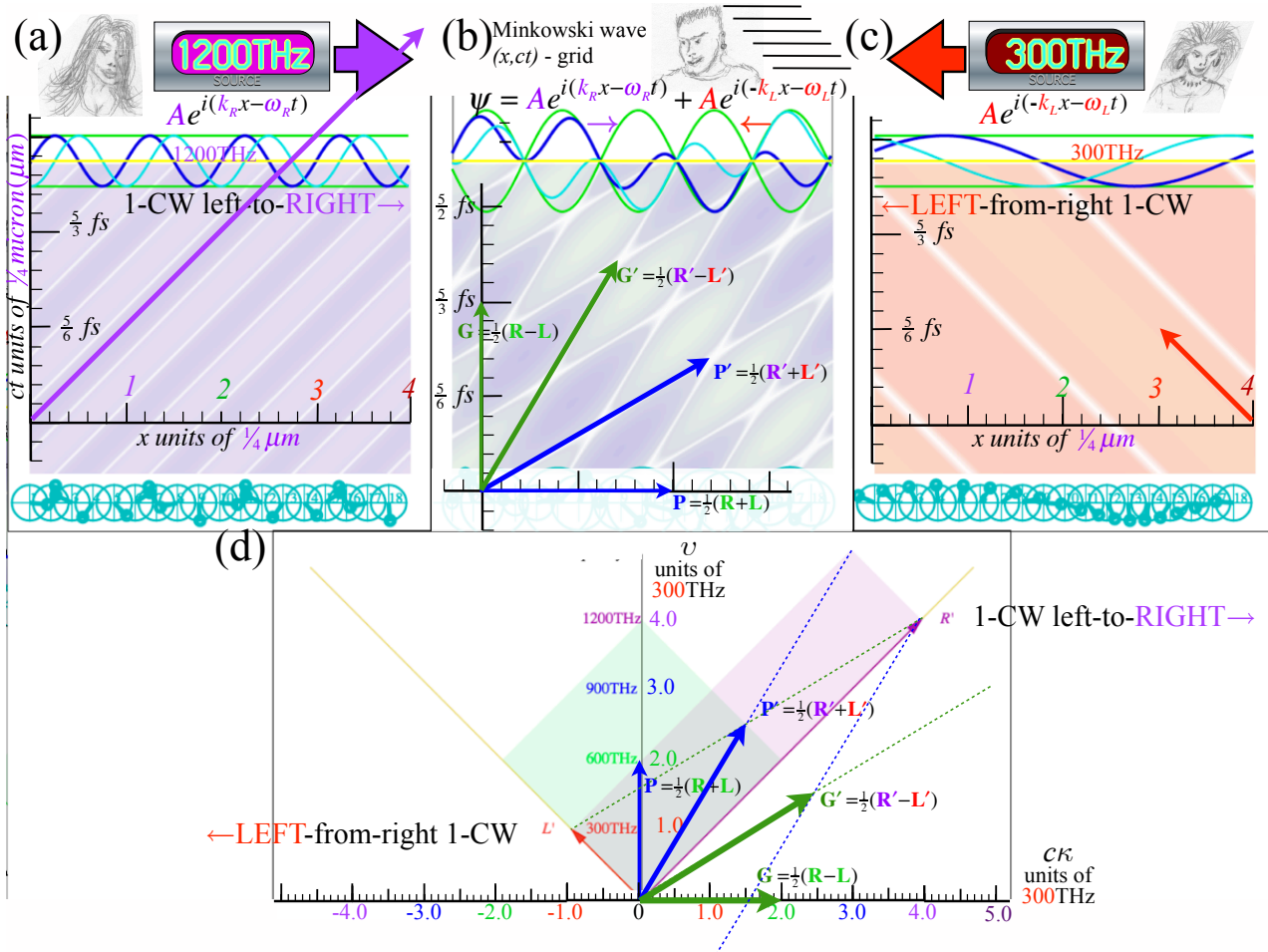


Fig.10 (x, ct) wave plots (a) Alice’s **R'**-CW (b) Bob’s Group **G'** over Phase **P'** (c) Carla’s **L'**-CW (d) $(c\kappa, v)$ plots of \mathbf{P}' over \mathbf{G}'

Alice’s rightward blue-shifted wave $e^{iR'}$ plus Carla’s leftward red-shifted wave $e^{iL'}$ has factors like (12).

$$\Psi'(x, t) = e^{iR'} + e^{iL'} = e^{\frac{i(R'+L')}{2}} \left(e^{\frac{i(R'-L')}{2}} + e^{-\frac{i(R'-L')}{2}} \right) = e^{\frac{i(R'+L')}{2}} 2 \cos \frac{R'-L'}{2} = \Psi'_{phase} \Psi'_{group} \quad (13)$$

Zeros of Real parts of wave factors $\psi_{phase}\psi_{group}$ in (12) make a square “rest-frame” lattice in Fig. 9b.

$$0 = \text{Re}\psi_{phase} = \text{Re}e^{i\frac{R-L}{2}} = \text{Re}e^{-i\omega_A t} = \cos\omega_A t \quad \text{define horizontal time-lines: } t = \pm\frac{\pi}{2\omega_A}, \pm\frac{3\pi}{2\omega_A} \dots \quad (14a)$$

$$0 = \text{Re}\psi_{group} = \text{Re}e^{i\frac{R-L}{2}} = \text{Re}e^{-ik_A x} = \cos k_A x \quad \text{define vertical x-space-lines: } x = \pm\frac{\pi}{2k_A}, \pm\frac{3\pi}{2k_A} \dots \quad (14b)$$

They are (x, ct) coordinate lines marking half-periods $\frac{\tau_A}{2} = \frac{\pi}{\omega_A} = \frac{1}{2\nu_A}$ and half-wavelengths $\frac{\lambda_A}{2} = \frac{\pi}{k_A} = \frac{1}{2\kappa_A}$ that lie mid-way between crests (lighter regions) and troughs (darker regions) in Fig. 9b. Its square lattice turns into a “moving-frame” rhombus lattice of Fig. 10b when the Doppler parameter ρ_{AB} is non-zero. Then Bob sees blue-shift $\langle B|A \rangle v_A = v_A e^{\rho_{AB}}$ going toward Alice’s v_A -laser source and red-shift $\langle B|C \rangle v_C = e^{-\rho_{BC}} v_C$ as he goes away from Carla’s v_C -laser. Time inversion flips roles of receiver-source pairs. That flips ratio $\langle R|S \rangle = v_{RECEIVER}/v_{SOURCE} \rightarrow \langle S|R \rangle$ while changing the \pm sign of $\rho_{AB} = -\rho_{BA}$ and relative velocity $u_{AB} = -u_{BA}$.

A single rhombus in “reciprocal” $(c\kappa, v)$ -per-space-time of Fig. 10d has geometry similar to every rhombus cell of (x, ct) wave zeros in Fig. 10b. This geometry also relates ρ_{AB} to u_{AB} as shown below.

Geometry of Minkowski phase and group wave-lattices

Bob sees Alice’s $v_A = 600\text{THz}$ laser beam blue-shifted by $\langle B|A \rangle = e^{\rho_{BA}} = 2 = b_{BA}$ as he approaches her. So a vector $\mathbf{R}' = \begin{pmatrix} v \\ c\kappa \end{pmatrix}$ that Bob plots for Alice is her original vector $\mathbf{R} = v_A \begin{pmatrix} 1 \\ +1 \end{pmatrix}$ *doubled* in length by the blue shift to $\mathbf{R}' = b_{BA} v_A \begin{pmatrix} 1 \\ +1 \end{pmatrix} = v_A \begin{pmatrix} 2 \\ +2 \end{pmatrix}$ along the 1st baseline (45°) in Fig. 10d. This runs head-on into Carla’s $v_C = 600\text{THz}$ laser beam that is red-shifted by $\langle B|C \rangle = e^{-\rho_{BC}} = \frac{1}{2} = r_{BC}$ as Bob runs away from Carla. So her original vector $\mathbf{L} = v_A \begin{pmatrix} 1 \\ -1 \end{pmatrix}$ is *halved* in length to $\mathbf{L}' = r_{BC} v_A \begin{pmatrix} 1 \\ -1 \end{pmatrix} = v_A \begin{pmatrix} 1/2 \\ -1/2 \end{pmatrix}$ along 3rd baseline (-45°). (Evenson’s axiom confines 1-CW light to 1st-baseline for positive κ and to 3rd-baseline for negative κ .)

Alice’s right-going vector \mathbf{R} (Bob’s view \mathbf{R}') and Carla’s left-going vector \mathbf{L} (Bob’s view \mathbf{L}') go according to (12) or (13) into a half-sum $\mathbf{P} = \frac{1}{2}(\mathbf{R} + \mathbf{L})$ (Bob’s view $\mathbf{P}' = \frac{1}{2}(\mathbf{R}' + \mathbf{L}')$) for phase wave factor.

$$\mathbf{P}' = \begin{pmatrix} v'_{phase} \\ c\kappa'_{phase} \end{pmatrix} = \frac{1}{2}(\mathbf{R}' + \mathbf{L}') = v_A \begin{pmatrix} \frac{1}{2}(e^\rho + e^{-\rho}) \\ \frac{1}{2}(e^\rho - e^{-\rho}) \end{pmatrix} = v_A \begin{pmatrix} \cosh \rho \\ \sinh \rho \end{pmatrix} = v_A \begin{pmatrix} \frac{5}{4} \\ \frac{3}{4} \end{pmatrix} \quad \text{or: } v_A \begin{pmatrix} 1 \\ 0 \end{pmatrix} \quad (15a)$$

Bob's View Alice's View

Group wave factor of (12) or (13) calls for a half-difference $\mathbf{G} = \frac{1}{2}(\mathbf{R} - \mathbf{L})$ (Bob’s view $\mathbf{G}' = \frac{1}{2}(\mathbf{R}' - \mathbf{L}')$).

$$\mathbf{G}' = \begin{pmatrix} v'_{group} \\ c\kappa'_{group} \end{pmatrix} = \frac{1}{2}(\mathbf{R}' - \mathbf{L}') = v_A \begin{pmatrix} \frac{1}{2}(e^\rho - e^{-\rho}) \\ \frac{1}{2}(e^\rho + e^{-\rho}) \end{pmatrix} = v_A \begin{pmatrix} \sinh \rho \\ \cosh \rho \end{pmatrix} = v_A \begin{pmatrix} \frac{3}{4} \\ \frac{5}{4} \end{pmatrix} \quad \text{or: } v_A \begin{pmatrix} 0 \\ 1 \end{pmatrix} \quad (15b)$$

Bob's View Alice's View

The slope of Bob’s group vector \mathbf{G}' in $(c\kappa, v)$ -plot of Fig. 10d is actual group wave velocity in c -units.

$$\frac{V^{group}}{c} = \frac{v'_{group}}{c\kappa'_{group}} = \frac{\sinh \rho}{\cosh \rho} = \tanh \rho = \frac{\frac{3}{4}}{\frac{5}{4}} = \frac{3}{5} \equiv \frac{u}{c} \equiv \beta \quad (16a)$$

This is the speed $\frac{u}{c} = \frac{3}{5}$ of Alice and Carla’s *group* or *envelope* wave in Bob’s space-time plot of Fig. 10b. u/c is the conventional *relativity-parameter* $\beta \equiv \frac{u}{c}$ for velocity of Alice and Carla relative to Bob. This group wave is, for Alice or Carla, a *standing* wave held by their laser cavities. In the same picture is the much faster *phase* or *carrier* wave that Bob would (if he could!) record going $\frac{5}{3}$ faster than light.

$$\frac{V^{phase}}{c} = \frac{v'_{phase}}{c\kappa'_{phase}} = \frac{\cosh \rho}{\sinh \rho} = \coth \rho = \frac{\frac{5}{4}}{\frac{3}{4}} = \frac{5}{3} \equiv \frac{c}{u} \equiv \frac{1}{\beta} \quad (16b)$$

After Fig. 9b we noted “instantons” seen by Bob that had infinite phase velocity. That is what Alice or Carla see for phase velocity in Fig. 10b while Bob sees two or three phase-zero white lines intersecting the dark blue wave curves near the top of the figure. There they have slowed down to a super-luminal speed (16b) of $\frac{u}{c} = \frac{5}{3}$. (\mathbf{P}' line slope is $\frac{5}{3}$ relative to x' -axis in Fig. 10b but it is $\frac{5}{3}$ relative to $c\kappa'$ -axis in reciprocal Fig. 10d. Recall that \mathbf{P} and \mathbf{G} lines get switched between reciprocal spaces.)

Fig. 11 shows detail in (a) per-Space-Time $(c\kappa, v)$ and (b) Space-Time $(\lambda, c\tau)$. In Fig. 11a, $(c\kappa, v)$ -coordinates of \mathbf{P}' are proportional to $\kappa_{phase}=1/\lambda_{phase}$ and $v_{phase}=1/\tau_{phase}$ while $(c\kappa, v)$ -coordinates of \mathbf{G}' are proportional to $\kappa_{group}=1/\lambda_{group}$ and $v_{group}=1/\tau_{group}$. In Fig. 11b, the interval between successive intercepts of \mathbf{P}' -lines (or \mathbf{G}' -lines) with the space x' -axis is proportional to wavelength λ_{phase} (or λ_{group}), and the corresponding intercepts with time ct' -axis give the period τ_{phase} (or τ_{group}).

Table 1. displays eight relativity parameters including Doppler shifts and wave velocities given as functions of rapidity ρ and the old $\beta=\frac{u}{c}$ parameter. Numerical values for the $\beta=\frac{3}{5}$ case are at bottom.

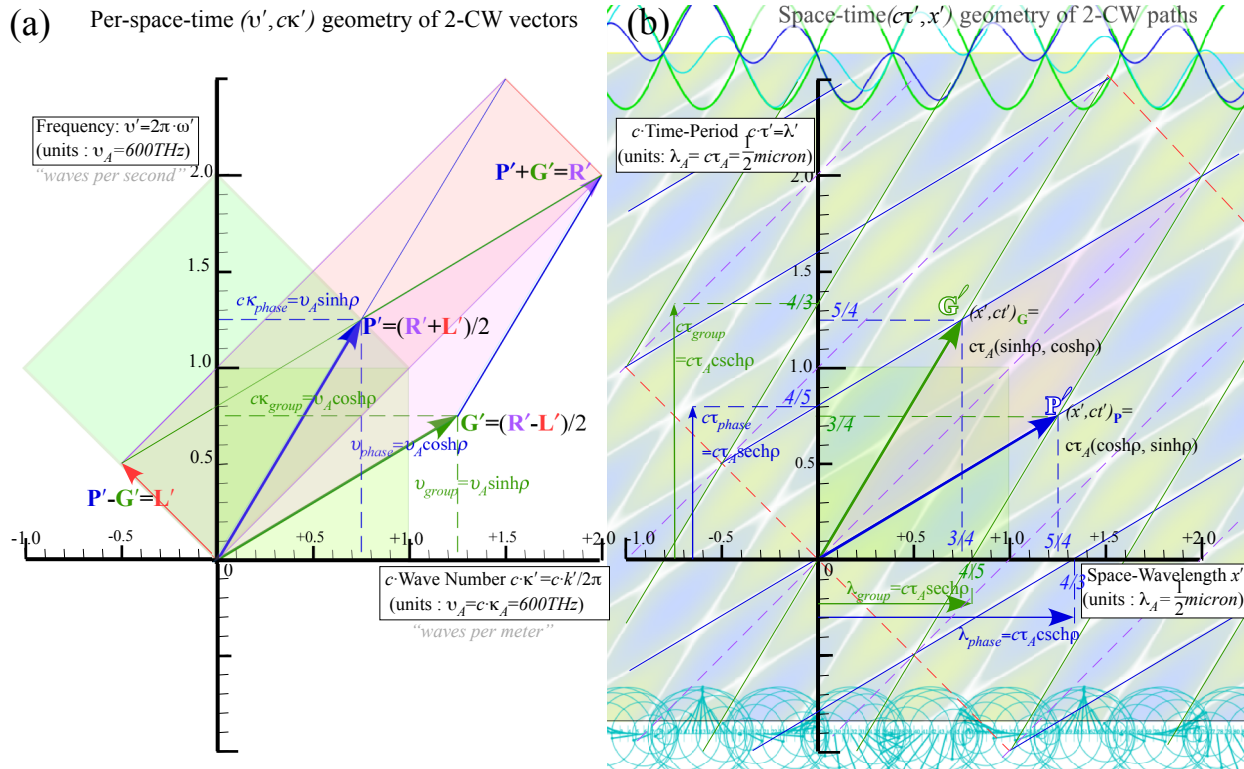


Fig. 11. Relativity parameters given as ρ -functions as they appear in (a) Per-space-time and (b) Space-time Table 1. Relativity parameter formulae. Last row gives numeric values for blue-shift $b_{BLUE}^{Doppler} = 2$ or $\beta = \frac{u}{c} = \frac{3}{5}$

<i>phase</i>	$b_{RED}^{Doppler}$	$\frac{c}{V_{phase}}$	$\frac{\kappa_{phase}}{\kappa_A}$	$\frac{\tau_{phase}}{\tau_A}$	$\frac{v_{phase}}{v_A}$	$\frac{\lambda_{phase}}{\lambda_A}$	$\frac{V_{phase}}{c}$	$b_{BLUE}^{Doppler}$
<i>group</i>	$\frac{1}{b_{BLUE}^{Doppler}}$	$\frac{V_{group}}{c}$	$\frac{v_{group}}{v_A}$	$\frac{\lambda_{group}}{\lambda_A}$	$\frac{\kappa_{group}}{\kappa_A}$	$\frac{\tau_{group}}{\tau_A}$	$\frac{c}{V_{group}}$	$\frac{1}{b_{RED}^{Doppler}}$
<i>rapidity</i> ρ	$e^{-\rho}$	$\tanh \rho$	$\sinh \rho$	$\operatorname{sech} \rho$	$\cosh \rho$	$\operatorname{csch} \rho$	$\operatorname{coth} \rho$	$e^{+\rho}$
$\beta \equiv \frac{u}{c}$	$\frac{\sqrt{1-\beta}}{\sqrt{1+\beta}}$	$\frac{\beta}{1}$	$\frac{1}{\sqrt{\beta^2-1}}$	$\frac{\sqrt{1-\beta^2}}{1}$	$\frac{1}{\sqrt{1-\beta^2}}$	$\frac{\sqrt{\beta^2-1}}{1}$	$\frac{1}{\beta}$	$\frac{\sqrt{1+\beta}}{\sqrt{1-\beta}}$
<i>value for</i> $\beta=3/5$	$\frac{1}{2} = 0.5$	$\frac{3}{5} = 0.6$	$\frac{3}{4} = 0.75$	$\frac{4}{5} = 0.80$	$\frac{5}{4} = 1.25$	$\frac{4}{3} = 1.33$	$\frac{5}{3} = 1.67$	$\frac{2}{1} = 2.0$

Note that the ratio in column- $(l+n)$ is the inverse of the ratio in column- $(8-n)$ for $n < 8$. Some discussion is required of the Table 1 and plot thereof in Fig. 11 in order to avoid pitfalls in the application and interpretation of the ratios. This begins in the following section.

Understanding relativity parameters and Lorentz transformations

Some of the parameters listed in Table 1 and plotted in Fig. 11 have famous names attached. In some cases there are several such names and contexts, and these will be recalled in due time. We begin with just two pairs of mutually reciprocal parameters $\text{sech}\rho$ and $\text{cosh}\rho$ that show up in sophomore physics.

$$\lambda_{group} = \lambda_A \text{sech}\rho = \lambda_A \sqrt{1-\beta^2} \quad (17a) \quad v_{phase} = v_A \cosh\rho = \frac{v_A}{\sqrt{1-\beta^2}} \quad (17b)$$

Sophomores learn two names: *Lorentz length contraction* and *Einstein time dilation*. Group velocity $V_{group} = c \tanh\rho$ is related to $\beta \equiv u/c$ in (16a). So the β -forms in (17a-b) follow by hyper-identity $\cosh^2\rho - \sinh^2\rho = 1$. (17c)

More difficult is learning what lies under these “contractions” and “dilations” and realizing that they are primary (really *secondary*) effects of greater but not-quite-canceling Doppler contractions and dilations.

By now it should be clear that the hyper-trigonometry lessons in Fig. 2 and Fig. 3 have $\text{sech}\rho$ and $\text{cosh}\rho$ functions along with **R**, **L**, **P**, and **G** points in precisely the places they appear in Fig. 10 or Fig. 11. (All involve 3:4:5 triangles and $\text{sech}\rho = \frac{4}{5}$.) Fig. 11b has two parallel **G'**-lines (group velocity $\frac{3}{5}$) cross Bob's x' -axis at $x'=0$ and $x'=\frac{4}{5}x_A$, respectively. So Alice's standing wave is contracted to 80% (or $\frac{4}{5}$) of its original λ_A , that is, $\lambda_{group} = \lambda_A \frac{4}{5}$ as listed in Table 1 (column-4) and Fig. 11b, and due to (17a).

Lorentz contraction comes with a well-worn paradox. Suppose Bob criticizes Alice for her 80% foreshortened meter-stick. (Actually, it is a *micrometer* stick if it holds two 600Thz standing $\lambda_A = \frac{1}{2}\mu\text{m}$ waves.) But, if Alice checks out Bob's equipment as well as he did hers, then she could reply, “No Bob! You're the one that's 80% short of a full deck!”

So begins a physical lovers-quarrel made all the worse by the fact that *both* parties are *right*. This also questions a relativity assumption that a Lorentz contraction of an ethereal light wave would imply the same contraction of a solid steel laser cavity set to precisely hold that wave.

This hi-lights a main point of relativity: *All* things are wavelike as in *quantum* wavelike. The steel cavity obeys the same space-time rules as light itself while the standing wave in Alice's laser is behaving like a tiny mass making its own frame. Furthermore, both the tiny wave and its steel cavity must contract *together* to keep the laser in *resonance*. Waves are very particular about resonance.

As the GPS and LIGO projects have shown, quantum interference can be excruciating exercise in precision of timing. While Lorentz contraction (17a) involves the “skin” or *group-envelope* of a wave, the v_{phase} dilation effect embodied by (17b) involves the “guts” or *phase frequency* of a wave (and an old showman's adage, “*Timing is everything!*”) It has no famous name so let's call it the *Planck frequency dilation effect* since, as seen later, v_{phase} is the “heartbeat” of quantum matter that gives it its energy.

Einstein time dilation is one of the more poorly explained effects since it involves Bob reading a moving clock (Alice's in this case) located far down-track using co-observers (Bob's in this case) that have clocks co-moving and synced with Bob's. Imagine Alice's clock in Fig. 11b to be passing thru point **G'** at the instant Bob and observers occupy the horizontal dashed line where all their ct' clocks read $\frac{5}{4}=1.25$ in Alice's units. ($\tau_A = \frac{5}{3}$ femto seconds) That is a 25% dilation of 1.0 that Alice's clock will read at the right end of the dashed line. (Alice is crossing a **P'** line that is all $ct=1$.) So from that scenario her clocks appear 25% slower than Bob's. This is another lover's quarrel like that of the Lorentz effect.

Since that **P'** line Alice just crossed points back to Bob's time of ($ct' = \frac{4}{5} = 0.8$) she could claim to be even younger, 80% of Bob's age. Time and space reading by non-local observers is problematic due to another 1st-order time shift (besides Doppler). It is future-to-past shift due to slope of **P** and **G** lines. As Alice passes Bob his observers further to her left get to look farther into Alice's future while those further to her right can see farther into her past. This strange shift turns out to vary as $x \cdot \sinh\rho$.

The future-to-past time shift due to spatial position x is part of the famous²⁰ *Lorentz space-time* $(x, ct) \leftrightarrow (x', ct')$ transformation. First, the *relativity* $(c\kappa, v) \leftrightarrow (c\kappa', v')$ *per-space-time transformation* (not properly due to Lorentz but quite similar in form) follows from definitions (15a) and (15b) of Bob's phase vector \mathbf{P}' and group \mathbf{G}' vector in terms of Alice's vectors of phase \mathbf{P} and group \mathbf{G} .

$$\mathbf{P}' = \begin{pmatrix} v'_{phase} \\ c\kappa'_{phase} \end{pmatrix} = v_A \begin{pmatrix} \cosh \rho \\ \sinh \rho \end{pmatrix} = \begin{pmatrix} v_A \\ 0 \end{pmatrix} \cosh \rho + \begin{pmatrix} 0 \\ v_A \end{pmatrix} \sinh \rho = \mathbf{P} \cosh \rho + \mathbf{G} \sinh \rho \quad (18a)$$

$$\mathbf{G}' = \begin{pmatrix} v'_{group} \\ c\kappa'_{group} \end{pmatrix} = v_A \begin{pmatrix} \sinh \rho \\ \cosh \rho \end{pmatrix} = \begin{pmatrix} v_A \\ 0 \end{pmatrix} \sinh \rho + \begin{pmatrix} 0 \\ v_A \end{pmatrix} \cosh \rho = \mathbf{P} \sinh \rho + \mathbf{G} \cosh \rho \quad (18b)$$

This gives a matrix $(c\kappa', v') \leftarrow (c\kappa, v)$ *per-space-time transformation* and its inverse $(c\kappa, v) \leftarrow (c\kappa', v')$.

$$\begin{pmatrix} v' \\ c\kappa' \end{pmatrix} = \begin{pmatrix} \cosh \rho & +\sinh \rho \\ +\sinh \rho & \cosh \rho \end{pmatrix} \begin{pmatrix} v \\ c\kappa \end{pmatrix} \Rightarrow \begin{pmatrix} v \\ c\kappa \end{pmatrix} = \begin{pmatrix} \cosh \rho & -\sinh \rho \\ -\sinh \rho & \cosh \rho \end{pmatrix} \begin{pmatrix} v' \\ c\kappa' \end{pmatrix} \quad (19)$$

You may re-order c -scaled vectors: $(c\kappa, \omega) = 2\pi(c\kappa, v)$ transforms just like $(\omega, c\kappa) = 2\pi(v, c\kappa)$.

Bob's \mathbf{P}' vector lies on a phase hyperbola it shares with Alice's \mathbf{P} and similarly for \mathbf{G}' and \mathbf{G} .

$$\mathbf{P}\text{-hyperbola: } v^2 - c^2\kappa^2 = v'^2 - c^2\kappa'^2 = v_A^2 \quad (20a) \quad \mathbf{G}\text{-hyperbola: } c^2\kappa^2 - v^2 = c^2\kappa'^2 - v'^2 = c\kappa_A^2 \quad (20b)$$

These are hyperbolas first plotted in Fig. 2 and 3. They are invariant to Lorentz-like transformation (18).

Invariance of phase to Lorentz transformation

A laser phasor sketched in Fig. 4 should be taken seriously as a gauge of time (clock) and of space (metric ruler) for giving time (wave period τ) and distance (wavelength λ) in Fig. 11b. A reading of phase ϕ by Alice at a space-time point must equal reading ϕ' by Bob in spite of unequal readings (x, t) and (x', t') for that point and unequal readings (ω, k) and (ω', k') for a laser group-wave or its phase-wave. (Here angular $(c\kappa, \omega) = 2\pi(c\kappa, v)$ replace Kayser-Hertz $(c\kappa, v)$ to do phase calculations.)

$$\begin{aligned} \phi'_{phase} &\equiv k'_{phase}x' - \omega'_{phase}t' = k_{phase}x - \omega_{phase}t \equiv \phi_{phase} \\ \phi'_{group} &\equiv k'_{group}x' - \omega'_{group}t' = k_{group}x - \omega_{group}t \equiv \phi_{group} \end{aligned} \quad (21)$$

Bob's (ω', k') components are in (15) or (18). Alice's (ω, k) are the same with $\rho = 0$. This derives an Einstein-Lorentz Transformation (ELT) $(x, ct) \leftarrow (x', ct')$ of Bob's (x', ct') to Alice's (x, ct) .

$$\begin{aligned} \phi_{phase} &\equiv x' \frac{\omega_A}{c} \sinh \rho - t' \omega_A \cosh \rho = 0 \cdot x - \omega_A t \quad \Rightarrow \quad ct = ct' \cosh \rho - x' \sinh \rho \\ \phi_{group} &\equiv x' \frac{\omega_A}{c} \cosh \rho - t' \omega_A \sinh \rho = \frac{\omega_A}{c} x - 0 \cdot t \quad \Rightarrow \quad x = -ct' \sinh \rho + x' \cosh \rho \end{aligned}$$

ELT matrix and inverse resolve Bob-Alice space-time (Fig. 11b) and matches per-space-time form (19).

$$\begin{pmatrix} ct' \\ x' \end{pmatrix} = \begin{pmatrix} \cosh \rho & +\sinh \rho \\ +\sinh \rho & \cosh \rho \end{pmatrix} \begin{pmatrix} ct \\ x \end{pmatrix} \Rightarrow \begin{pmatrix} ct \\ x \end{pmatrix} = \begin{pmatrix} \cosh \rho & -\sinh \rho \\ -\sinh \rho & \cosh \rho \end{pmatrix} \begin{pmatrix} ct' \\ x' \end{pmatrix} \quad (22)$$

Quite similar invariant hyperbolas appear in space-time. A key space-time ρ -invariant is *proper time* τ .

$$(c\tau_A)^2 = (ct')^2 - (x')^2 = (ct'')^2 - (x'')^2 = \dots \quad (23a)$$

$$c\tau_A = ct' \sqrt{1 - \frac{(x')^2}{(ct')^2}} = ct' \sqrt{1 - \frac{u^2}{c^2}} \quad (23b)$$

Thales-Euclid means and geometry of hyperbolic invariants

A reverse analysis of the Alice, Bob, and Carla laser thought experiment is instructive. Imagine as before, that Bob detects counter-propagating laser beams of frequency ω_R going left-to-right (due to Alice's laser) and ω_L going right-to-left (due to Carla's laser). We ask two questions:

- (1.) To what velocity u_E must Bob accelerate so he sees beams with equal frequency ω_E ?
- (2.) What is that frequency ω_E ?

Query (1.) has a Jeopardy-style answer-by-question: What beam group velocity does Bob see?

$$u_E = V_{group} = \frac{\omega_{group}}{k_{group}} = \frac{\omega_R - \omega_L}{k_R - k_L} = c \frac{\omega_R - \omega_L}{\omega_R + \omega_L} \quad (24)$$

Query (2.) similarly: What ω_E is blue-shift $b\omega_L$ of ω_L and red-shift ω_R/b of ω_R ?

$$\omega_E = b\omega_L = \omega_R/b \Rightarrow b = \sqrt{\omega_R/\omega_L} \Rightarrow \omega_E = \sqrt{\omega_R \cdot \omega_L} \quad (25)$$

V_{group}/c is ratio of difference mean $\omega_{group} = \frac{\omega_R - \omega_L}{2}$ to arithmetic mean $\omega_{phase} = \frac{\omega_R + \omega_L}{2}$. Frequency $\omega_E = B$ is the geometric mean $\sqrt{\omega_R \cdot \omega_L}$ of left and right-moving frequencies defining the geometry in Fig.12 as detailed in Fig.12a. Line sum of $\omega_L = \omega_E e^{-\rho}$ and $\omega_R = \omega_E e^{+\rho}$ is bisected at center C of a circle connecting shifted phase vector \mathbf{P}' to its $\sqrt{\omega_R \cdot \omega_L}$ original \mathbf{P} .

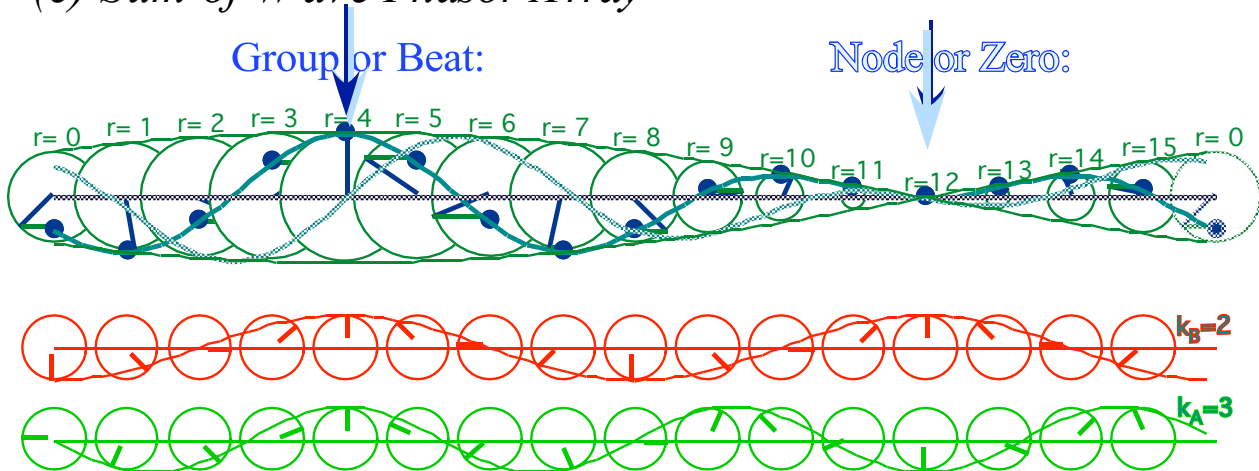
Original \mathbf{P} (Pitcher's mound) is the geometric mean point $\sqrt{1 \cdot 4} = 2$ at Alice's base frequency of $B = \nu_A = 600$ THz. (Fig.12 units are 300 THz.). That lets you construct points \mathbf{P}' , \mathbf{P}'' , \mathbf{P}''' ,... on a hyperbola that all frames will claim to also be their 600 THz invariant curve. Geometry begins by choosing to prick a \mathbf{C} -point ck' with compass needle. Then compass pencil is set to point- \mathbf{P} , and arc $\mathbf{P}\mathbf{P}'$ is drawn to the next hyperbola point $\omega'(k')$ on the new axis ck' . (Arc is optional if graph paper locates vertical $\mathbf{P}'\mathbf{C}$ line.)

Time-symmetry axiom ($e^{-\rho} e^{+\rho} = r \cdot b = 1$) implies phase points \mathbf{P}' , \mathbf{P}'' , \mathbf{P}''' ,... lie upon equilateral hyperbolas ($xy = const.$ or $\omega_R \cdot \omega_L = \omega_A^2$) whose $\pm 45^\circ$ asymptotes frame Doppler-shifted rectangles that all have the same area $2\omega_A^2$ of the initial ($\rho = 0$) baseball diamond in Fig.9d. Fig. 12b shows plots of upper branches for two (ω' , ck')-hyperbolas belonging to constants $\omega_A = 2$ and $\omega_A = 4$. This oblique $\pm 45^\circ$ view of the invariant hyperbolas emphasizes the Doppler shift ($r \cdot b = const.$) relations that are not immediately obvious from the usual straight Cartesian invariant equations such as (23).

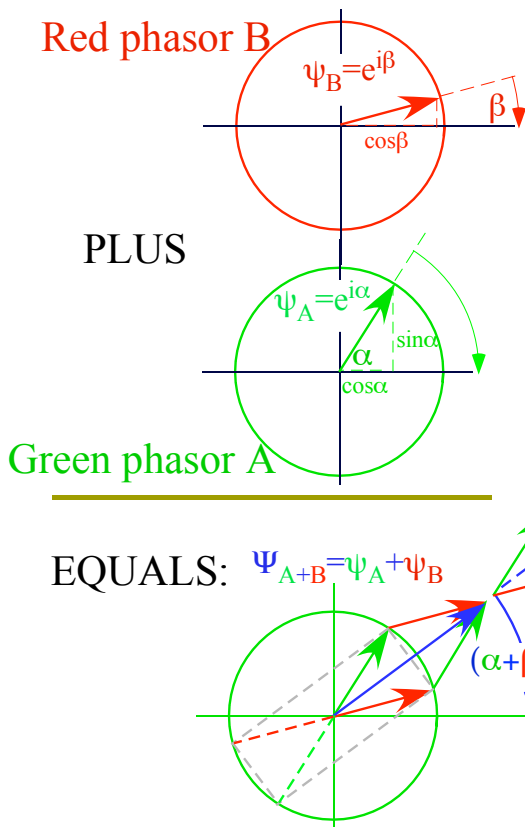
The geometry behind Fig. 12a or Fig. 12b is ancient and goes back to Thales of Miletus (*circa 600 BCE*) about three centuries before Euclid. Thales construction of means follows from his proof by symmetry that each point on a circle subtends a right (90°) angle which in turn is based on inscribed rectangles (dashed lines in Fig. 12). The same geometry applies to half-sum and half differences of phase angles involved in the wave interference sum sketched in Fig. 12c for each pair of phasors added in Fig. 12d. That is the geometry of factoring equations (12) and (13) giving Minkowski grids.

Adding waves ψ_A and ψ_B gives new and valid $\psi_{AB} = \psi_A + \psi_B$ solution to Maxwell wave equations due to linearity of differential equations. Then one may entertain a Galilean relativity of phase angular velocity ω as sketched in Fig. 12e, a *2nd-Galileo-revenge*, the *1st* being ρ -addition in Fig. 8, another argument of wave function exponentials. So Galilean addition of linear velocity fails so that we may trust it when adding lightwave phase angular velocity ω . Would we have it any other way?

(c) Sum of Wave Phasor Array



(d) Typical Phasor Sum:



(e) Phasor-relative views

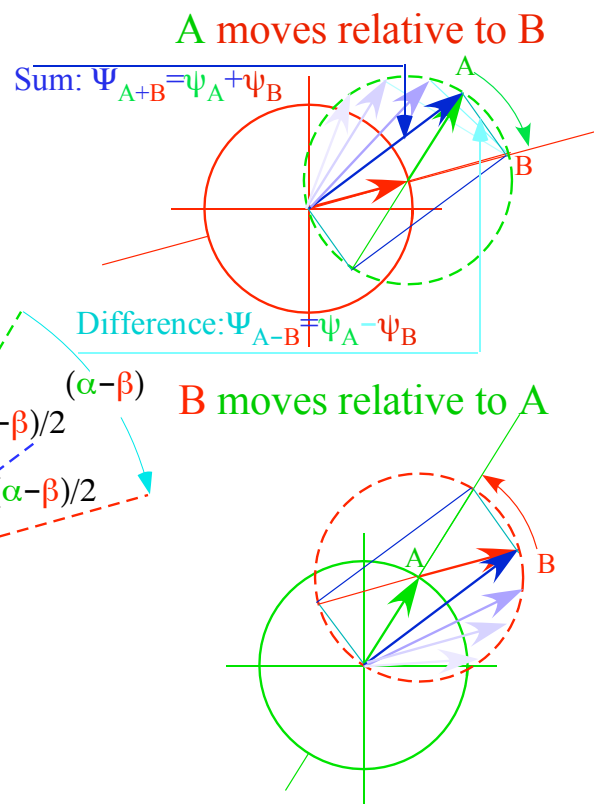


Fig. 12 (c) Sum $\psi_{AB} = \psi_A + \psi_B$. (d) Sum of individual phasors. (e) Phasor A moves relative to B and vice-versa.

PW Sums of multiple CW harmonics and Doppler effects

A sum of n -CW harmonics ($1v_A, 2v_A, 3v_A, 4v_A, \dots, nv_A$) traces a “baseball-diamond” lattice of PW (Pulse-Wave) paths in space-time as shown in Fig. 12g. Crests in CW plot of Fig. 9 are PW peaks at baseline intersections that surround a flat diamond area in Fig. 12g where a CW trough was in Fig. 9. Fig. 12i shows a Doppler shifted version of PW diamonds made into equal area rectangles framed by \mathbf{R}' and \mathbf{L}' paths drawn in Fig. 10 and Fig. 11a and sketched by dash-lines in Fig. 12i.

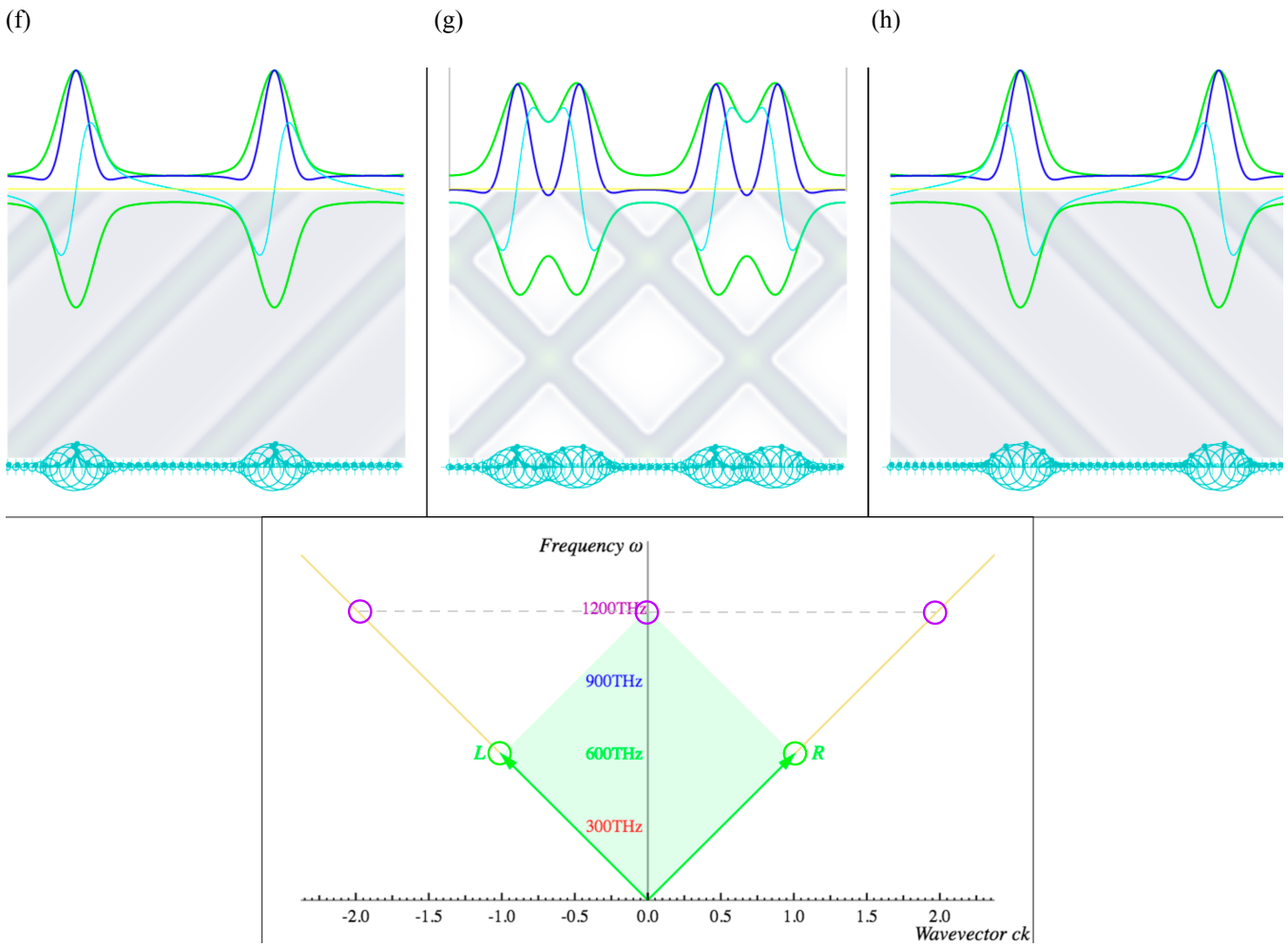


Fig. 12 (f) Right moving PW $k=2,4,6\dots$ (g) Sum of colliding $k=\pm 2, \pm 4, \pm 6, \dots$ PW. (h) Left-moving PW $k=-2,-4,-6\dots$

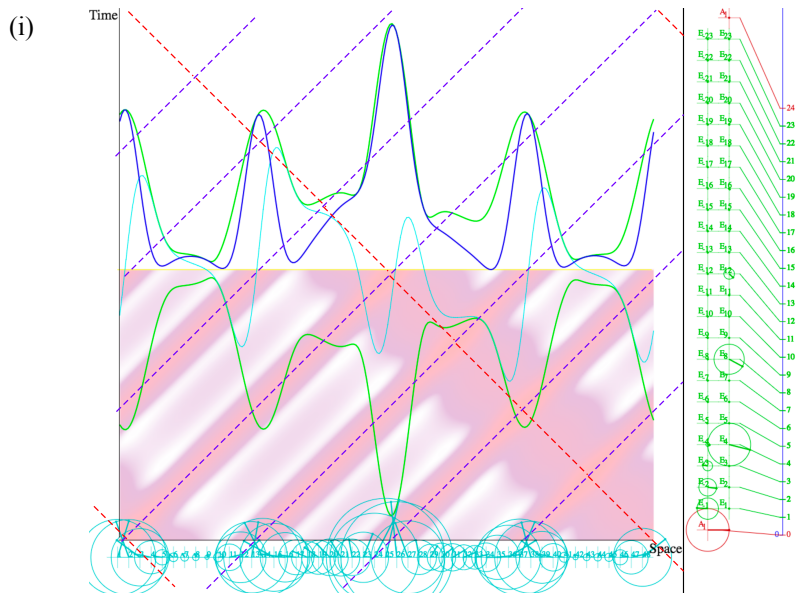


Fig. 12(i) Colliding PW of Fig. 12g as viewed in frame moving at $u=3c/5$.

5. Properties and applications of relativity geometry

The *relativity* quantities q in Table 1 are dimensionless ratios q_B/q_A including 1-CW Doppler shifts (*blue* $b=e^\rho$ and *red* $r=1/b$) and 2-CW phase or group wave-velocity $V_{group}=1/V_{phase}$, wavelength λ , wavenumber $\kappa=1/\lambda$, wave-period τ , or wave-frequency $\nu=1/\tau$, given for a frame moving at rapidity ρ_{AB} relative to a rest frame that starts with Alice's value q_A that Bob records as q_B . Ratios are also functions of the conventional velocity parameter $\beta=u/c$ where $u=V_{group}$ is relative group velocity u_{AB} .

Table 2 that follows this section includes the circular angle parameter σ that began the review of trigonometry. Here σ measures rotation of laser beams *transverse* to Bob's x -axis instead of *longitudinal* Doppler shift e^ρ he sees going parallel to a beam. This σ is the stellar aberration angle and is the key parameter in a novel space-proper-time approach to relativity pioneered by Lewis Epstein²¹. It is also useful as the wave \mathbf{k} -angle of Transverse-Electric (TE) waveguide and cavity modes.

Space-proper-time plots and the stellar-aberration angle

Lewis C. Epstein²² developed a novel approach to space-time relativity that uses the transverse stellar aberration angle σ to define relative velocity by $u = c \sin \sigma$ as sketched in Fig.13. This is in place of longitudinal Doppler definition $u = c \tanh \rho$ (16a) in terms of rapidity ρ as derived in (16a).

(a) Fixed observer sees star directly overhead

(b) Moving observer sees star shift angle σ in direction of \mathbf{u}

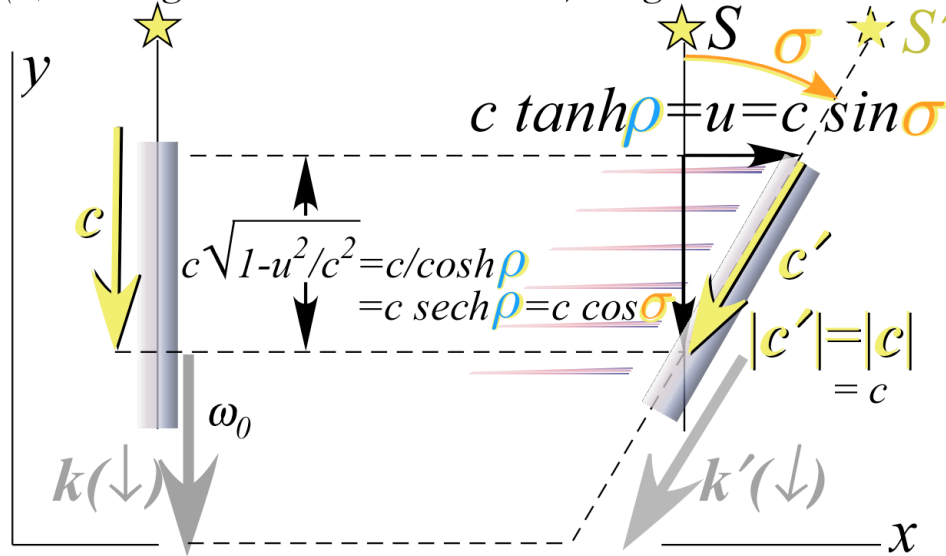


Fig. 13 Stellar aberration angle σ of light beam normal to direction of velocity \mathbf{u} .

This alternative to Minkowski- (x, ct) -plots involves flipping proper-time definition (23) as follows into a Cartesian Pythagorean relation.

$$(c\tau)^2 = (ct')^2 - (x')^2 \quad \Rightarrow \quad (c\tau)^2 + (x')^2 = (ct')^2 \quad (26)$$

A Pythagorean geometry for space-proper-time or $(x, c\tau)$ -plots is shown by Fig. 14. There it is imagined all things travel at light-speed c including a stationary object ($x' = 0$) that “moves” parallel to the $(c\tau)$ -axis. Moving object P is indicated by a vector (ct') that is inclined at aberration angle σ and also grows at rate c as given by (26) with $(x' = ut')$. Both the longitudinal parameter ρ for hyperbolic geometry and the transverse σ for circular geometry are useful and insightful. Applications to wave guide and cavity relativity and quantum wave mechanics follow a use of ρ and σ relations developed in Fig. 1 to Fig. 3. As group speed u becomes low ($u \ll c$) both ρ and σ converge on the old parameter $\beta = u/c$.

Applications that follow use a pattern-recognition aid labeled Occam'sSword in Fig.15(inset). It focuses mostly on geometry of $(\sin \rightleftharpoons \tan)$ and $(\cos \rightleftharpoons \sec)$ columns of Table 2. The $(\cot \rightleftharpoons \csc)$ intercepts are outliers for low to moderate u/c values. The sword has a staircase whose steps belong to a $(\cosh \rho)^n$ -geometric series: $(B \cosh \rho, B, B \sec \rho, \dots)$. Multiplying series by $\tanh \rho$ gives line $(|\mathbf{C}'\mathbf{P}'|=B \sinh \rho)$, then line $(|\mathbf{PB}|=B \tanh \rho)$, and lowest step $(|\mathbf{AB}'|=B \tanh \rho \operatorname{sech} \rho)$. Steps subtend a triple-cross- \mathbf{X} -point of tangents $\mathbf{C}'\mathbf{XS}$, \mathbf{AXP}' , and b -baseline \mathbf{PXB} . Extensions of the tangents have κ -axis $(\cot \rightleftharpoons \csc)$ -intercepts on either side of the sword in Fig.15. The sword's leading \mathbf{k} -edge defines wavevectors for waveguides and for free-electron lasers and this makes them easier to analyze and visualize. Compare Fig. 15 to Fig. 3.

TE-Waveguide geometry

Consider a sum of plane waves with wave-vectors $\mathbf{k}^{(+)}=(k \sin \sigma, +k \cos \sigma)=(k_x, k_y)$ pointing up in Fig. 16a and $\mathbf{k}^{(-)}=(k \sin \sigma, -k \cos \sigma)=(k_x, k_y)$ pointing down, each an angle $\pm \sigma$ relative to the y -axis in Fig 16.

$$E_z(\mathbf{r}, t) = e^{i(\mathbf{k}^{(+)} \cdot \mathbf{r} - \omega t)} + e^{i(\mathbf{k}^{(-)} \cdot \mathbf{r} - \omega t)} = e^{i(k_x x - \omega t)} [e^{ik_y y} + e^{-ik_y y}] \quad (27)$$

The result in xy -plane is a Transverse-Electric-(TE)-mode \mathbf{E} -field with plane-normal z -component E_z that vanishes on metallic floor and ceiling ($y = \pm Y/2$) of the waveguide.

$$E_z(\mathbf{r}, t) = e^{i(k_x \sin \sigma - \omega t)} 2 \cos(k_y \cos \sigma) \Big|_{y=\pm \frac{Y}{2}} = 0 \quad \text{implies: } k \frac{Y}{2} \cos \sigma = n \frac{\pi}{2} \quad (28)$$

Fig.16 shows two cases of lowest ($n = 1$) guide modes with Occam-sword geometry. Projection $Y \cos \sigma$ of floor-to-ceiling Y onto $\mathbf{k}^{(\pm)}$ -vectors is shown by right triangles at guide ends (28) to be $\frac{\pi}{k} = \frac{\lambda}{2}$, that is a half wave $\frac{\lambda}{2}$. Waveguide angle σ and dispersion function $v(\kappa)$ follows.

$$v = c\kappa = c \sqrt{\kappa_x^2 + \kappa_y^2} = c \sqrt{\kappa_x^2 + \kappa^2 \cos^2 \sigma} = \sqrt{c^2 \kappa_x^2 + \left(\frac{c}{2Y}\right)^2} = \sqrt{c^2 \kappa_x^2 + v_A^2} \quad (29)$$

Surprising insight into Fig.16 waves results if we note it is what Bob sees if Alice and Carla point their $v_A = 600\text{THz}$ 2-CW beam *across* Bob's x -line of motion at angle σ to y and not *along* x as in Fig. 9b. Bob can Doppler shift his wave-number κ_x and angle σ to zero and reduce frequency v in (29) to $v = v_A$.

Then Bob will be co-moving with Alice and Carla and see Alice's $\mathbf{k}^{(+)}$ -vector at zero aberration angle ($\sigma = 0$) if she is below Fig. 16 beaming straight up the y -axis. Meanwhile, Carla's $\mathbf{k}^{(-)}$ -vector points straight down. For ($\sigma = 0$) the wave given by (28) is a y -standing wave of wavelength $\lambda_A = 2Y$ between Alice and Carla and not just a half-wave section ($Y = \frac{\lambda}{2}$) modeling a lowest mode of this xy -wave guide.

Ideally Alice and Carla's laser mode viewed along y looks like their x -standing wave in Fig.9b or Fig. 10b and appears the same over its x -beam-width by having zero x -wave number ($\kappa_x = \kappa_A \sin \sigma = 0$). Zero- κ_x or infinite x -wavelength ($\lambda_x = \lambda_A \csc \sigma = \infty$) is a flat-line wave parallel to the x -axis oscillating at Alice's (or Carla's) 600THz frequency v_A .

This x -flat wave is better known in wave guide theory as a *cut-off-frequency* mode where the cut-off-frequency $v_{\text{CUTOFF}} = \frac{c}{2Y} = v_A$ is the lower bound to frequency that can enter a waveguide of width Y . In Fig. 16b it corresponds to dispersion function bottom point B (or \mathbf{P}) that is well separated from its phase point \mathbf{P}' in the upper right of the figure. That separation $|\mathbf{OC}| = B \sinh \rho = B \tanh \sigma$ gives a mode in Fig. 16a that is more robust than the near-cutoff mode in Fig. 16c having less $|\mathbf{OC}|$ and a more nearly vertical \mathbf{k} -vector in Fig.16c-d.

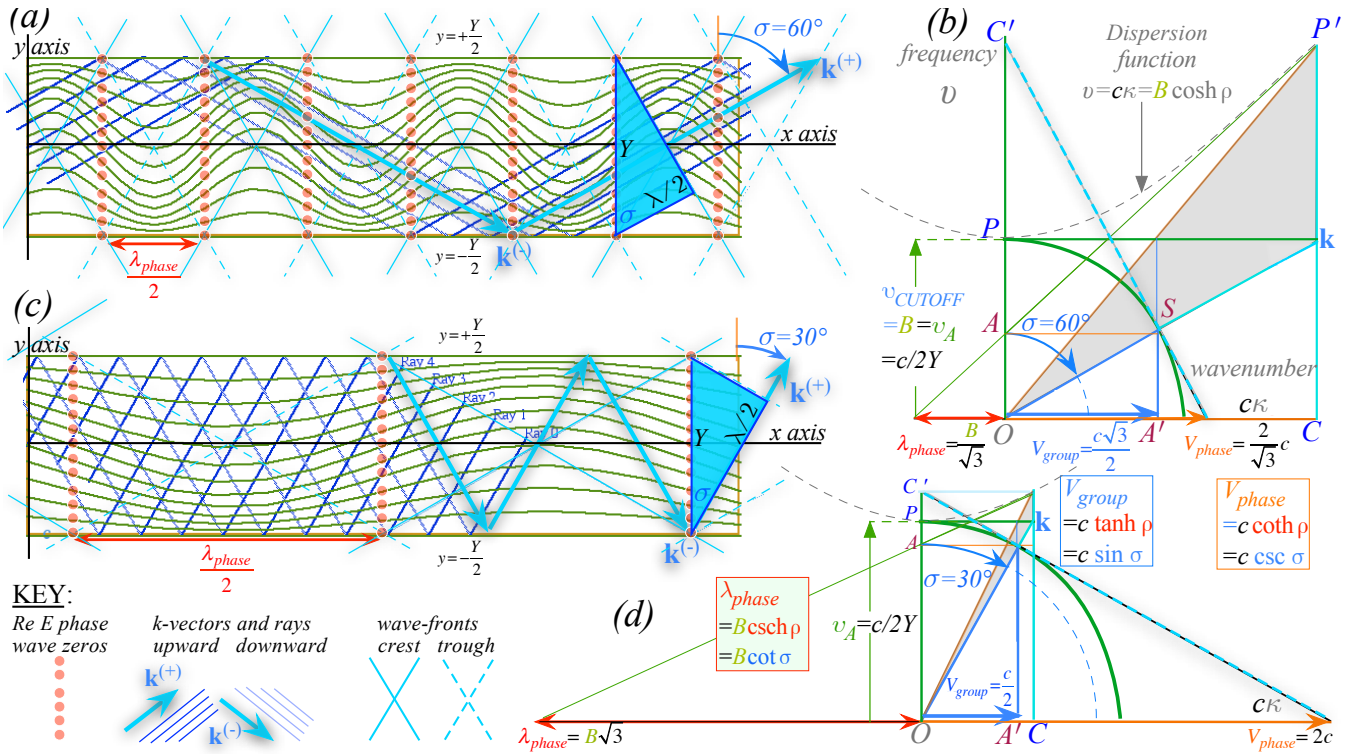


Fig. 16 TE-Waveguide and Occam sword geometry for stellar angle (a-b) $\sigma = 60^\circ$ and (c-d) $\sigma = 30^\circ$.

The $\tan\sigma$ -column of Table 2 represents the phase wave-number ratio κ_{phase}/κ_A of Bob's κ_{phase} to κ_A that Alice and Carla claim is their output. Later it is shown that $|\mathbf{OC}| = \kappa_x$ is mode wave *momentum* while vertical interval $|\mathbf{CP}'| = B \cosh \rho = B \sec \sigma = v_{phase}$ or phase frequency ratio v_{phase}/v_A in Table 2 correspond to mode carrier wave *energy*. These determine wave robustness and phase velocity V_{phase}/c is equal to their ratio $v_{phase}/\kappa_{phase} = \lambda_{phase}/\tau_{phase}$.

The importance of waveguide phase or carrier behavior is matched by that of group or signal wave dynamics. Each has six of twelve variables listed in Table 2. Matching phase velocity $V_{phase}/c = \coth \rho = \csc \sigma$ is reciprocal to $V_{group}/c = \tanh \rho = \sin \sigma$. Both are indicated by arrow lengths at the base of Occam Sword plots in Fig. 16b or Fig. 16d. The latter has V_{group} much lower than V_{phase} while the former has both closing in on light speed c .

Group velocity V_{group} equals projection $c \sin \sigma$ of $c \hat{\mathbf{k}}$ -vector onto the waveguide x -axis. One may imagine a signal bouncing off guide floor or ceiling riding on the \mathbf{k} -vectors normal to phase wavefronts moving at speed c along $\mathbf{k}^{(+)}$ or $\mathbf{k}^{(-)}$ in Fig. 16a or Fig. 16c. So a signal wastes time bouncing around the guide x -axis while the phase crests proceed via a greater speed $c \csc \sigma$. A signal may be imagined as an extra wrinkle in symmetry of identical wave crests due to lately added Fourier components limited by envelope group velocity as an established underlying phase maintains Evenson's c -lockstep. Per-space-time $(v, c\kappa_x)$ geometry of Fig. 16b or Fig. 16d rules that of space-space (x, y) in Fig. 16a or Fig. 16c.

Wave parameter variation with group velocity

As relative group velocity u/c or rapidity ρ grows, so do most of the eight wave-ratio variables listed in Table 2 with some approaching infinity while others approach zero. Fig. 17 shows a plot of those eight quantities versus group velocity ($u/c = V_{group}/c$) with their values for $u/c = 3/5$ appearing mid-plot in the order listed in Table 2.

There near $u/c = 3/5 = 0.6$, the function pair $\text{csch}\rho$ and $\text{cosh}\rho$ and pair $\text{sech}\rho$ and $\sinh\rho$ are close to their respective crossing points one above the other on the vertical line $u/c = G_-$ where the sub-unit Golden Mean is $G_- = \frac{\sqrt{5}-1}{2} = 0.618\dots$ is a root pair with $G_+ = \frac{\sqrt{5}+1}{2} = 1.618\dots$

The sech - \sinh pair cross at the Golden Root $\sqrt{G_-} = 0.7862\dots$ and csch - \cosh pair cross at inverse root $\sqrt{G_+} = 1/\sqrt{G_-} = 1.272\dots$ of G_+ . The $\text{csch}\rho$ and $\tanh\rho$ pair cross at plot point $(\frac{u}{c} = \sqrt{G_-}, y = \sqrt{G_-})$. The \sinh - coth pair cross at $(\frac{u}{c} = \sqrt{G_-}, y = \sqrt{G_+})$.

Between the ‘‘Golden’’ intersections are three more crossing points on the vertical line $\frac{u}{c} = x = \frac{1}{\sqrt{2}}$. They are sech - \tanh at $y = \frac{1}{\sqrt{2}}$, csch - \sinh at $y = 1$, and \cosh - coth at $y = \sqrt{2}$. Crossings correspond to a singular case of symmetry in a trigonometric map like Fig. 15.

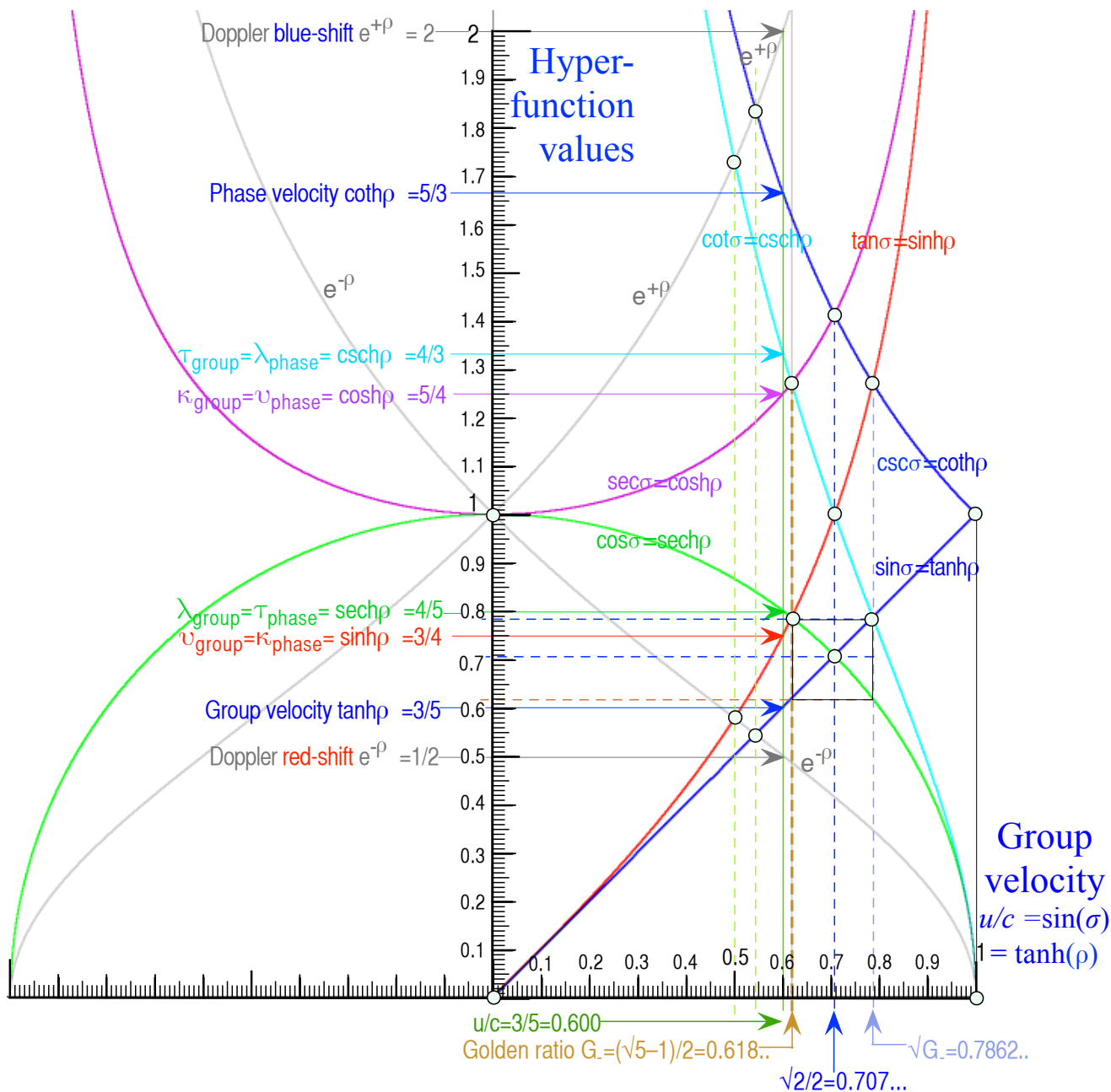


Fig. 17. Plot of Table 2 ratios values versus group velocity u/c . (List is labeled for $u/c = 3/5$.)

Table 2. Relativity ratios versus rapidity- ρ , guide angle- σ , and $\beta=u/c$

<i>group</i>	$b_{RED}^{Doppler}$	$\frac{V_{group}}{c}$	$\frac{v_{group}}{v_A}$	$\frac{\lambda_{group}}{\lambda_A}$	$\frac{\kappa_{group}}{\kappa_A}$	$\frac{\tau_{group}}{\tau_A}$	$\frac{c}{V_{group}}$	$b_{BLUE}^{Doppler}$
<i>phase</i>	$\frac{1}{b_{BLUE}^{Doppler}}$	$\frac{c}{V_{phase}}$	$\frac{\kappa_{phase}}{\kappa_A}$	$\frac{\tau_{phase}}{\tau_A}$	$\frac{v_{phase}}{v_A}$	$\frac{\lambda_{phase}}{\lambda_A}$	$\frac{V_{phase}}{c}$	$\frac{1}{b_{RED}^{Doppler}}$
<i>rapidity</i> ρ	$e^{-\rho}$	$\tanh \rho$	$\sinh \rho$	$\operatorname{sech} \rho$	$\cosh \rho$	$\operatorname{csch} \rho$	$\operatorname{coth} \rho$	$e^{+\rho}$
<i>stellar</i> ∇ <i>angle</i> σ	$1/e^{+\rho}$	$\sin \sigma$	$\tan \sigma$	$\cos \sigma$	$\sec \sigma$	$\cot \sigma$	$\csc \sigma$	$1/e^{-\rho}$
$\beta \equiv \frac{u}{c}$	$\sqrt{\frac{1-\beta}{1+\beta}}$	$\frac{\beta}{1}$	$\frac{1}{\sqrt{\beta^{-2}-1}}$	$\frac{\sqrt{1-\beta^2}}{1}$	$\frac{1}{\sqrt{1-\beta^2}}$	$\frac{\sqrt{\beta^{-2}-1}}{1}$	$\frac{1}{\beta}$	$\sqrt{\frac{1+\beta}{1-\beta}}$
<i>value for</i> $\beta=3/5$	$\frac{1}{2}=0.5$	$\frac{3}{5}=0.6$	$\frac{3}{4}=0.75$	$\frac{4}{5}=0.80$	$\frac{5}{4}=1.25$	$\frac{4}{3}=1.33$	$\frac{5}{3}=1.67$	$\frac{2}{1}=2.0$

6. Relativity gives basic wave mechanics of matter

Since the last century, fundamental developments of quantum mechanics have relied on concepts from advanced classical mechanics of Lagrange, Hamilton, Legendre, Jacobi, and Poincare that were developed mostly in the preceding (19th) century. The latter contain a formidable web of formalism using ecclesiastical terms such as *canonical* that once implied higher levels of truthiness, but for modern physics students, they mean not so much.

Below is a simpler approach that connects wave geometry of Sec.4 to 16th through 18th century mechanics of Galileo, Kepler, and Newton and then derives mechanics fundamentals for the 20th and 21st centuries. It also clarifies some 19th century concepts that are often explained poorly or not at all. This includes Legendre contact transformations, canonical momentum, Poincare invariant action, and Hamilton-Jacobi equations. Understanding of these difficult classical ideas and connections is helped by wave geometry or *relawavity*.

2-CW geometry of Fig. 15 has hyperbolic coordinates of phase frequency $v_{phase} = B \cosh \rho$ and c -scaled wave number $c\kappa_{phase} = B \sinh \rho$ with slope equal to group velocity $V_{group}/c = u/c = \tanh \rho$. Each depends on rapidity ρ that approaches u/c for Galilean-Newtonian speeds $u \ll c$.

$$\begin{aligned} v_{phase} &= B \cosh \rho \approx B + \frac{1}{2} B \rho^2 & (\text{for } u \ll c) \\ c\kappa_{phase} &= B \sinh \rho \approx B \rho & (\text{for } u \ll c) \\ u/c &= \tanh \rho \approx \rho & (\text{for } u \ll c) \end{aligned} \quad (30)$$

At these low speeds κ_{phase} and v_{phase} are functions of group velocity $u = c\rho$ or $u^2 = c^2\rho^2$. The hyperbolic base coefficient B has frequency units ($1\text{Hz} = 1\text{s}^{-1}$) of v_{phase} and $c\kappa_{phase}$ so B/c^2 multiplies u^2 and u .

$$v_{phase} \approx B + \frac{1}{2} [B/c^2] u^2 \quad \Leftarrow \text{for } (u \ll c) \Rightarrow \quad \kappa_{phase} \approx [B/c^2] u \quad (31)$$

From freshman physics is recalled kinetic energy $KE = \text{const.} + \frac{1}{2} Mu^2$ and Galilean momentum $p = Mu$. One *Joule-s* scale factor $h = Mc^2/B$ gives v_{phase} energy units and κ_{phase} momentum units. Then these wave coordinates give classical KE and p formulas. But, an annoying (and large) constant Mc^2 is added to KE !

$$h v_{phase} \approx Mc^2 + \frac{1}{2} Mu^2 \quad \Leftarrow \text{for } (u \ll c) \Rightarrow \quad h \kappa_{phase} \approx M u \quad (32)$$

One may ask, "Is this just a lucky coincidence?"

The answer involves the base or bottom value $B = v_A$ of Alice's frequency hyperbola. It is also Bob's bottom due to hyperbola invariance to ELT. The constant $\text{const.} = hB = h v_A = Mc^2$ may be the most famous formula in physics. Here it is Einstein's rest-mass-energy equation. It is an add-on to Newton's kinetic energy $\frac{1}{2} Mu^2$ that is perhaps the *second* most famous physics formula. This add-on does not contradict Newton's result. Physical effects depend only on *difference* or *change* of energy so any add-on constant (*const.*) has no observable effect. The question of false coincidence criticizes (32) for Galilean-Newtonian formulas valid only at low velocity ($u \ll c$) and low ρ . The approximate v_{phase} and κ_{phase} in (32) need to be replaced by Table 2 formulas $v_{phase} = B \cosh \rho$ and $c\kappa_{phase} = B \sinh \rho$ that hold for *all* ρ .

$$\begin{aligned} E = h v_{phase} &= Mc^2 \cosh \rho & \Leftarrow \text{for all } \rho \Rightarrow & p = h \kappa_{phase} = Mc \sinh \rho \\ &= \frac{Mc^2}{\sqrt{1 - u^2/c^2}} & \Leftarrow \text{for } |u| < c \Rightarrow & = \frac{Mu}{\sqrt{1 - u^2/c^2}} \end{aligned} \quad (33)$$

The old-fashioned $\beta=u/c$ form of $\cosh \rho$ (Table 2) is Einstein²³ 1905 total energy formula. Later in 1923, DeBroglie gives wave momentum formula²⁴ $p=\hbar k=h\kappa$ that has a $\beta=u/c$ form for $\sinh \rho$, too. Three lines above derive both ρ -forms from Table 2. This allows physics students to enjoy one-button-press calculator-recall as well as the geometric and algebraic elegance of relativity discussed below.

Underlying (33) is considerable physics and mystery of “scale factor” h (or $\hbar \equiv h/2\pi$) the Planck constant $h=6.62607 \cdot 10^{-34}$ Joule·sec that appears in his cavity energy axiom $E_N=hN\nu$. Thus (33) gives just the lowest quantum level ($N=1$) of Planck's axiom²⁵. (Modern form $E_N=\hbar N\omega$ has angular frequency $\omega=2\pi\nu$ and angular $\hbar=1.05 \cdot 10^{-34}$ Js.) A quick-fix replaces h with hN , but underlying quantum oscillator theory of electromagnetic cavity waves still needs to be discussed.

So far, the only axioms needed by SR results (33) are Evenson's (*All colors go c!*) and time reversal symmetry following Fig.7 and Fig. 8. These involve space, time, frequency and phase factors of plane light waves that are sufficient to develop the special relativity theory. But this phase approach has so far ignored amplitude factor A of light wave $\psi = Ae^{i(\mathbf{k}\cdot\mathbf{r}-\omega t)}$. While phase factor $e^{i(\mathbf{k}\cdot\mathbf{r}-\omega t)}$ describes the *quality* aspects of the light, an amplitude factor A describes the *quantity* of light, or more to the point, an average number N of *quanta* or *photons* in a wave having the N factor of Planck's axiom. Raising N raises overall phase frequency $N\nu_{phase}$ and in proportion, both total energy $hN\nu_{phase}$ and total wave *quantum-mass* $M_N=(hN\nu_{phase})/c^2$. (As seen below, this “light-weight” is tiny unless N is astronomical.)

The logical efficiency of optical axioms leading to (33) sheds some light on the three of the most logically opaque concepts of physics, namely energy, momentum and mass by expressing them as phase frequency ν (inverse time τ) and wavenumber κ (inverse length λ). Perhaps, the terms *energy* and *momentum* could someday go the way of *phlogiston!*

What is energy?

Once I asked a professor lecturing on energy, “What is *Energy?*” He replied, “It measures ability to do *Work.*” So, I asked, “What is *Work?*” He replied, “Well, it's Energy, of course!”

Probably, he would give the same circular logic if asked about *momentum*, another *sine qua non* of basic physics. A favorite flippant response to E and p questions is that momentum is the “*Bang*” and energy is the *\$Buck\$* that pays for it. ($\$1.00=10kWhr$ is close to national average.) This makes sense given an (unfortunate) U.S expression “Get more bang for your buck!” but only on the 4th of July.

Wave energy and momentum results (33) defeat such circular logic by showing how energy E is proportional to temporal frequency (ν_{phase} waves per second) and momentum p_α is proportional spatial frequency (κ_{phase} waves per meter in direction α). One should note the ratio of momentum p and energy E in (33) is $\frac{p}{E}=\frac{h\kappa}{h\nu}=\frac{\kappa}{\nu}$. It is a wave velocity relation for any scale-factor h (or hN).

The answer in (33) for wave energy inside Alice's laser cavity is a product of her quantum tick-rate $\nu_{phase}=\nu_A=600\text{THz}$, scale factor h (actually hN), and Einstein dilation factor $\cosh \rho$ that is $\cosh 0=1$ for her and $\cosh \rho=\frac{5}{4}$ for Bob in Fig.10b. Bob might complain about her $\frac{4}{5}$ -shortened wavelength $\lambda_{group}=(\frac{1}{2}\mu m)sech \rho=\frac{1}{2}\frac{4}{5}\mu m$ instead of complimenting her for $\frac{5}{4}$ more wave energy. (When you can't say something nice...) Bob may not see her considerable increase of momentum from zero ($\sinh 0=0$) to

$$p=hN\kappa_{phase}=hN\kappa_A \sinh \rho=hN\frac{\nu_A}{c}\frac{3}{4}.$$

He could be excused for overlooking such a tiny momentum. (p has a $\frac{1}{c}$ -factor that E lacks.)

$$E=hN\nu_A \cosh \rho=hN\nu_A \frac{5}{4}$$

A most remarkable thing about (energy, momentum) $\propto (\nu_{phase}, \kappa_{phase})$ relations (33) (now with hN in for h) and the Alice-Bob story is that (33) applies not just to Alice's light wave but also to its laser cavity frame. (Recall discussion after Fig.11.) In fact *any* mass M (including Alice and Bob themselves) is made of waves with an internal “heartbeat” frequency $\nu_{phase}=\frac{Mc^2}{Nh}$ that is *incredibly* fast due to the

c^2 -factor and tiny Planck- h divisor. Also, Alice's light wave with $v_{phase}=v_A$ has a mass $M_A=Nh\nu_A/c^2$ that is *incredibly* tiny here due to *both* a tiny Planck- h factor and enormous c^2 -divisor.

What's the matter with energy?

Evenson axioms of optical dispersion and time symmetry imply a 2-CW light geometry that leads directly to exact mass-energy-momentum and frequency relations (33) with low-speed approximations (32). A light wave with rest mass and rest energy proportional to a proper invariant phase frequency

$$v_{phase}=v_A=v'_A$$

is effectively a quantum matter wave that, due to its phase frequency, acquires intrinsic rest mass

$$M_{A_N} = Nh\nu_A/c^2.$$

In so doing, concepts of mass or matter lose classical permanence and become fungible. We define three types of mass M_{rest} , M_{mom} , and M_{eff} distinguished by their dependence on rapidity ρ or velocity u . The first is $M_{rest} = M_{A_N}$. The other two approach M_{rest} at low $u \ll c$.

Einstein rest mass M_{A_N} is invariant to ρ . It labels a hyperbola with a bottom base level B .

$$E_N(\rho=0) = hB = M_{A_N} c^2.$$

This label is respected by all observers including Alice and Bob. Each mode A of Alice's cavity has a stack of $N=1,2,3,\dots$ hyperbolas, one for each quantum number N -value.

$$\begin{aligned} E_N^2 &= (hN\nu_A)^2 = (M_{A_N} c^2)^2 \cosh^2 \rho = (M_{A_N} c^2)^2 (1 + \sinh^2 \rho) \\ &= (M_{A_N} c^2)^2 + (cp_N)^2 \end{aligned} \quad (34)$$

(E, cp) -space hyperbola $E = \sqrt{(Mc^2)^2 + (cp)^2}$ in Fig. 18 is a plot of an exact Einstein-Planck matter wave dispersion (33). The inset is a plot of approximation (31) for low p and $u \ll c$. Properties and pitfalls of this *Bohr²⁶-Schrodinger²⁷ approximation* to quantum theory are discussed later.

The second type of mass M_{mom} is *momentum-mass* defined by ratio p/u of relativistic momentum $p=Mc \sinh$ from (33) with group velocity $u=c \tanh \rho$. M_{mom} satisfies Galileo's very old quasi-definition $p=M_{mom} u$, but now using the newly defined relativistic wave quantities.

$$\begin{aligned} \frac{p}{u} &\equiv M_{mom} = \frac{M_{rest} c}{u} \sinh \rho = M_{rest} \cosh \rho \xrightarrow{u \rightarrow c} M_{rest} e^\rho / 2 \\ &= \frac{M_{rest}}{\sqrt{1 - u^2 / c^2}} \xrightarrow{u \ll c} M_{rest} \end{aligned} \quad (35)$$

The third type of mass M_{eff} is *effective-mass* defined by ratio dp/du of *change* of momentum $p=Mc \sinh \rho$ from (33) with *change* of group velocity $du=c \operatorname{sech}^2 \rho d\rho$. M_{eff} satisfies Newton's quite old definition $F=M_{eff} a$, but now using relativistic wave quantities.

$$\frac{F}{a} \equiv M_{eff} \equiv \frac{dp}{du} = \frac{dp}{d\rho} \bigg/ \frac{d\rho}{du} = M_{rest} c \cosh \rho / c \operatorname{sech}^2 \rho = M_{rest} \cosh^3 \rho \quad (36)$$

Another derivation of M_{eff} uses group velocity $V_{group} = \frac{d\nu}{d\kappa} = u$ as the independent variable.

$$\begin{aligned} \frac{F}{a} &\equiv M_{eff} \equiv \frac{dp}{du} = \frac{h d\kappa}{dV_{group}} = h \bigg/ \frac{d}{d\kappa} \frac{d\nu}{d\kappa} = h \bigg/ \frac{d^2\nu}{d\kappa^2} \\ &= M_{rest} \bigg/ (1 - u^2 / c^2)^{3/2} \xrightarrow{u \ll c} M_{rest} \end{aligned} \quad (37)$$

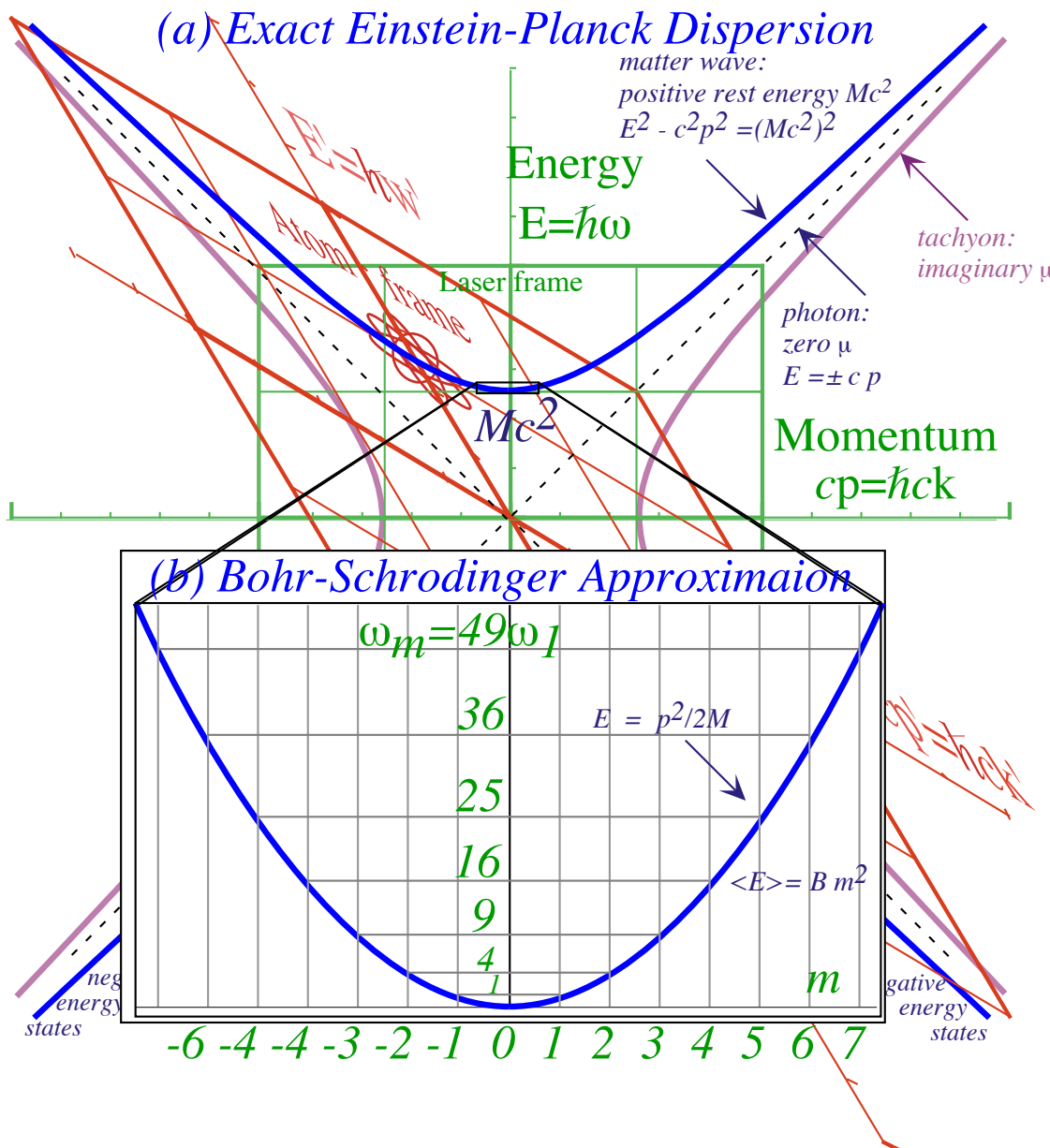


Fig. 18 (a) Einstein-Planck energy-momentum dispersion (b) Bohr-Schrodinger approximation

Group velocity and its tangent geometry is a crucial but hidden part of the matter wave theory. Physicists tend to commit to memory a derivative formula $\frac{dv}{dk} = \frac{d\omega}{dk}$ for group velocity and forget $\frac{\Delta v}{\Delta \kappa} = \frac{\Delta \omega}{\Delta k}$ that is a finite-difference formula from which the former is derived. This may give wrong results since the latter is *exact* for discrete frequency spectra while the former may be ill-defined. The wave Minkowski coordinate geometry starts with half-difference ratios to give V'_{group} in primary u -formulae (15) and (16).

$$V'_{group} / c = \frac{\Delta v}{c \Delta \kappa} = \frac{v_R - v_L}{v_R + v_L} = \frac{e^\rho - e^{-\rho}}{e^\rho + e^{-\rho}} = \tanh \rho \tag{38}$$

What follows in Fig. 10 through Fig. 12 and Fig. 15 is based entirely upon the more reliable finite-difference definition $\frac{\Delta v}{\Delta \kappa} = \frac{\Delta \omega}{\Delta k}$ that gives exactly desired slope.

Nevertheless, Nature is kind to derivative definition $\frac{dv}{dk} = \frac{d\omega}{dk}$ as seen in Fig.15. There hyperbolic tangent slope of line **RL** with altitude $\Delta v = v_R - v_L$ and base $\Delta \kappa = \kappa_R - \kappa_L$ has a finite-difference slope exactly equal to the derivative of the hyperbola at tangent point **P'** on phase velocity line **OP'**. Geometry

of Doppler action (38) is at play. That slope $\frac{dv}{d\kappa} = \frac{d\omega}{dk}$ equals $V'_{group} = u$ and is the velocity of Alice relative to Bob. It is also related to the momentum/energy ratio $\frac{p}{E} = \frac{c\kappa}{\omega} = \frac{u}{c}$ noted before.

$$V_{group} = u = \frac{\Delta v}{\Delta \kappa} = \frac{dv}{d\kappa} = \frac{d\omega}{dk} = \frac{dE}{dp} = \frac{c^2 p}{E} \quad (39)$$

As slope $\frac{dv}{d\kappa} = u$ of dispersion hyperbola $v(\kappa)$ affects velocity u and relations with momentum p , so does curvature $\frac{d^2v}{d\kappa^2}$ affect acceleration a and its relation to force F or momentum time rate of change $\frac{dp}{dt}$ in the effective-mass M_{eff} equations (36) and (37). One is inclined to regard M_{eff} as a quantum mechanical result since it is a product of Planck constant h with inverse $\frac{d^2v}{d\kappa^2}$, the approximate *Radius of Curvature* $RoC = 1/\frac{d^2v}{d\kappa^2}$ of dispersion function $v(\kappa)$. Geometry of a dispersion hyperbola $v = v_A \cosh \rho$ is such that its bottom ($\rho = 0 = u$) radius of curvature RoC equals the rest frequency $v_A = M_{rest} c^2 / h$ that is labeled as the *b-circle* radius B in Fig.15. Hyperbola curvature decreases as ρ increases, and so its RoC and M_{eff} grow according to (52) and (53) in proportion to exponential $e^{3\rho}$ as velocity u approaches c , three times faster than the e^ρ for high- ρ growth of momentum mass M_{mom} in (35).

How light is light?

Since 1-CW dispersion $v = \pm c\kappa$ is flat, its RoC and photon effective mass are infinite $M_{eff}^\gamma = \infty$. This is consistent with the Evenson's axiom prohibiting c -acceleration. (All colors *always* go c .) The other extreme is photon rest mass which is zero $M_{rest}^\gamma = 0$. Between these extremes, photon momentum-mass M_{mom}^γ depends on quality, that is, CW color or frequency v .

$$\begin{aligned} (a) \gamma - \text{rest mass: } M_{rest}^\gamma &= 0, \\ (b) \gamma - \text{momentum mass: } M_{mom}^\gamma &= \frac{p}{c} = \frac{h\kappa}{c} = \frac{h\nu}{c^2}, \\ (c) \gamma - \text{effective mass: } M_{eff}^\gamma &= \infty. \end{aligned} \quad (40)$$

Newton's *Optics* text is famous for his rejection of wave nature of light in favor of a corpuscular one. He described interference effects as light's 'fits.' Perhaps, light having three mass values in (39) would, for Newton, verify its schizophrenic insanity. Also, the fact that 2-CW 600THz cavity momentum \mathbf{p} must average to zero while each photon adds a tiny mass M_{mom}^γ , might support his corpuscular view.

$$M_{mom}^\gamma = \frac{h\nu}{c^2} = \nu(7.4 \cdot 10^{-51}) \text{kg} \cdot \text{s} = 4.4 \cdot 10^{-36} \text{kg} \quad (\text{for: } \nu=600\text{THz})$$

A 1-CW state has zero M_{rest}^γ , but ($N=1$)-photon momentum (33) is a non-zero quantity $p^\gamma = M_{mom}^\gamma c$.

$$p^\gamma = h\kappa = \frac{h\nu}{c} = \nu(2.2 \cdot 10^{-42}) \text{kg} \cdot \text{m} = 1.3 \cdot 10^{-27} \text{kg} \cdot \text{m} \cdot \text{s}^{-1} \quad (\text{for: } \nu=600\text{THz})$$

In the form $p^\gamma = M_{mom}^\gamma c$ Galileo's $p = MV$ is exact for light. It is another "Galilean Revenge" like the exact Galilean addition (Fig. 8) of rapidity ρ and of phase angular velocity ω (Fig. 9). Photons are light! With numbers so tiny it is a wonder subtle relativistic or quantum effects were ever noticed. That is so, unless the photon quantum number N is huge as in thermonuclear blast²⁸ or a star²⁹.

Then light can be many tons!

7. Relativity geometry of Hamiltonian and Lagrangian functions

The 2-CW matter-wave in Fig. 9 has a rest frame with origin $x'=0$ and $k'=0=k_{phase}$ where the invariant phase function $\Phi = kx - \omega t = k'x' - \omega't'$ reduces to $\Phi = 0 - \omega\tau$, a product of its proper or base frequency $B = \omega = Mc^2/\hbar$ defined after (32) with proper time $t' = \tau$ defined by (23). The (x, t) -differential of phase is reduced as well to a similar negative mass-frequency (ω)-term.

$$d\Phi = kdx - \omega dt = 0 \cdot 0 - \frac{Mc^2}{\hbar} d\tau \equiv -\omega d\tau \quad (41)$$

A proper-time interval $d\tau$ dilates to ρ -moving frame time interval dt by Einstein dilation relations.

$$dt = \frac{d\tau}{\sqrt{1-u^2/c^2}} = d\tau \cosh \rho \quad \Leftrightarrow \quad d\tau = dt \sqrt{1-u^2/c^2} = dt \operatorname{sech} \rho \quad (42)$$

One of the more interesting tales of modern physics is a first meeting³⁰ between Dirac³¹ and the younger Richard Feynman³². Both had been working on aspects of quantum phase and classical Lagrangian mechanics. Dirac mused about some formulas in one of his papers that showed similarities between a Lagrangian function and quantum phase. Feynman said abruptly, "That's because the Lagrangian *is* quantum phase!" That was a fairly radical bit of insight for the time. It needs its geometry clarified.

Phase, action, and Lagrangian functions

Feynman's observation needs some adjustment for units since Lagrangian L has *Joule* units of energy while phase Φ is a dimensionless invariant. A quantity S called *Action* is quantum phase Φ scaled by Planck's angular constant $\hbar = \frac{h}{2\pi} = 1.05 \cdot 10^{-34} \text{ J}\cdot\text{s}$ and is the following time integral of L .

$$S \equiv \hbar \Phi \equiv \int L dt \quad \text{where:} \quad \hbar \equiv \frac{h}{2\pi} = 1.05 \cdot 10^{-34} \text{ Joule}\cdot\text{Second} \quad (43)$$

Differentials of action and phase (40) with time (41) combine to re-express Ldt .

$$dS \equiv Ldt = \hbar d\Phi = -Mc^2 d\tau = -Mc^2 \sqrt{1-u^2/c^2} \cdot dt = -Mc^2 dt \operatorname{sech} \rho \quad (44)$$

From ρ -frame time derivative $dt/d\tau$ (40) arises the Lagrangian in terms of rapidity ρ or stellar angle σ .

$$L = -Mc^2 \sqrt{1-u^2/c^2} = -Mc^2 \operatorname{sech} \rho = -Mc^2 \cos \sigma \quad (45)$$

Table 2 supplies identity $\operatorname{sech} \rho = \cos \sigma$ for L in (44) and $\tanh \rho = \sin \sigma$ for group velocity u .

$$u \equiv V_{group} = c \tanh \rho = c \sin \sigma \quad (46)$$

A classical convention has Lagrangian L be explicit function of velocity. This is consistent with the low- $\rho \approx \frac{u}{c}$ approximation to Lagrangian (44) that recovers the Newtonian $KE = \frac{1}{2}Mu^2$ term in (32).

$$L = -Mc^2 \sqrt{1-u^2/c^2} \xrightarrow{u \ll c} -Mc^2 + \frac{1}{2}Mu^2 + \dots \quad (47)$$

A following discussion of explicit functionality for Hamiltonian $H(p)$ and Lagrangian $L(u)$ involves the geometry of Legendre contact transformation depicted in Fig. 19a-b below and a Fig. 20 that follows.

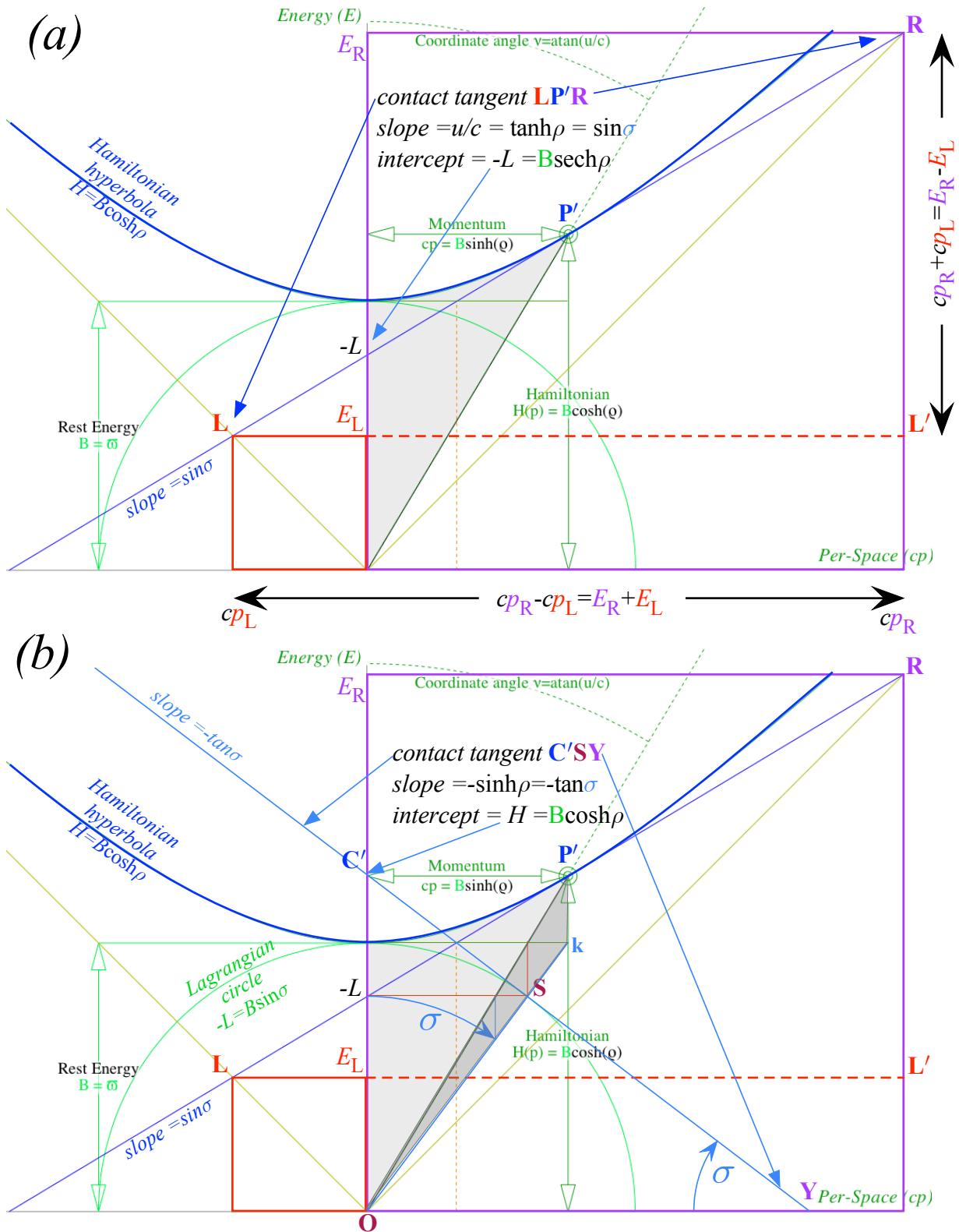


Fig. 19 (a) Slope u/c and intercept $-L$ of $H(p)$ -tangent LP' give (u, L) point S on $L(u)$ -circle.
 (b) Slope cp and intercept H of $L(u)$ -tangent $C'S$ give (p, H) point P' on $H(p)$ -hyperbola.

Hamiltonian functions, Poincare invariants, and Legendre contact transformation

The invariant phase differential (40) with an \hbar -factor as in (43) is a key relation.

$$dS \equiv Ldt \equiv \hbar d\Phi = \hbar k dx - \hbar \omega dt \quad (48)$$

Energy $E = \hbar \nu_{\text{phase}} = \hbar \omega = H$ and momentum $p = \hbar \kappa_{\text{phase}} = \hbar k$ from (33) for $N=1$ are used.

$$dS \equiv Ldt \equiv \hbar d\Phi = p dx - H dt \Rightarrow L = p \frac{dx}{dt} - H = p\dot{x} - H \quad (49)$$

Here energy E is identified with Hamiltonian function H . Results include the classical *Poincare differential invariant* $Ldt = p dx - H dt$ and the *Legendre transform* $L = pu - H$ between Lagrangian L and Hamiltonian H . Remarkably, it shows L/Mc^2 is the negative reciprocal of H/Mc^2 .

$$H = \hbar \omega = Mc^2 \cosh \rho = Mc^2 \sec \sigma = \frac{Mc^2}{\sqrt{1-u^2/c^2}} \quad (50a)$$

$$L = \hbar \dot{\Phi} = -Mc^2 \operatorname{sech} \rho = -Mc^2 \cos \sigma = -Mc^2 \sqrt{1-u^2/c^2} \quad (50b)$$

Except for a (-)sign, H and L are co-inverse (cos,sec)-cousin functions (mid-columns of Table 2). So are Einstein t -dilation and Lorentz x -contraction, respectively. H is explicit function of momentum p and L is explicit function of velocity u . So are u and p a 1st *cousin* (sin,tan) pair in Table 2.

$$cp = \hbar ck = Mc^2 \sinh \rho = Mc^2 \tan \sigma = \frac{Mc u}{\sqrt{1-u^2/c^2}} \quad (51a)$$

$$u \equiv V_{\text{group}} = c \tanh \rho = c \sin \sigma \quad (51b)$$

Legendre contact transformation $H(cp) = pu - L = cpu/c - L$ uses slope u/c and intercept $-L$ of tangent line **LR** contacting H -hyperbola in Fig. 19a to locate contact point $L(u)$ of Lagrangian plot. Inverse Legendre contact transformation $L(u) = pu - H$ uses slope p and intercept H of stellar tangent line **C'SY** contacting the L -circle in Fig. 19b to locate point $H(p)$ of Hamiltonian plot. This construction is further clarified by separate plots of $H(p)$ in Fig. 20a and $L(u)$ in Fig. 20b.

Tangent contact transformation is a concept based upon wave properties and goes back to the Huygens and Hamilton principles discussed below. The basics of this lie in construction of space-time (x, ct) wave-grids given frequency- \mathbf{k} -vectors $(\nu, c\kappa)$ like **P'** and **G'** in Fig. 10. Each **P'** or **G'** coordinate pair $(\nu, c\kappa)$ determines lines with speed ν/κ and t -intercept spacing $\tau = 1/\nu$ on ct -axis while x -intercept spacing is $\lambda = 1/\kappa$ on x -axis. These phase and group grid lines make Minkowski zero-line coordinates.

This geometry applies as well to energy-momentum $(E, cp) = \hbar(\nu, c\kappa) = \hbar(\omega, ck)$ spaces. Functional dependence of wave grid spacing and slopes determines classical variables, equations of motion, as well as functional *non*-dependence. For example, Lagrangian L is an explicit function of velocity u but *not* momentum p , that is, $\frac{\partial L}{\partial p} = 0$. Hamiltonian H is explicit function of momentum p but *not* velocity u , that is, $\frac{\partial H}{\partial u} = 0$. Such 0th-equations combined with $L = pu - H$ give 1st-Hamilton and 1st-Lagrange equations.

$$0 = \frac{\partial L}{\partial p} = \frac{\partial}{\partial p}(pu - H) \Rightarrow u = \frac{\partial H}{\partial p} \left(\begin{array}{l} \text{Hamilton's} \\ 1^{\text{st}} \text{ equation} \end{array} \right) \quad (52a)$$

$$0 = \frac{\partial H}{\partial u} = \frac{\partial}{\partial u}(pu - L) \Rightarrow p = \frac{\partial L}{\partial u} \left(\begin{array}{l} \text{Lagrange} \\ 1^{\text{st}} \text{ equation} \end{array} \right) \quad (52b)$$

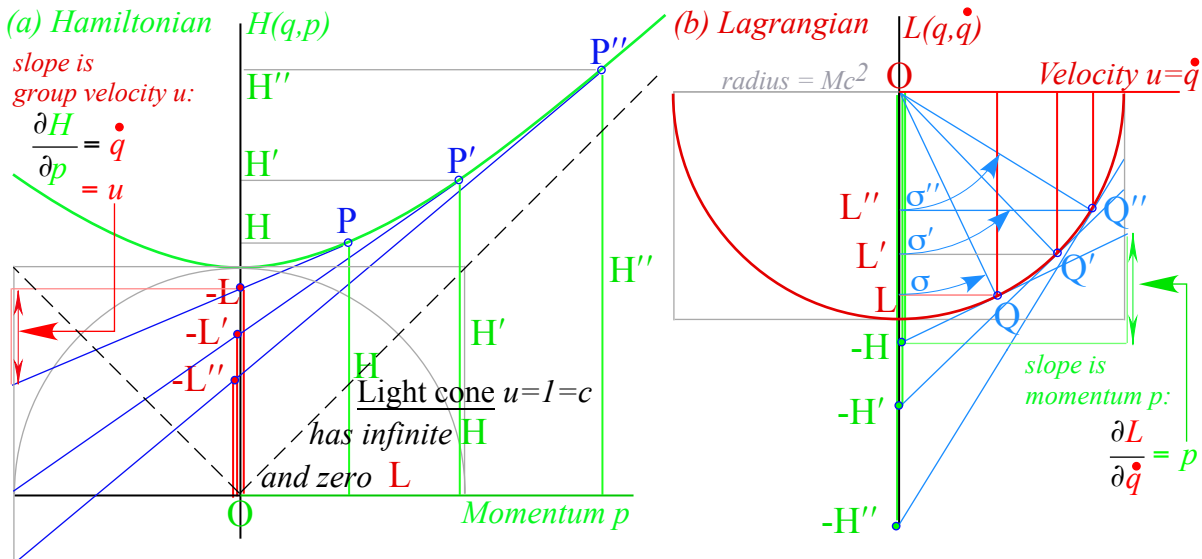


Fig. 20 Relativistic Legendre contact transformation between (a) Hamiltonian $H(p)$ (b) Lagrangian $L(u)$.

In Fig. 19a slope of $H(p)$ -hyperbola at tangent contact point P' is group velocity $u/c = \tanh \rho = \sin \sigma = 3/5$. In Fig. 19b slope of $-L(u)$ -circle at tangent point S is momentum $cp = B \sinh \rho = B \tan \sigma = (Mc^2)^{3/4}$ with a minus (-) sign. This minus sign in (49b) for Lagrangian $L = -Mc^2 \cos \sigma$, for example, is a result of (-) in basic phase $(kx - \omega t)$ and phasor conventions. (We like phasor clocks to turn clockwise (\curvearrowright), too.)

For a low- $(\rho \approx u/c)$ approximate Lagrangian (46), one may drop the $-Mc^2$ term and just keep the Newtonian kinetic energy term $(\frac{1}{2} Mu^2)$ that is equal to the corresponding kinetic term $(p^2/2M)$ in the approximate Hamiltonian. Of course, $p^2/2M$ reduces to $\frac{1}{2} Mu^2$ if approximate momentum $p = Mu$ is used, so students are well to ask, “Why are we so fussy about having only momentum p -dependence of H and only velocity u -dependence of L ?”

It is true that Hamiltonian $H(p)$ hyperbola minimum in Fig. 19 and Fig. 20a are nearly identical to the Lagrangian $L(u)$ circle minimum in Fig. 19b that lies below Fig. 20b. There both curves are nearly parabolic. But, at higher speeds the Lagrangian $L(u)$ approaches zero precipitously as stellar angle σ approaches $\pi/2$ and velocity u approaches c . Meanwhile, Hamiltonian $H(p) = B \cosh \rho$ and its momentum $p = B \sinh \rho$ each approach $Be^{\rho/2}$ as rapidity ρ grows without bound.

So it should be clear that hyperbolic “Country-cousin” functions involving rapidity ρ and momentum p must share a Hamiltonian with infinite horizon, while circular “City-cousin” functions of the very restricted stellar angle $-\pi < \sigma < \pi$ and velocity $-c < u < c$ must share a localized Lagrangian that is the keeper of quantum phase.

The third (csc, cot)-cousin pair $\lambda_{phase} = B \csc \rho = B \cot \sigma$ and $V_{phase} = B \coth \rho = B \csc \sigma$ from Table 2 do not appear in any discussions of classical correspondence. Instead, these describe the phase part or “quantum guts” of a 2-CW internal structure, and as such were nonexistent for 19-century classicists, and one might add, still today a bit sketchy and hard to observe. Now v_{phase} is seen as the “heartbeat” of quantum physics one may note DeBroglie wavelength λ_{phase} and velocity V_{phase} in Fig. 21 at the lower edges of geometric constructions just inside the Doppler blue shift ($b = e^{\rho}$)-bottom line of the **R** box.

One may compare Fig. 21 to Trigonometry Maps (TM) in Fig. 3. They share points $\mathbf{P} = \frac{1}{2} (\mathbf{R} + \mathbf{L})$ and $\mathbf{G} = \frac{1}{2} (\mathbf{R} - \mathbf{L})$. Fig. 3 exhibits fundamental and ancient geometry with triangular relations that have fundamental roles in Fig. 21 in describing a *relawavity* of relativistic quantum mechanics.

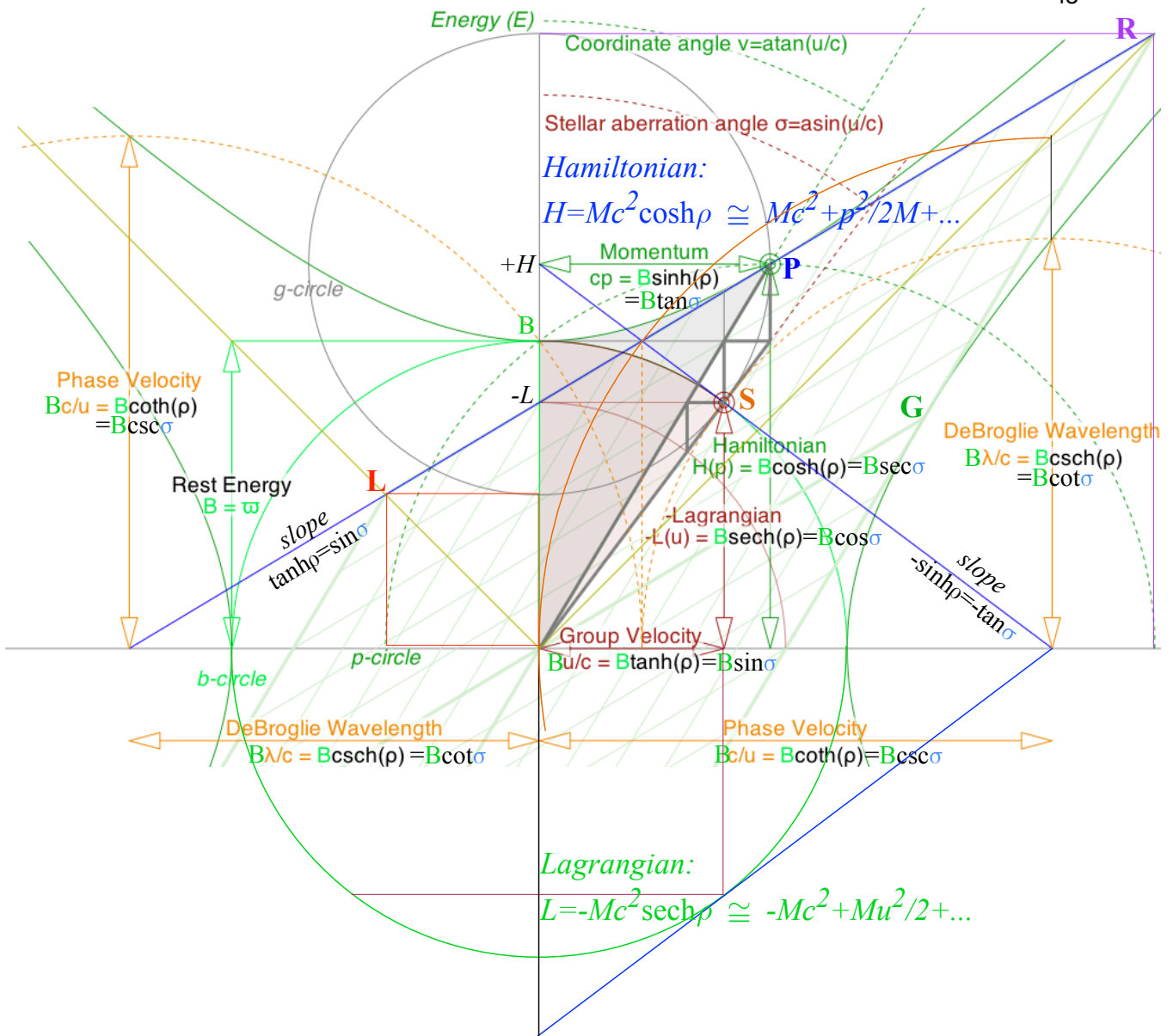


Fig. 21 Geometric elements of positive-energy relativistic quantum mechanics.

Hamilton-Jacobi quantization

Invariant phase Φ or action S differential (47) and (48) are integrable under certain conditions.

$$dS \equiv Ldt \equiv \hbar d\Phi = p dx - H dt = \hbar k dx - \hbar \omega dt \quad (53)$$

That is each coefficient of a differential term dq in dS must be a corresponding partial derivative $\frac{\partial S}{\partial q}$.

$$\frac{\partial S}{\partial x} = p, \quad \frac{\partial S}{\partial t} = -H. \quad (54)$$

These are known as *Hamilton-Jacobi equations* for the phase action function S . Classical *HJ-action* theory was intended to analyze families of trajectories (PW or particle paths). Dirac and Feynman related this to matter-wave mechanics (CW phase paths) by proposing approximate semi-classical wavefunction Ψ based on Lagrangian action $S = \hbar \Phi$ in its phase.

$$\Psi \approx e^{i\Phi} = e^{iS/\hbar} = e^{i \int L dt / \hbar} \quad (55)$$

Approximation symbol (\approx) indicates that phase but not amplitude is expected to vary here. The *HJ* form $\frac{\partial S}{\partial x} = p$ turns x -derivative of Ψ into standard quantum \mathbf{p} -operator form $\mathbf{p} = \frac{\hbar}{i} \frac{\partial}{\partial x}$.

$$\frac{\partial}{\partial x} \Psi \approx \frac{i}{\hbar} \frac{\partial S}{\partial x} e^{iS/\hbar} = \frac{i}{\hbar} p \Psi \quad \Rightarrow \quad \frac{\hbar}{i} \frac{\partial}{\partial x} \Psi = \mathbf{p} \Psi \quad (56a)$$

The *HJ* form $\frac{\partial S}{\partial t} = -H$ turns t -derivative of Ψ similarly into Hamiltonian operator $\mathbf{H} = \hbar i \frac{\partial}{\partial t}$.

$$\frac{\partial}{\partial t} \Psi \approx \frac{i}{\hbar} \frac{\partial S}{\partial t} e^{iS/\hbar} = -\frac{i}{\hbar} H \Psi \quad \Rightarrow \quad \hbar i \frac{\partial}{\partial t} \Psi = \mathbf{H} \Psi \quad (56b)$$

Action integral $S = \int L dt$ is to be minimized. Feynman's interpretation of this is depicted in Fig. 22.

Any mass M appears to fly so that its phase proper time τ is maximized. The proper mass-energy frequency $\varpi = Mc^2/\hbar$ is constant for a mass M . Minimizing $-\varpi\tau$ is thus the same as maximizing $+\tau$.

Clocks near light cone tick slowly compared ones near $\max\text{-}\tau$. Those on light cone do not tick!

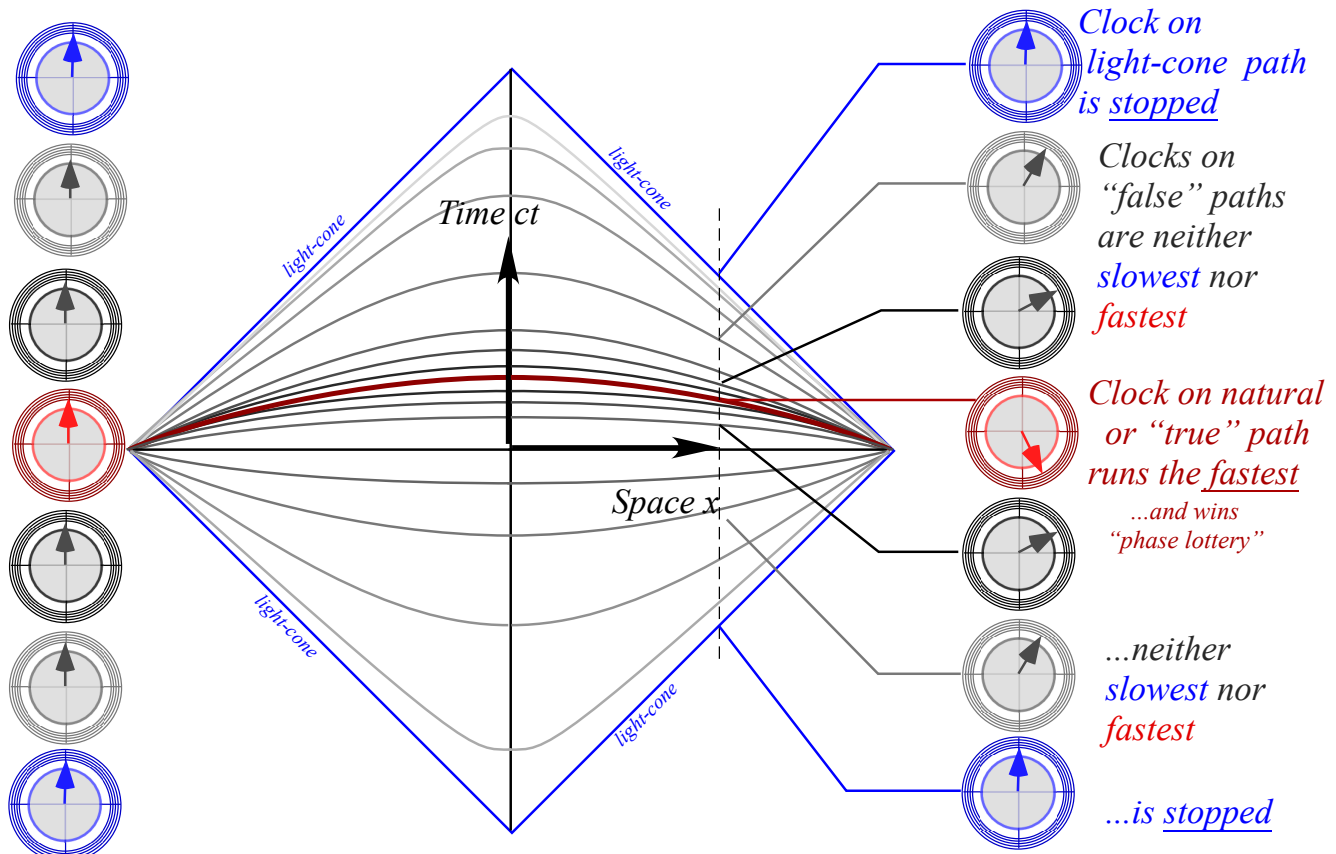


Fig. 22 Feynman's flying clock contest winner has the greatest advance of time.

One may explain how a flying mass finds and follows its $\max\text{-}\tau$ path by imagining it is first a wave that could spread Huygen's wavelets out over many paths. But, an interference of Huygen wavelets favors stationary and extreme phase. This quickly builds constructive interference in the stationary phase regions where the the fastest possible clock path lies. Nearby paths contain a continuum of non-extreme or non-stationary wavelet phase that interfere *destructively* to crush wave amplitude off the well-beaten $\max\text{-}\tau$ path as sketched in Fig. 23.

The very "best" are so-called stationary-phase rays that are extremes in phase and thereby satisfy Hamilton's Least-Action Principle requiring that $S = \int L dt$ is minimum for "true" classical trajectories.

This in turn enforces Poincare invariance by eliminating, by de-phasing, any “false” or non-classical paths because they do not have an invariant (and thereby stationary) phase. So “bad” rays” cancel each other in a cacophonous mish-mash of mismatched phases.

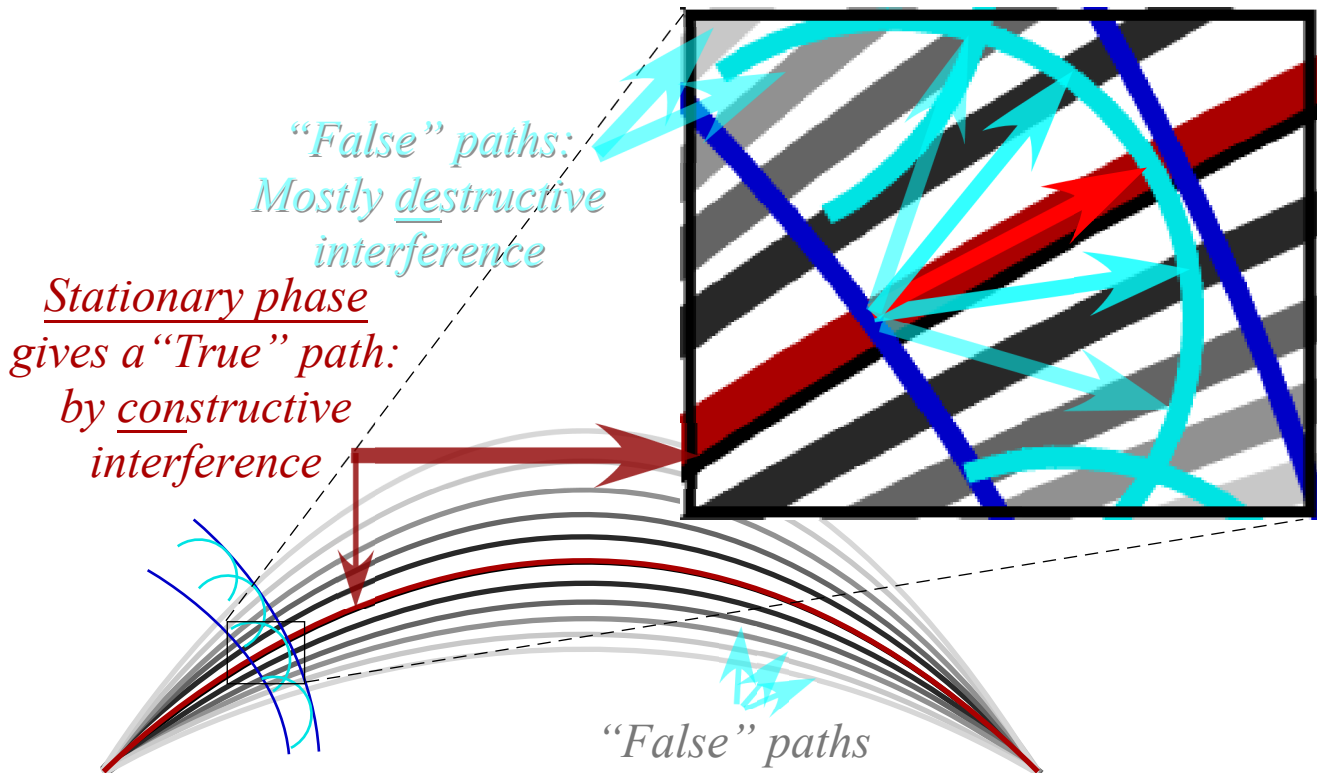


Fig. 23 Quantum waves interfere constructively on “True” path but mostly cancel elsewhere.

Each Huygen wavelet in Fig. 23 is tangent to the next wavefront being produced. That contact point is precisely on a ray or true classical trajectory path of minimum action and on the resulting “best” wavefront. Time evolution from any wavefront to the next is thus a contact transformation between two wavefronts described by this geometry of Huygens Principle.

Thus a Newtonian clockwork-world appears to be the perennial cosmic gambling-house winner in a kind of wave dynamical lottery on an underlying wave fabric. Einstein's God may not play dice³³, but some persistently wavelike entities seem to be gaming at enormous Mc^2/\hbar -rates down in the cellar! And in so doing, geometric order is created out of chaos.

It is ironic that Evenson and other metrologists have made the greatest advances of precision in human history, not with metal bars or ironclad classical mechanics, but by using the most ethereal and dicey stuff in the universe, light waves. This motivates a view of classical matter or particle mechanics that is more simply and elegantly done by its relation to light and its built-in relativity, resonance, and quantization that occurs when waves are subject to boundary conditions or otherwise confined. While Newton was grouching about “fits” of light, perhaps his crazy stuff was just trying to tell him something!

Derivation of quantum phenomena using a classical particle paradigm seems as silly now as deriving Newtonian results from an Aristotelian paradigm. It now seems much more likely that particles are made by waves, optical or otherwise, rather than vice versa as Newton believed. Also, CW trumps PW as CW axioms of Evenson (*All colors go c.*) and Doppler time-reversal ($r=1/b$) can easily derive Lorentz-Einstein-Minkowski algebra and geometry summarized in Table 2 and re-derive exact relations (33) for relativity and quantum wave mechanics using geometry summarized in Fig. 21.

8. Relativity geometry of quantum transitions

Preceding theory uses combinations of states $|N, \mathbf{k}_n, \omega\rangle$ or wavefunctions $\Psi_{N, \mathbf{k}, \omega} = A_N e^{i(\mathbf{k}\cdot\mathbf{r} - \omega t)}$ of an ideal optical cavity that are quantized by quantum mode numbers n for phase and photon numbers N for amplitude. This leads to geometry of elementary quantum transitions that involve change or transition of one such state into another. Such a discussion begins with symmetry and related conservation rules that restrict such transitions.

Symmetry and conservation principles

In Newtonian mechanics the first law or axiom is one of momentum conservation. Such physical axioms, by definition, have only experimental proof or justification. Logical proof or disproof is possible only if an older theory like classical mechanics becomes undermined by a more general theory like relativity or quantum mechanics having finer axioms. Then an older axiom might be proved using newer and more basic axioms, or else it might be disproved or reduced to an approximate or conditional result.

Patient teachers respect critically thinking students having doubt about the classical momentum conservation law. Indeed, How *does* Nature avoid losing even the tiniest bit of a momentum current however large it may be? This seems miraculous as does conservation of energy, though the latter is a classically provable result of the former given time reversal symmetry.

So it provides pedagogical relief to unite momentum and energy conservation rules in the wave nature of light seemingly shared by all matter. Newton's momentum axiom replaced by Evenson CW axiom gives Einsein-Planck-DeBroglie results (33) that match momentum \mathbf{p} to phase wavenumber vector $\boldsymbol{\kappa} = \mathbf{k}/2\pi$ scaled in h or Nh units while doing the same to energy E and phase frequency ν .

A rough statement of how CW axioms undermine or "prove" \mathbf{p} -or- E conservation axioms is that their conservation is required by wave coherence and so $\mathbf{p} = \hbar\boldsymbol{\kappa}$ and $E = \hbar\nu$ must be conserved, too. However, this oversimplifies deeper concepts of symmetry logic, a kind of "grown-up" geometry.

CW axioms are symmetry principles due to the Lorentz-Poincare isotropy of space-time. That invokes invariance to a translation $\mathbf{T}(\vec{\delta}, \tau)$ that has plane wave eigenfunctions $\psi_{k, \omega} = A e^{i(kx - \omega t)}$ and eigenstates $|\psi_{k, \omega}\rangle$ with roots-of-unity eigenvalues $e^{i(k\delta - \omega\tau)}$ as in the bra-ket relations below.

$$\mathbf{T}(\delta, \tau) |\psi_{k, \omega}\rangle = e^{i(k\delta - \omega\tau)} |\psi_{k, \omega}\rangle, \quad \langle \psi_{k, \omega} | \mathbf{T}^\dagger(\delta, \tau) = \langle \psi_{k, \omega} | e^{-i(k\delta - \omega\tau)}. \quad (57)$$

The relations apply also to N -factor (or " N -particle") states $\Psi_{K, \Omega} = \psi_{k_1, \omega_1} \psi_{k_2, \omega_2} \cdots \psi_{k_N, \omega_N}$ where exponents add (k_j, ω_j) -values of each constituent to a total \mathbf{K} -vector $K = k_1 + k_2 + \dots + k_N$ with a total frequency $\Omega = \omega_1 + \omega_2 + \dots + \omega_N$ to give the $\mathbf{T}(\vec{\delta}, \tau)$ -eigenvalue in exponential form $e^{i(K\delta - \Omega\tau)}$.

\mathbf{T} -symmetry requires quantum time evolution operator \mathbf{U} not be affected by \mathbf{T} movement. This means $\mathbf{U} = \mathbf{T}\mathbf{U}\mathbf{T}^\dagger$ and \mathbf{U} commute with \mathbf{T} ($\mathbf{U}\mathbf{T} = \mathbf{T}\mathbf{U}$ for any \mathbf{T}). So transition matrix $\langle \Psi_{K', \Omega'} | \mathbf{U} | \Psi_{K, \Omega} \rangle$ equals $\langle \Psi_{K', \Omega'} | \mathbf{T}\mathbf{U}\mathbf{T}^\dagger | \Psi_{K, \Omega} \rangle$, and relations (56) yield (K, Ω) conservation rules: $(K', \Omega') = (K, \Omega)$.

$$\begin{aligned} \langle \Psi_{K', \Omega'} | \mathbf{U} | \Psi_{K, \Omega} \rangle &= \langle \Psi_{K', \Omega'} | \mathbf{T}^\dagger(\delta, \tau) \mathbf{U} \mathbf{T}(\delta, \tau) | \Psi_{K, \Omega} \rangle \quad (\text{if } \mathbf{U}\mathbf{T} = \mathbf{T}\mathbf{U} \text{ for all } \delta \text{ and } \tau) \\ &= e^{-i(K'\delta - \Omega'\tau)} e^{i(K\delta - \Omega\tau)} \langle \Psi_{K', \Omega'} | \mathbf{U} | \Psi_{K, \Omega} \rangle = 0 \text{ unless } : K' = K \text{ and } : \Omega' = \Omega \end{aligned} \quad (58)$$

\mathbf{T} -symmetry implies total energy $E = \hbar\Omega$ and total momentum $\mathbf{P} = \hbar\mathbf{K}$ conservation for ideal CW states. However, laboratory CW have momentum uncertainty $\Delta k = l/\Delta x$ due to finite beam size Δx and energy uncertainty $\Delta E = \hbar\Delta\omega = \hbar/\Delta\tau$ due to finite lifetime $\Delta\tau$. Newton's 1st-law is verified only to the extent that lifetime or beam-width accommodates greater numbers of wavelengths or wave periods.

Single-photon transitions and Feynman diagram geometry

The geometric analysis of photon-affiliated transitions begins with the simple Doppler shifted or Lorentz transformed “baseball-diamond” geometry shown in Fig. 24. Most figures showing this geometry so far, including Fig. 15, Fig. 12 and the original Fig. 10, are drawn for velocity $u/c=3/5$ or Doppler shift $b=2$. Here, Fig. 24 uses odd values $b=3/2$ or $u/c=5/13$ to avoid distracting crossings found in Fig. 17 level plot. The Planck-Einstein-DeBroglie relation (33) is labeled by *energy* $E=\hbar\Omega$ plotted versus c -scaled momentum $cp=\hbar ck$ so that both have the same dimensions of energy.

Photon transitions obey rocket-science formula

Tiny photon momentum $p=\hbar k$ needs a c -factor to show up in plots. Also, Fig. 24 is bisected by a wavy right-angle $\mathbf{HP'K}$ inscribed in a g -circle that represents photon (ω, ck) -vectors connecting levels of high-state $|\omega_h\rangle$ at rest frequency $\omega_h=3$, middle-state $|\omega_m\rangle$ at $\omega_m=2$, and low-state $|\omega_\ell\rangle$ at $\omega_\ell=4/3$. Each frequency relates to one above it (or below it) by blue-shift factor $e^{+\rho}=3/2$ (or red-shift factor $e^{-\rho}=2/3$). Thus the middle frequency $\omega_m=2$ is the geometric mean $\omega_m=\sqrt{\omega_h\omega_\ell}$ of those above and below.

$$3=\omega_h=e^{+\rho}\omega_m \quad 2=\omega_m=e^{+\rho}\omega_\ell \quad \frac{4}{3}=\omega_\ell=e^{-\rho}\omega_m=e^{-2\rho}\omega_h \quad (59)$$

Wavy segment $\mathbf{HP'}$ represents a photon of energy $\hbar\Omega_{\mathbf{HP'}}=\hbar\omega_m \sinh\rho$ that would be emitted in a transition from a stationary mass $M_H=\hbar\omega_h/c^2$ at point \mathbf{H} to a mass $M_P=\hbar\omega_m/c^2$ moving with rapidity ρ at point $\mathbf{P'}$. Implicit in Fig. 24 is the choice of right-to-left direction for the outgoing photon momentum $cp=-\hbar\omega_m \sinh\rho$ recoiling left-to-right by just enough to conserve momentum as (57) requires. Mass M_H loses energy (frequency) equal to momentum (wavevector) of outgoing photon. Since M_H is initially stationary, it must lose energy by reducing rest-mass from M_H to M_P by Doppler shift ratio $e^{+\rho}$.

$$\frac{M_H}{M_P} = \frac{\omega_h}{\omega_m} = e^\rho \quad (60)$$

A rest mass formula results for recoil rapidity ρ with a simple low- ρ ($\rho \approx u/c$)-approximation.

$$\rho = \ln \frac{M_H}{M_P} \xrightarrow{\rho \rightarrow \frac{u}{c}} u = c \ln \frac{M_H}{M_P} \quad (61)$$

Interestingly, this quantum recoil formula is reminiscent of a famous rocket formula.

$$V_{\text{burnout}} = c_{\text{exhaust}} \ln \frac{M_{\text{initial}}}{M_{\text{final}}} \quad (62)$$

One might recall a popular expression, “This isn't rocket science!” Usual notions are that quantum transitions are infinite discrete “jumps” with emitted (or absorbed) photons acting like bullets. This appears wrong-headed in light of a more complete relativistic picture of an atom or nucleus in (60). It gradually exhales its mass like a rocket with an optical exhaust velocity of c .

One may also recall classical Lorentz resonance models of atomic transitions. Lorentz of ELT did non-relativistic theory to show atoms undergo over 10^5 oscillations during decay lifetimes of roughly 10^{-8} seconds, hardly ∞ -jumps. Nuclear transitions may involve much greater frequency and mass-energy phase velocity $\omega_h=M_H c^2/\hbar$, but an atomic transition with THz beats $\Delta_{hm}=\omega_h-\omega_m-\delta$ has a tiny recoil downshift δ due to the atom getting tiny photon recoil momentum. (Lorentz did not consider δ .) The exact δ in Fig. 24 is the height of point $\mathbf{P'}$ above ω_m -baseline, and $\hbar\delta$ is KE acquired by mid-mass M_P .

$$\delta = \omega_m \cosh\rho - \omega_m \approx \frac{\omega_m}{2} \rho^2 \Rightarrow KE_{\text{recoil}} \approx \frac{\hbar\omega_m}{2} \rho^2 \approx \frac{M_P}{2} u^2 \quad \text{with: } \rho \approx \frac{u}{c} \quad (63)$$

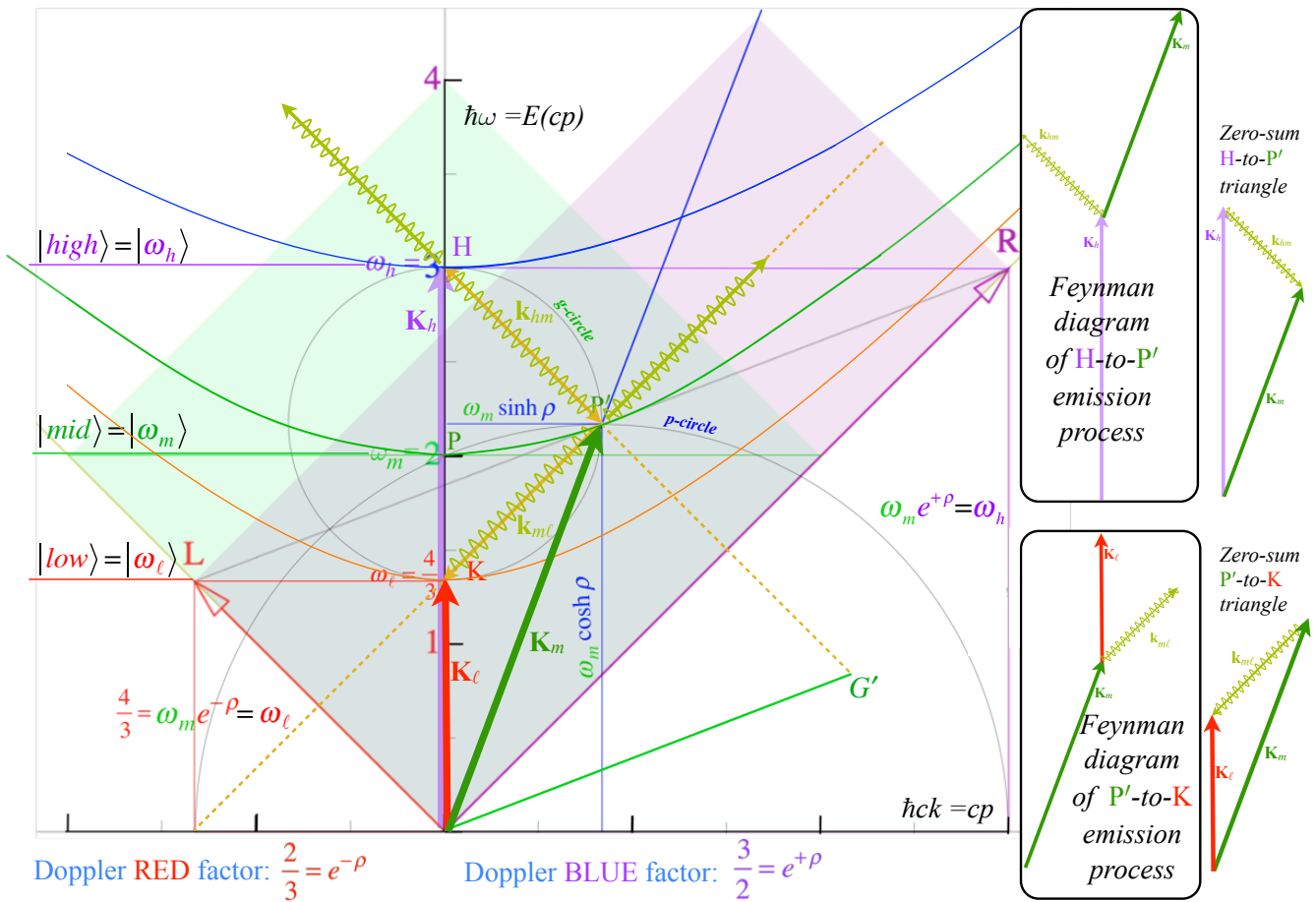


Fig. 25 Feynman diagrams of 1-photon transitions connecting 3-levels ω_h , ω_m , and ω_ℓ .

This labels a geometric sequence stack of hyperbolas shown in Fig.26. Meanwhile, rapidity $\rho = \ln \frac{3}{2}$ labeling velocity line- $(u/c=5/13)$ is boosted thru a sequence of ρ_p -values $\{\dots, -2\rho, -\rho, 0, 2\rho, 3\rho, \dots, p\rho, \dots\}$ and defines p -points of momentum $cp_{p,q} = b^q \omega_m \sinh \rho_p$ (where: $\rho_p = p \cdot \rho$) on each $b^q \omega_m$ -hyperbola.

The result is a lattice in Fig. 26 of transition points $P_{p,q} = (cp_{p,q}, E_q)$ that are scaling-and-Lorentz-boost-equivalent to the point $P = P_{0,0}$ at the center of Fig. 24 and Fig. 25 or else the point $P' = P_{1,0}$ that is the center of transitions in those figures. Choice of origin is quite arbitrary in a symmetry manifold defined by group operations. The $\pm 45^\circ$ -light-cone boundaries and their intersection $(cp, E) = (0, 0)$ lie outside of this open set of $P_{p,q}$ points. The choice of the base Doppler ratio $b = e^{+\rho}$ is also arbitrary and may be irrational. However, a rational b guarantees all 16 functions in Table.2 are also rational. The lattice in Fig. 26 may be viewed at $\pm 45^\circ$ as a quasi-Cartesian grid of lines. Each line is positioned according to rest-frequency power $\omega_m e^{q\rho}$ at its meeting point on the vertical ω -axis (or 2nd-base of a Doppler baseball diamond) as shown in Fig 27. The $+45^\circ$ R -axis (1st-baseline) is marked-off by sequence $\omega_R = \omega_m e^{R\rho}$ ($R = -2, -1, 0, 1, 2, \dots$) and the -45° L -axis (3rd-baseline) is marked-off by sequence $\omega_L = \omega_m e^{L\rho}$ ($L = -2, -1, 0, 1, 2, \dots$). (Here base constants $b = e^\rho = \frac{3}{2}$ and $\omega_m = 2$ are fixed.) At the intersections of R and L grid-lines are discrete transition (p, q) -points $P_{p,q}$.

$$P_{p,q} = (ck_{p,q}, \omega_{p,q}) = \omega_m e^{q\rho} (\sinh p\rho, \cosh p\rho) \quad (65)$$

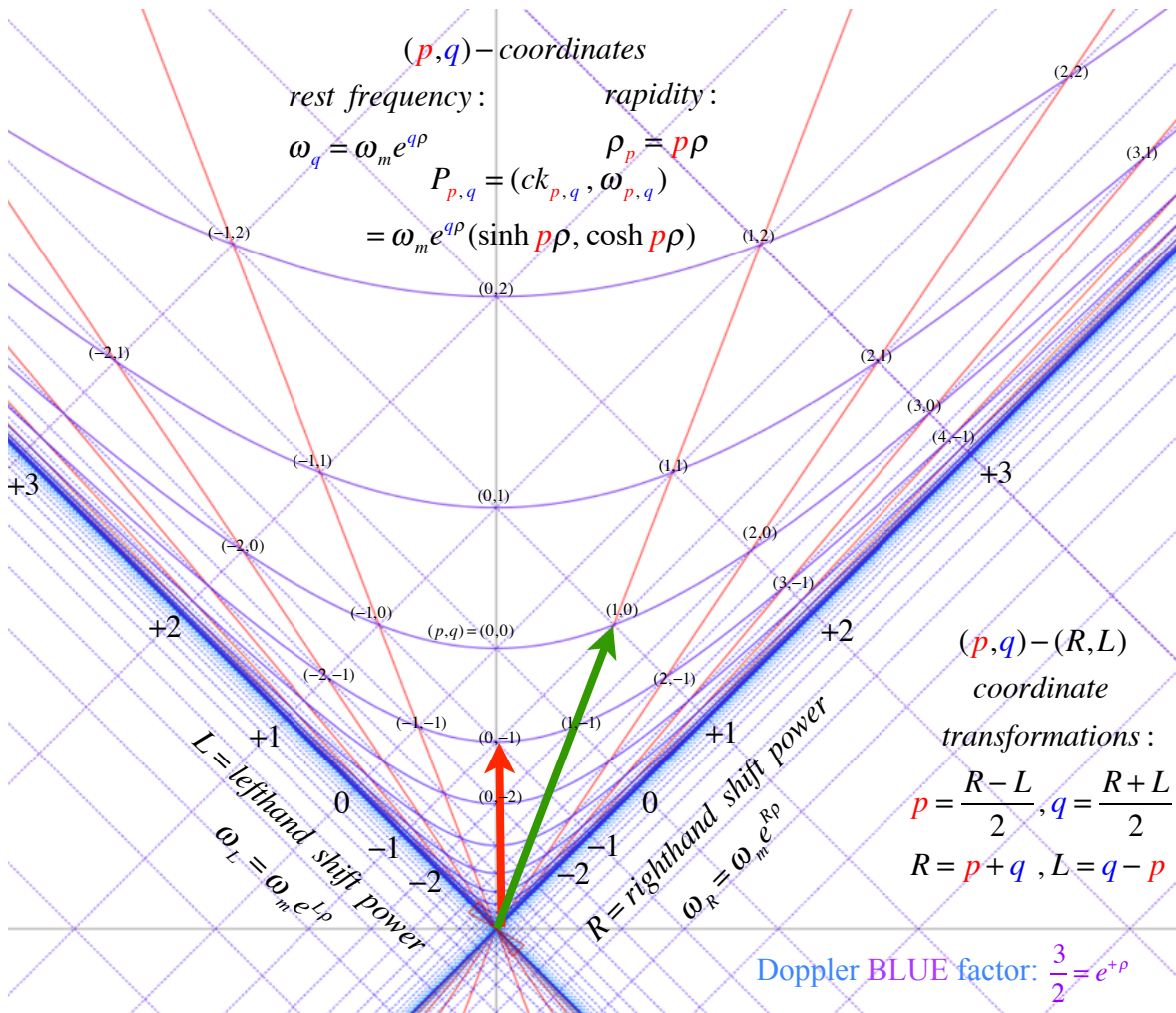


Fig. 27 Hyperbolic lattice of (p,q) -transition points for base $b=e^\rho=\frac{3}{2}$ and half-sum-difference coordinate relations.

9. Accelerated frames and optical Einstein-elevator

Fig. 9b and Fig. 10b show Lorentz-Minkowski space-time frames made by a 2-CW pair of lasers. Fig. 9b shows a Cartesian (x,ct) -grid made as Alice's and Carla's lasers collide 600THz beams. Fig. 10b shows Bob's view of Alice closing at $u/c=3/5$ with her laser beam Doppler blue-shifted by an octave factor $(B|A)=2=e^{+\rho}$ to 1200THz and Carla going away at $u/c=-3/5$ with her beam Doppler red-shifted by $(B|C)=1/2=e^{-\rho}$ to 300THz. If Bob attenuates Alice's beam E-field amplitude by 1/2 so its amplitude matches Carla's then he may see the Alice-Carla (x,ct) -grid in Fig. 9b form the Minkowski (x',ct') -grid shown in Fig. 10b.

Alice and Carla can provide Bob with the same $\rho=\ln 2=0.69$ grid without expending the energy needed to move their lasers to enormous speeds of $u/c=3/5$ relative to him. Instead they may be at rest in his frame and gradually tune up or up-chirp Alice's laser from $\nu_A=600\text{THz}$ to $e^{+\rho}\nu_A=1200\text{THz}$ while Carla is down-chirping from ν_A to $\nu_A e^{-\rho}=300\text{THz}$.

This opens the possibility of projecting accelerating frames for optical "Einstein elevators" with curving space-time coordinates that span a finite region between the lasers for a finite time interval. One may imagine Bob has a space ship that accelerates to a velocity $u=c \tanh \rho$ that Doppler shifts the Alice and Carla beams back to their initial green frequency $\nu_A=600\text{THz}$. (Or else, an excited atom b could be

imagined to be trapped in a single group-wave anti-node space-time cell so b accelerates with that cell while staying in resonance with the cell's constant phase frequency ν_A .)

The instantaneous velocity u of Bob (or the atom b) relative to Alice and Carla depends on their chirp factors $e^{\pm\rho}$ that vary with rapidity ρ . Bob can find his ρ relative to Alice if she broadcasts a fixed frequency ν_A that he sees at $\nu_B = \nu_A e^{-\rho}$. Rapidity is a function $\rho = \rho(\tau)$ of proper time τ for Bob (or atom b) and τ is related by (41) to time t for Alice or Carla.

$$u = \frac{dx}{dt} = c \tanh \rho \quad \text{where: } \frac{dt}{d\tau} = \cosh \rho \quad \text{and: } \frac{dx}{d\tau} = \frac{dx}{dt} \frac{dt}{d\tau} = c \tanh \rho \cosh \rho = c \sinh \rho \quad (67a)$$

Integrating the relations (66a) gives Bob's time-space path (ct, x) as seen by Alice or Carla.

$$ct = c \int \cosh \rho(\tau) d\tau \quad \text{and: } x = c \int \sinh \rho(\tau) d\tau \quad (67b)$$

The simple case with constant rapidity $\rho = \text{const.}$ gives a Minkowski τ -axis of slope $x/ct = \sinh \rho / \cosh \rho$.

$$ct = c\tau(\cosh \rho) \quad \text{and: } x = c\tau(\sinh \rho) \quad (67c)$$

This case is sketched in Fig. 28a as a tiny CW Minkowski frame at the intersection of paths of PW light waves from Alice and Carla. This repeats the situation described for Fig. 10.

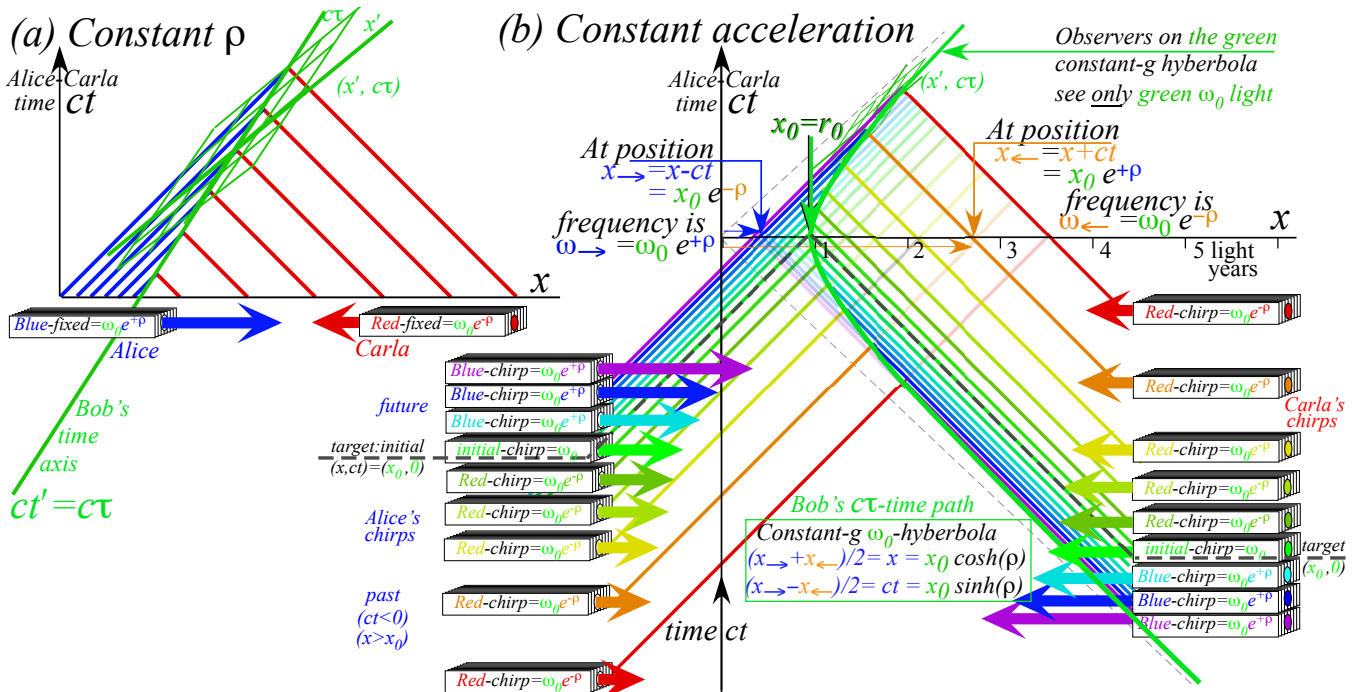


Fig. 28 Space-time laser-formed paths of constant g -acceleration (a) $g=0$, (b) $g=9.8m/s^2$

Fig. 28b path has constant acceleration $g=9.8m/s^2$ where rapidity is linear in Bob's proper time $c\rho = g\tau$.

$$ct = c \int \cosh \rho d\tau = \frac{c^2}{g} \sinh \left(\frac{g\tau}{c} \right) \quad (\text{for } u = \rho c = g\tau), \quad x = c \int \sinh \rho d\tau = \frac{c^2}{g} \cosh \left(\frac{g\tau}{c} \right) \quad (68)$$

Recall that low rapidity ($\rho \ll 1$) is approximated by u/c , and so setting $c\rho$ equal to $g\tau$ gives the classical uniform acceleration equation $u=g\tau$. The resulting space-time path shown in Fig. 28b is a hyperbola of radius $a=c^2/g$. That radius is enormous unless "gravity" g is also enormous. For terrestrial $g=9.8m/s^2=9.8$ the radius is $a=0.97LightYr$. However, a traveler with even this small $1g$ acceleration can, over several years, rack up considerable light-year mileage. One should recall both $\cosh \rho$ and $\sinh \rho$ contain e^ρ .

After the first year of $\tau_1=3.15 \cdot 10^7 \text{sec}$. the rapidity is $\rho_1=g\tau_1/c=1.03$ giving an x -coordinate of $x=a \cosh(g\tau_1/c)=1.53 \text{ LightYr}$ with a total mileage of $x-a=0.56 \text{ LightYr}$. But, after 21 years (the age of legality) x balloons to $x=a \cosh(21g\tau_1/c)=1.22 \cdot 10^9 \text{ LightYr}$! Now hyperbolic radius a is an insignificant part of a billion light-year journey. After 25 years (about the age of Einstein as he developed relativity theory) the mileage is 76 billion light-years, well beyond age-of-universe estimates in the frame of Alice. (Who, by then has long since passed away in the lab frame. Why *did* she have to stay at home?).

The geometric and exponential behavior of relativistic Doppler components dominates this example of space-time inflation and takes Alice-Bob sagas beyond any realm of possibility. Still it is instructive to explore such surprising thought experiments as far as possible and note the asymptotic extremes of scaling and curvature. Recall that rapidity ρ is defined in Fig. 2b as twice the area subtended by a unit hyperbola, its radius vector, and the horizontal axis. Half that is the area α shaded in Fig 29a.

$$\alpha(\rho_1)=\frac{x \cdot ct}{2}-\int_0^{x_1} ct dx =\frac{x \cdot ct}{2}-\int_0^{\rho_1} ct \cdot \frac{dx}{d\rho} d\rho =a^2 \frac{\cosh \rho_1 \sinh \rho_1}{2}-\int_0^{\rho_1} a \sinh^2 \rho d\rho =a^2 \rho_1 / 2 \quad (69)$$

Coordinates $x=a \cosh \rho$ and $ct=a \sinh \rho$ from (68) are used. (Circle area is $\alpha=r^2 \sigma / 2$.) Hyperbolic radius $r_0=a=c^2/g$ then gives c -scaled proper time $c\tau_1$ as a radius-rapidity product $a\rho_1$.

$$a\rho_1 = c\tau_1 \quad (70)$$

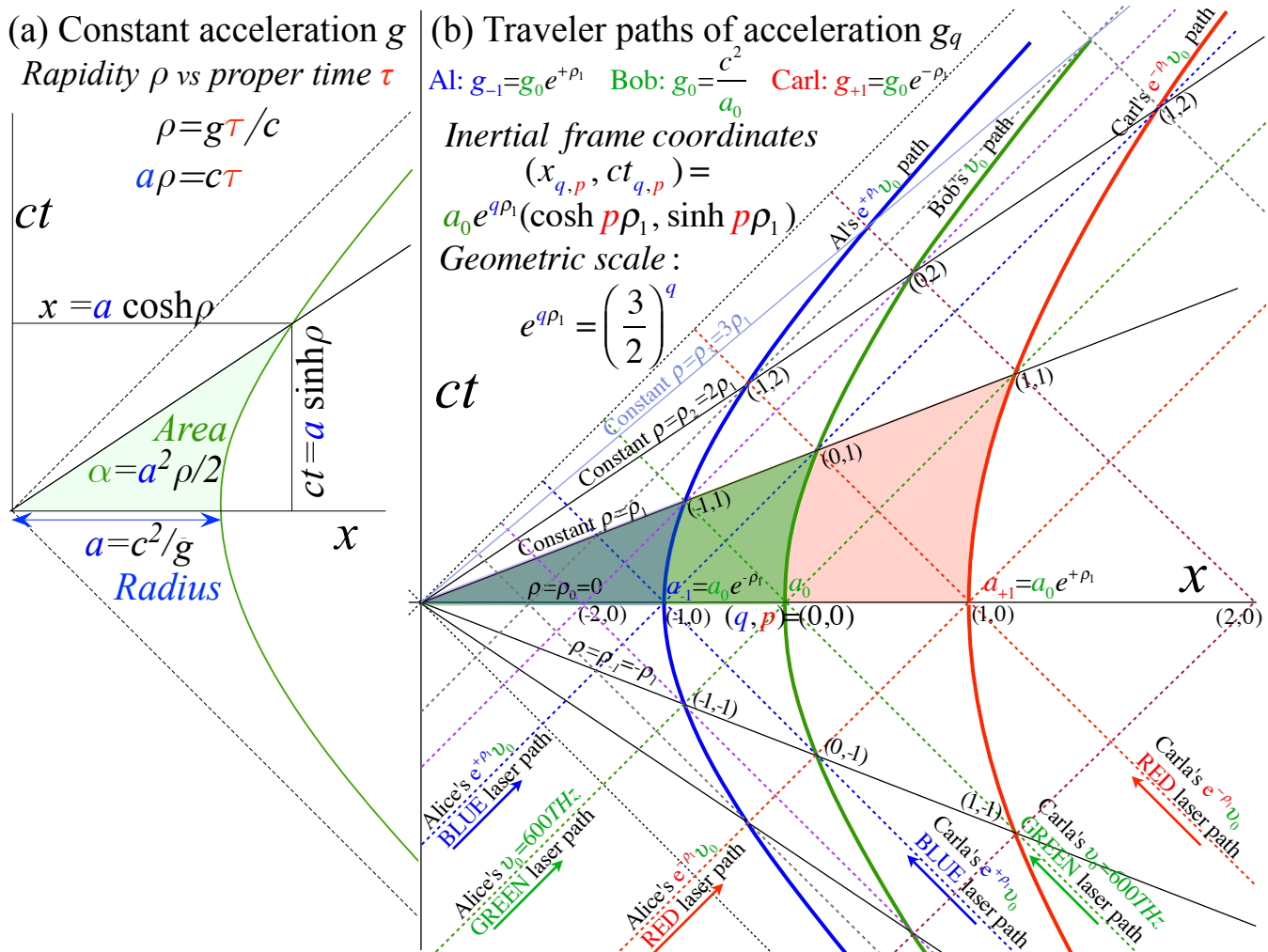


Fig. 29 (a) Constant- $g_q=c^2/a_q$ paths proper time vs area (b) $q_{Al}=-1, q_{Bob}=0, q_{Carl}=1$ vary $\rho_p=p\rho_1=p \ln(3/2)$ from $p=-1$ to 3.

Colliding Alice-versus-Carla laser beams in Fig. 28b are detailed in Fig.29b, a plot of an inertial space-time (x, ct) -frame with Alice and Carla sitting on left or right sides, respectively. Alice gradually up-tunes from infrared while Carla just as gradually down-tunes from ultra-violet. They start their beams over a year before and time their tuning so the central GREEN (lab frequency $\nu_0=600\text{THz}$) beam-pair meets at $t_0=0$ on the x -axis at $x_0=a_0$ where Bob is briefly stationary but accelerating right at his constant $g_0=c^2/a_0$. (See Fig. 29b. Tuning is gradual but only two other tuning paths are plotted and labeled.)

The right-hand RED (lab frequency $\nu_I=\nu_0 e^{-\rho_I}$) beam-pair meet at $t_0=0$ on the x -axis at the point $x_I=a_I=a_0 e^{+\rho_I}$ where Bob's companion Carl is also briefly stationary but accelerating right at $g_I=c^2/a_I$. The left-hand BLUE (lab frequency $\nu_{-I}=\nu_0 e^{+\rho_I}$) beam-pair meet at $t_0=0$ on the x -axis at the point $x_{-I}=a_{-I}=a_0 e^{-\rho_I}$ where Bob's companion Al is also briefly stationary but accelerating right at $g_{-I}=c^2/a_{-I}$.

Bob and his companions share a line of rising slope $x/ct=\coth\rho$ as they travel up their respective hyperbolic paths in Fig. 29b according to (67). All points on such a line share the same rapidity ρ and the same tangent slope $dx/dct=\tanh\rho$ or lab velocity u/c , and so Al, Bob, and Carl on the ρ_1 -line in Fig. 29b apply the same Doppler blue-shift factor $b_I=e^{+\rho_I}$ to light they meet head-on and the same red-shift factor $r_I=e^{-\rho_I}$ to light that catches them from behind. Thus Bob down-shifts Carla's blue beam from its lab BLUE frequency $\nu_{BLUE}=\nu_0 e^{+\rho_I}$ to his observed GREEN $\nu_0=600\text{THz}$ and up-shifts Carla's red beam from its lab RED frequency $\nu_{RED}=\nu_0 e^{-\rho_I}$ to the same base frequency $\nu_0=600\text{THz}$.

This is consistent with Alice and Carla's original plan for Bob on an optically accelerated "Einstein elevator" but now it includes two companions Al and Carl that travel in spatial lock-step beside Bob in Fig. 29b with Al maintaining a fixed distance $\Delta a_0=a_0-a_{-I}$ below Bob as Carl maintains a larger fixed distance $\Delta a_I=a_I-a_0=e^{+\rho_I} \Delta a_0$ above Bob (As plotted in their frames of equal rapidity ρ_1 .)

Meanwhile, the lab x -view in Fig. 29b clearly shows their relative spatial separations suffering Lorentz contraction. Each hyperbolic path is invariant so a boost in rapidity by $\Delta\rho$ moves any of its points of rapidity ρ_p to $\rho_p+\Delta\rho$ on the same hyperbola.

While Al, Bob, and Carl maintain initial spatial separations tallied by Alice and Carla at zero rapidity or velocity $\rho_0=0=u_0/c$, they do not maintain equal proper time- τ readings. According to (70) proper time $c\tau_{p,q}$ on hyperbola- q is a product of its radius $a_q=e^{q\rho_1} a_0$ with rapidity $\rho_p=p\rho_1$ for any given p -line shared by travelers $q=-I, 0$, and $+I$, namely, Al, Bob, and Carl.

$$c\tau_{q,p} = a_q \rho_p = a_0 e^{q\rho_1} p \rho_1 \quad \text{where: } q=-1(\text{Al}), 0(\text{Bob}), \text{ and } +1(\text{Carl}). \quad (71)$$

Hyperbolas of smaller radius a_q have proportionally slower local or proper time evolution and proportionally greater acceleration $g_q=c^2/a_q$ hence more curvature of hyperbolas closer to origin in Fig. 29. Indeed, each (q,p) -cell has the same number of wavelengths and wave-periods packed into a tighter space-time as the radius a_q is reduced.

The hyperbolic acceleration geometry of space-time in Fig. 29b has similar geometry (rotated by 90°) to that of Compton scattering in per-space-time of Fig. 27, but the physics is inverted. A boost of Bob ($q=0$) from ρ_0 to ρ_I ($p=0 \rightarrow I$) in Fig. 29b corresponds to a Compton transition of a rest-mass $q=0$ from ρ_0 to ρ_I in Fig. 27. Increased energy $E=h\nu$ and momentum $p=h\kappa$ on reciprocal (E, cp) lattice Fig. 27 is decreased wave length $\lambda=I/\kappa$ and wave period $\tau=I/\nu$ for space-time (x, ct) in Fig. 29. And vice-versa, a low-hyper-radius $a_q=c^2/g_q$ or high acceleration $g_q=c^2/a_q$ in Fig. 29 has high energy E (or frequency ν) and momentum p (or wavenumber κ) in Fig.27.

This mythical odyssey of intrepid accelerating voyagers (Al, Bob, and Carl) depends on optical metrology provided by a pair of laser-chirping Sirens (Alice and Carla) stationed for years at the left and right edges of Fig. 28b and Fig. 29b. While Carla leisurely de-tunes her right-to-left beam, Alice tries to meet an impossible up-tuning schedule of her left-to-right beam, planned to end with an exponential chirp and explosion of infinite frequency at $ct=0$. Her $ct_0=-a_0$ emission of frequency $\nu_0=600\text{THz}$ hits Bob at $x=a_0$, one of a geometric sequence of frequencies $\nu_q/\nu_0=e^{\rho_1}, e^{2\rho_1}, e^{3\rho_1}, \dots, e^{q\rho_1}$ emitted at times $ct_q=-e^{-\rho_1}, -e^{-2\rho_1}, -e^{-3\rho_1}, \dots, -e^{-q\rho_1} \rightarrow 0$ to hit a point $x_q = a_0 e^{-q\rho_1}$ at $ct=0$. (The geometric ratio in Fig. 29b is $e^{\rho_1}=3/2$ and arbitrarily chosen to provide a lattice in the (x, ct) -continuum.)

No light emitted by Alice after $t=0$ can reach Al, Bob, Carl or any fellow traveler- q maintaining enough acceleration to stay under hyperbolic asymptote or “event-horizon” $x=ct$ in Fig. 29b. Carla, the right-to-left half of this 2-CW metrology, hits the same q -points $x_q = a_0 e^{-q\rho_1}$ on the $ct=0$ -line (x -axis) with the same frequencies $\nu_q = \nu_0 e^{q\rho_1}$ that Alice sent to each traveler- (q) . She can continue hitting Carl (traveler $q=1$) at (q,p) -points $(1,1)$ and $(1,2)$ with beams that later hit Bob (traveler $q=0$) at (q,p) -points $(0,1)$, $(0,2)$ and $(0,3)$ and Al (traveler $q=-1$) at (q,p) -points $(-1,2)$, $(-1,3)$ and $(-1,4)$. However, Carl passes Carla soon thereafter (upper right hand corner of Fig. 29b) and so also will Bob followed by Al. Thus laser coordination by either Siren, Alice or Carla, is quite restricted in its coverage.

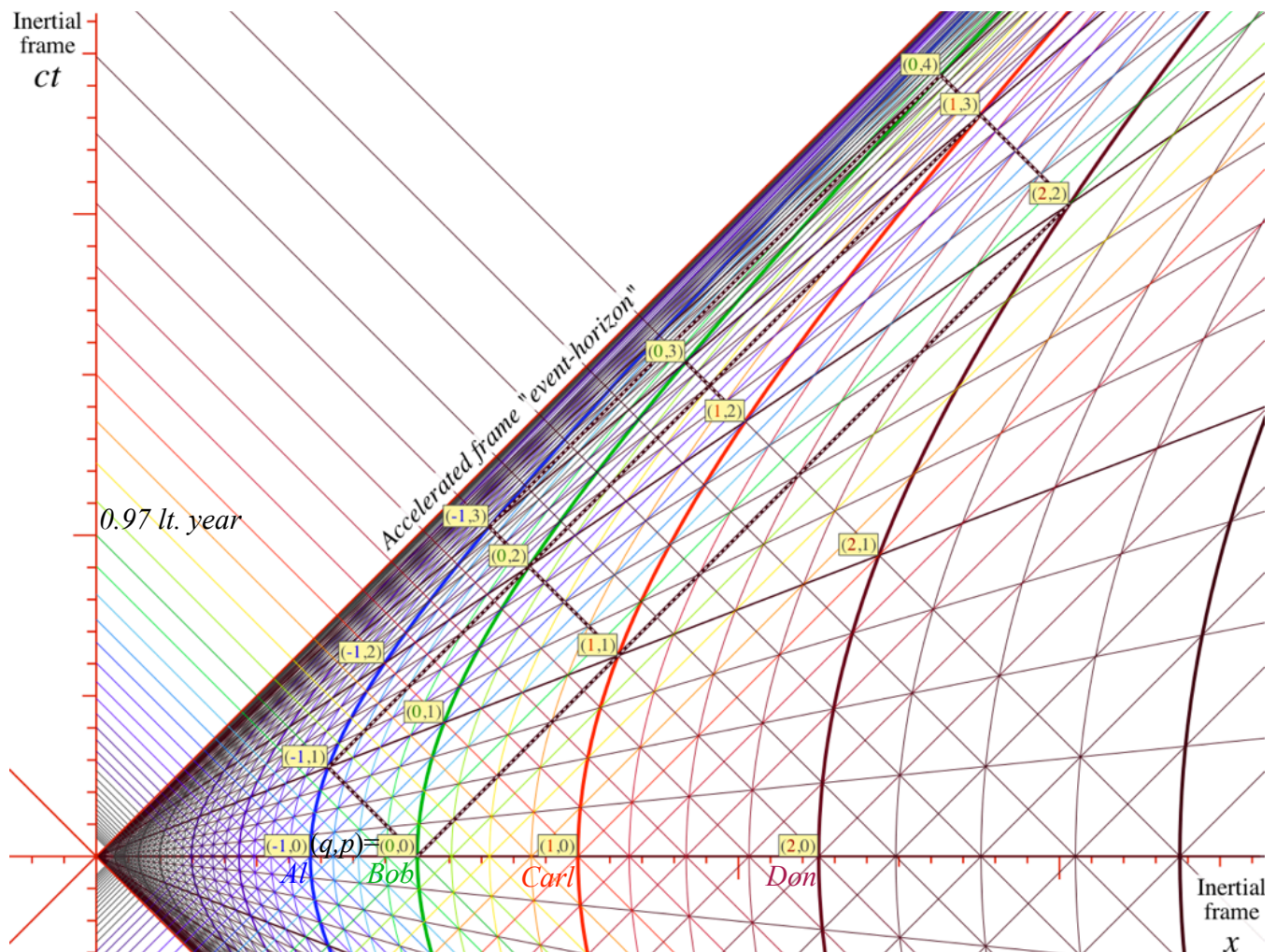


Fig. 30 CW Doppler and PW radar metrology for frame of constant acceleration $g=9.8m\cdot s^{-2}$.

Metrology in accelerated frames

Accelerated frame metrology of space, time, and relative velocity is quite counter-intuitive and easily misinterpreted. The space-time grid of CW and PW paths provided by Alice and Carla in Fig. 28b (and with greater detail in Fig. 29b) help to analyze what Al, Bob, and Carl might be able to observe at each (q,p) -intersection of light beams sent by Alice and Carla.

Let us assume each intersection marks colliding pulse waves (PW) that are separated by the same number N of CW wavelengths in space and N wave periods in time. In Fig. 30 the CW paths for $N=4$ are drawn as the finer CW grid for the sake of clarity, but it should be evident that increasing integer scale N sharpens the space-time fine-grid precision.

The course-grid defined by integer coordinates (q,p) mark equally spaced proper time p -instants $c\tau_{q,p}=a_q\rho p$ along the q -path hyperbola of traveler q according to (70). Bob ($q=0$), starting from his origin ($p=0$) at rest in Fig. 30, accelerates past his proper time points $c\tau_{0,p}=a_0\rho_1(0,1,2,3,4)$ before exiting at the very top of the plot. Bob sees the same proper time interval $c\tau_{0,1}=a_0\rho_1$ between each of his p -instants wherein he gains the same unit $\rho_1=\ln(3/2)=0.405$ of rapidity per interval or velocity $u/c=\tanh\rho_1=0.385$. The distance x traveled in inertial frame (x,ct) of Fig. 30 grows only quadratically at first but soon explodes exponentially due to hyperbolic cosine $x=a_0\cosh\rho$ in (67).

Meanwhile, Bob's companions, Al ($q=-1$) and Carl ($q=+1$), also see equal proper time intervals between p -points, but each $c\tau_{q,p}$ is proportional to q^{th} hyperbolic radial constant $a_q=a_0e^{q\rho_1}$. So Al's proper time interval $c\tau_{-1,1}=a_0e^{-\rho_1}=(2/3)a_0$ is $(2/3)$ of Bob's interval while Carl's interval $c\tau_{1,1}=a_0e^{\rho_1}=(3/2)a_0$ is $(3/2)$ -times greater. But, each traveler gains the same rapidity $\rho_1=\ln(3/2)=0.405$ in each interval.

Having uniform proper $\Delta\tau_q$ -intervals allows spatial intervals between each pair of accelerating neighbors to be easily measured by radar echo ranging. A dash-line rectangle connecting $[q,p]$ -points $[0,0]$, $[1,1]$, $[0,2]$, and $[-1,1]$ outlines paths of Bob's radar pulses he might send rightward (That is “up” in his perceived “gravity” field.) from $[0,0]$ to reflect from Carl at $[1,1]$ and leftward (that is down-field) to reflect from Al at $[-1,1]$. Both pulses return to Bob simultaneously at $[2,2]$ at precisely $c\tau_{0,2}=2a_0\rho_1$ or two “ticks” of his proper time given in distance units. ($a_0=0.97lt\text{-yr}$ derived by (68) for $g=9.8m\cdot s^{-2}$.)

Thus Bob finds a radar-range distance $x_{[-1,1]}=-a_0\rho_1=-0.39lt\text{-yr}$ for Al below him and a distance $x_{[1,1]}=a_0\rho_1=0.39lt\text{-yr}$ of equal distance for Carl above him. Bob gets the same $\pm a_0\rho_1$ distances if he sends out radar pulses one “tick” earlier from the $[0,-1]$ point (below $[0,0]$ and not visible in Fig. 30) that return to him simultaneously two “ticks” later at point $[0,1]$.

If Bob's radar pulses could echo off next-nearest neighbor's paths having radius $a_{\pm 2}=a_0e^{\pm 2\rho_1}$ or $a_{\pm 3}=a_0e^{\pm 3\rho_1}$ then they would return four “ticks” later at $[0,4]$ (as shown in Fig. 30) or six “ticks” later at $[0,6]$ (not shown in Fig. 30). Such echo range values would indicate uniformly spaced neighbors at constant positions $\pm a_0\rho_1$, $\pm 2a_0\rho_1$, and $\pm 3a_0\rho_1$, above and below Bob. Such uniformity of spacing seems paradoxical in light of a decidedly non-uniform spacing of neighbor- q positions $x_q(0)=a_q=a_0e^{q\rho_1}$ on the x -axis of Alice and Carla's inertial frame at time $ct=0$ (and rapidity $\rho=0$). They see a geometric series $a_q=a_0\{\dots,e^{-2\rho_1},e^{-\rho_1},1,e^{+\rho_1},e^{+2\rho_1},\dots\}$ of hyperbolic radii that includes Bob's radius a_0 at origin $[0,0]$.

However, the initial ($ct=0$)-spacing of travelers, that is $\Delta a_q=a_0(e^{q\rho_1}-e^{(q-1)\rho_1})$ in Alice's inertial frame, is to 1st-order in ρ_1 , a uniform $\Delta a_q=a_0\rho_1$ that agrees with Bob's radar-range values. Later, as traveler- q gains speed according to its respective acceleration $g_q=c^2/a_q$, Alice will see neighbor intervals Lorentz contract non-uniformly by $\Delta a_q\text{sech}\rho_p$ factors.

When a neighbor- q of Bob sends his own inquiring radar-echo ranging pulses he will get results that differ by the same exponential factor $e^{q\rho_1}$ relating his proper time value $\tau_{q,p}$ to the corresponding value $\tau_{0,p}$ for Bob intercepting echo-return- p . Bob's radar-range intervals are all seen by up-stairs

neighbor-(+|q|), to be uniformly expanded by $e^{+q\rho_1}$, while down-stairs neighbor-(-|q|), sees them uniformly contracted by $e^{-q\rho_1}$.

Consider Doppler blue-shifts $e^{+q\rho_1}$ seen by Bob for CW light sent by up-stairs neighbor-(+|q|) or a red-shift $e^{-q\rho_1}$ for a down-stairs neighbor-(-|q|) source. Each light beam on $\pm 45^\circ$ -paths in Fig.29b is a copy of laser light sent much earlier by Alice ($+45^\circ$) or Carla (-45°) and Doppler-shifted due to Bob's velocity so that he always sees a fixed green from either direction. Al and Carl are similarly seeing fixed colors as long as they can maintain their respective accelerations $g_q=g_{-1}$ and $g_q=g_{+1}$ through a field of up-chirped frequency sent by Alice and down-chirped frequency sent by Carla.

Thus each traveler only sends or receives its unique frequency: blue for Al, green for Bob, and red for Carl. So Bob always receives a green from Al down-stairs that is Doppler red-shifted by $e^{-q\rho_1}$ from Al's blue or else a green from Carl up-stairs that is blue-shifted by $e^{+q\rho_1}$ from Carl's red. It might seem travelers sharing a line of equal rapidity ρ and fixed radar-range separation should see no Doppler shift between them, that is $(R|S)=I$.

However, each $\pm 45^\circ$ -path connects a $[q,p]$ -point to the nearest up-stairs $[q+1,p\pm 1]$ -points of traveler $q+1$ who deals in reduced frequency and to the nearest down-stairs $[q-1,p\pm 1]$ -points of traveler $q-1$ who deals in higher frequency. In each case rapidity differs by one ρ_1 -unit implying a Doppler blue-shift factor $e^{+q\rho_1}$ for light is falling down-stairs or a Doppler red-shift factor $e^{-q\rho_1}$ for light having to rise up-stairs. Travelers must have identical and *constant* rapidity for their shifts to go away.

Mechanics in accelerated frames

The curved space-time in Fig.30 and Fig. 31 facilitate tracking light waves going back-and-forth between the co-accelerating travelers Al($q=-1$), Bob($q=0$), Carl($q=1$) and Don($q=2$) and reconciling them to Alice and Carla with their inertial frame laser sources. The same may be done for freely flying massive objects that travelers might drop or throw at each other. A simple example involves travelers dropping objects on downstairs companions at just the moment they all have zero velocity in the inertial (x,ct) frame. Alice and Carla would see such objects to be stationary and represented by vertical lines parallel to their inertial ct -axis as shown in Fig. 31.

Each object dropped by traveler-($q=Q$) will hit (or pass closely by) traveler-($q=Q-1$) then traveler-($q=Q-2$) and so forth as seen by examples in Fig. 31. The first example has Don($q=2$) drop something onto Carl($q=1$), Bob($q=0$), and Al($q=-1$) as is indicated at the top of the figure. Don's object hits Carl (or as witnessed by Alice and Carla: Carl hits Don's stationary object.) when Carl's x -coordinate equals a_2 of Don's object.

$$x_{2\text{HIT}1} = a_2 = a_0 e^{2\rho_1} = x_{\text{Carl}} = a_1 \cosh \rho_{2\text{HIT}1} = a_0 e^{\rho_1} \cosh \rho_{2\text{HIT}1} \quad (72a)$$

This is solved for the relative rapidity $\rho_{2\text{HIT}1}$ between Carl and Don's "falling" object.

$$\rho_{2\text{HIT}1} = \cosh^{-1} e^{\rho_1} = \cosh^{-1} \frac{3}{2} = 0.962 \Rightarrow u_{2\text{HIT}1} = 0.745c \quad (72b)$$

Course-grid scale factor $e^{\rho_1}=3/2$ yields high relative velocity. So, one hopes Don's object misses Carl. But, then it falls toward Bob ($q=0$) and Al ($q=-1$) with an ever increasing relative velocities.

$$\rho_{2\text{HIT}0} = \cosh^{-1} e^{2\rho_1} = 1.451 \Rightarrow u_{2\text{HIT}0} = 0.896c \quad (72c)$$

$$\rho_{2\text{HIT}-1} = \cosh^{-1} e^{3\rho_1} = 1.887 \Rightarrow u_{2\text{HIT}-1} = 0.955c \quad (72d)$$

From Fig. 31 it is seen that Don's object hits (or passes) Carl with the same relative speed that Carl's object hits Bob or that Bob's object hits Al. These hits (or passings) lie on a single line of rapidity

$\rho_{2\text{HIT}1} = \rho_{1\text{HIT}0} = \rho_{0\text{HIT}-1}$ as seen by generalizing (72a).

$$x_{\text{QHTT}_q} = a_Q = a_0 e^{Q\rho_1} = a_q \cosh \rho_{\text{QHTT}_q} = a_0 e^{q\rho_1} \cosh \rho_{\text{QHTT}_q} \quad (73a)$$

Thus rapidity ρ_{QHTT_q} and its hyper-cosine vary with the q -index difference (Q-q).

$$e^{(Q-q)\rho_1} = \cosh \rho_{\text{QHTT}_q} \quad (73b)$$

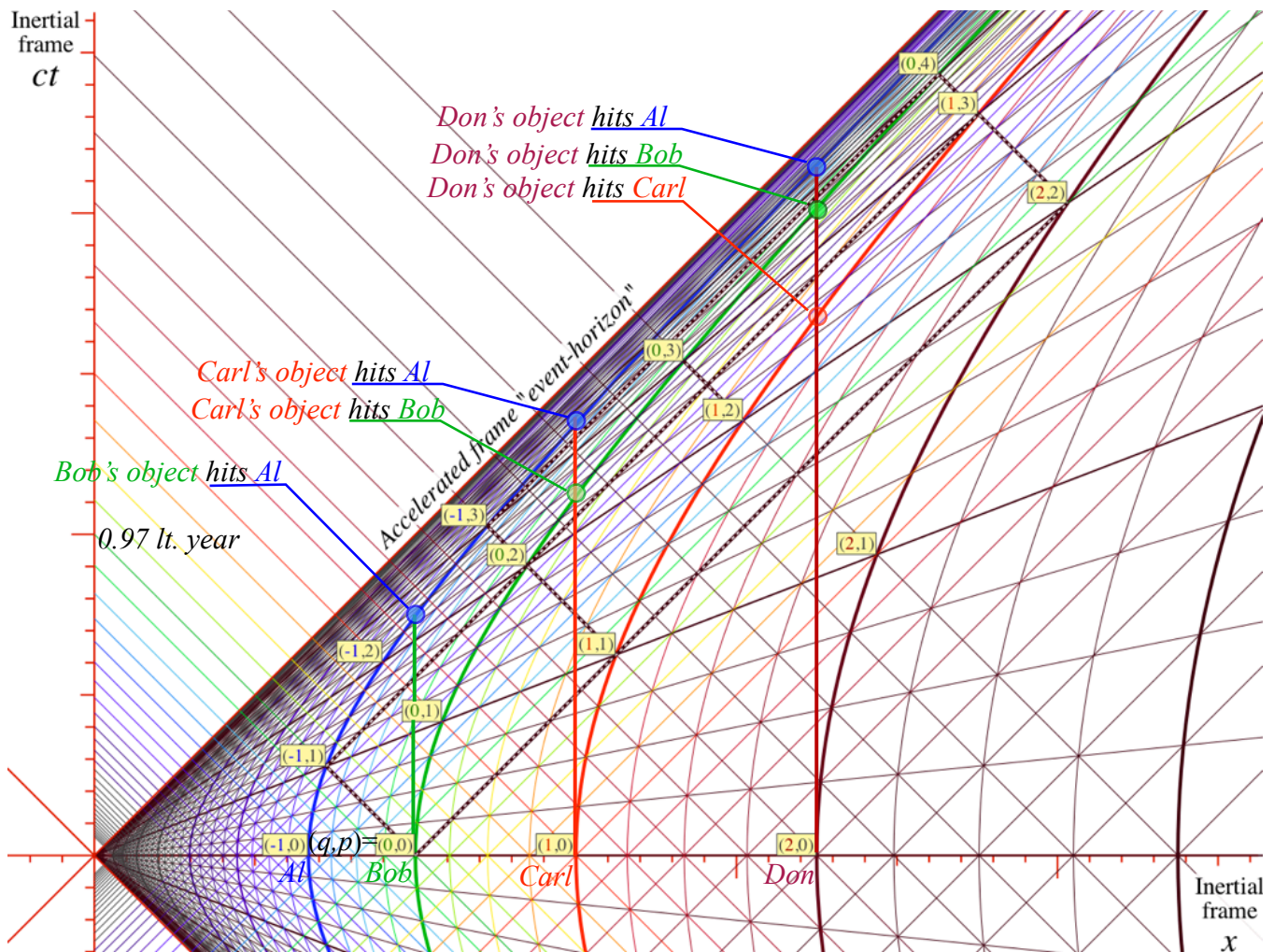


Fig. 31 Space-time paths of dropped objects hitting accelerating travelers.

The $[q,p]$ points or dots in Fig. 31 mark intersections of light rays or massive objects with members of a fleet of co-accelerating ships ($q = \dots -2, -1, 0, 1, 2, \dots$) located at each moment ($p = \dots -2, -1, 0, 1, 2, \dots$) on a line of equal rapidity $\rho_p = p\rho_1$ or velocity $u_p = c \tanh \rho_p$ with low- q ships accelerating more in the (x, ct) frame to have the same velocity u_p as their neighbors by gaining it sooner in local time τ or inertial time t than their high- q “upstairs” neighbors. Light acquires Doppler shift $e^{\rho_1} = 3/2$ in “falling” from a traveler to one below. A mass shifts its phase frequency ν_{phase} and Hamiltonian $H = Mc^2 \cosh \rho = h\nu_{\text{phase}}$ in the Planck-law equation (33) by e^{ρ_1} according to (73b).

The Purest Light and a Wave-Resonance Hero – Ken Evenson (1932-2002)

When travelers punch up their GPS coordinates they owe a debt of gratitude to an under sung hero who, alongside his colleagues and students, often toiled 18 hour days deep inside a laser laboratory lit only by the purest light in the universe.

Ken was an “Indiana Jones” of modern physics. While he may never have been called “Montana Ken,” such a name would describe a real life hero from Bozeman, Montana, whose extraordinary accomplishments in many ways surpass the fictional characters in cinematic thrillers like *Raiders of the Lost Arc*.

Indeed, there were some exciting real life moments shared by his wife Vera, one together with Ken in a canoe literally inches from the hundred-foot drop-off of Brazil’s largest waterfall. But, such outdoor exploits, of which Ken had many, pale in the light of an in-the-lab brilliance and courage that profoundly enriched the world.

Ken is one of few researchers and perhaps the only physicist to be twice listed in the *Guinness Book of Records*. The listings are not for jungle exploits but for his lab’s highest frequency measurement and for a speed of light determination that made c many times more precise due to his lab’s pioneering work with John Hall in laser resonance and metrology[†].

The meter-kilogram-second (mks) system of units underwent a redefinition largely because of these efforts. Thereafter, the speed of light c was set to $299,792,458\text{ms}^{-1}$. The meter was defined in terms of c , instead of the other way around since his time precision had so far trumped that for distance. Without such resonance precision, the Global Positioning System (GPS), the first large-scale wave space-time coordinate system, would have been much less practical.

Ken’s courage and persistence at the Time and Frequency Division of the Boulder Laboratories in the National Bureau of Standards (now the National Institute of Standards and Technology or NIST) are legendary as are his railings against boneheaded administrators who seemed bent on thwarting his best efforts. Undaunted, Ken’s lab painstakingly exploited the resonance properties of metal-insulator diodes, and succeeded in literally counting the waves of near-infrared radiation and eventually visible light itself.

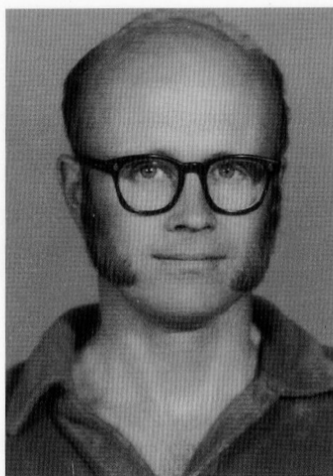
Those who knew Ken miss him terribly. But, his indelible legacy resonates today as ultra-precise atomic and molecular wave and pulse quantum optics continue to advance and provide heretofore unimaginable capability. Our quality of life depends on their metrology through the Quality and Finesse of the resonant oscillators that are the heartbeats of our technology.

Before being taken by Lou Gehrig’s disease, Ken began ultra-precise laser spectroscopy of unusual molecules such as HO_2 , the radical cousin of the more common H_2O . Like Ken, such radical molecules affect us as much or more than better known ones. But also like Ken, they toil in obscurity, illuminated only by the purest light in the universe.

In 2005 the Nobel Prize in physics was awarded to Glauber, Hall, and Hensch^{††} for laser optics and metrology.

[†] K. M. Evenson, J.S. Wells, F.R. Peterson, B.L. Danielson, G.W. Day, R.L. Barger and J.L. Hall, Phys. Rev. Letters 29, 1346(1972).

^{††} *The Nobel Prize in Physics, 2005*. <http://nobelprize.org/>



PAULINIA, BRASIL 1976

THE SPEED OF LIGHT IS
299,792,458 METERS PER SECOND!

- ¹ William of Occam (1245-1326) "*Pluralitas non est ponenda sine neccesitate*" (Do not assume plurality without necessity.)
- ² Max Planck "*Zur Theorie des Gesetzes der Energieverteilung im Normal-spectrum.*" Deutsche Physikalische Gesellschaft. Verhandlungen 2: 237-245 (1900).
- ³ A. Einstein, *Annalen der Physik* 17,891(1905). (Translation by W. Perrett and G.B. Jeffery, *The Principle of Relativity*(with notes by A. Sommerfield) (Methuen, London 1923), (republished by Dover, London 1952).
- ⁴ Albert Einstein "*Zur Elektrodynamik bewegter Korper.*" *Annalen der Physik* 18,639 (1905); *Annalen der Physik* 17,891(1905). (Translation: Perrett and Jeffery, *The Principle of Relativity*, (Methuen, London 1923), (Dover, 1952).
- ⁵ Albert Einstein "*Über einen die Erzeugung und Verwandlung des Lichtes betreffenden heuristischen Gesichtspunkt.*" *Annalen der Physik* 17: 132-148 (1905). (Translation by A.B. Aarons and M.B. Peppard, *Am. J. Phys.* 33, 367(1965).)
- ⁶ Louis de Broglie, *Nature* 112, 540 (1923); *Annalen der Physik* (10) 2 (1923).
- ⁷ W.G. Harter and T. C. Reimer, 2005 // www.uark.edu/ua/pirelli/html/poincare_inv_2.htm
- ⁸ R. P. Feynman, R. Leighton, and M. Sands, *The Feynman Lectures* (Addison Wesley 1964) Our development owes a lot to Feynman's treatment cavity wave dispersion in Vol. II Ch. 24 and Vol. III Ch. 7.
- ⁹ R. P. Feynman, F. B. Morinigo, and Wm. G. Wagner, *Feynman Lectures on Gravitation*, Perseus Books, Reading MA(1995)
- ¹⁰ W. G. Harter, J. Evans, R. Vega, and S. Wilson, *Am. J. Phys.* 53, 671(1985).
- ¹¹ W. G. Harter, *J. Mol. Spectrosc.* 210, 166(2001).
- ¹² L. C. Epstein, *Relativity Visualized*. (Insight Press 1981) Transverse rotation provides an alternative view of SR that is described later.
- ¹³ E.F.Taylor and J.A. Wheeler, *Spacetime Physics* (W. H. Freeman San Francisco 1966) p. xx.
- ¹⁴ D. F. Steyer, M. S. Balkin, K. M. Becker, M. R. Bums, C. E. Dudley, S. T. Forth, J. S. Gaumer, M. A. Kramer, D. C. Oertel, L. H Park, M. T. Rinkoski, C. T. Smith, and T. D. Wotherspoon, "Nine Formulations of Quantum Mechanics" *A. J. Phys.* 70. 288 (2002). The need for a more efficient logic is shown quite well.
- ¹⁵ K. M. Evenson, J.S. Wells, F.R. Peterson, B.L. Danielson, G.W. Day, R.L. Barger and J.L. Hall, *Phys. Rev. Letters* 29, 1346(1972).
- ¹⁶ Michelson, Albert A.; Morley, Edward W. (1887). "[On the Relative Motion of the Earth and the Luminiferous Ether](#)". *American Journal of Science*. **34**: 333–345.
- ¹⁷ H. Minkowski, *Mathematisch-Physikalische Klasse*, vol. 1, 53 (1908).
- ¹⁸ Einstein never used Minkowski's graphical view of SR (or even answer his teacher's letter). Minkowski died in 1909.
- ¹⁹ At this point a Faustian pact with the devil is made. For waves to make a Cartesian (x, ct) rest frame there must be a phase wave-zero traveling at infinite speed drawing a space- x grid-lines each with time ct constant. Here waves get weird!
- ²⁰ H. A. Lorentz Koninklijke Akademie van Wetenschappen te Amsterdam. Section of Science. Proc. 6: 809-831 (1904). Albert Einstein "*Zur Elektrodynamik bewegter Korper.*" *Annalen der Physik* 18,639 (1905); *Annalen der Physik* 17,891(1905). (Translation: Perrett and Jeffery, *The Principle of Relativity*, (Methuen, London 1923), (Dover, 1952).
- ²¹ L. C. Epstein, *Relativity Visualized*. (Insight Press 1981)
- ²² L. C. Epstein, *Relativity Visualized*. (Insight Press 1981) This novel approach to SR theory did not catch on likely due to not being connected to the conventional approaches. Perhaps this can be remedied as shown here.
- ²³ Albert Einstein "*Über einen die Erzeugung und Verwandlung des Lichtes betreffenden heuristischen Gesichtspunkt.*" *Annalen der Physik* 17: 132-148 (1905). (Translation by A.B. Aarons and M.B. Peppard, *Am. J. Phys.* 33, 367(1965).)

- ²⁴ Louis de Broglie, *Nature* 112, 540 (1923); *Annalen der Physik* (10) 2 (1923).
- ²⁵ Max Planck "Zur Theorie des Gesetzes der Energieverteilung im Normal-spectrum." Deutsche Physikalische Gesellschaft. *Verhandlungen* 2: 237-245 (1900).
- ²⁶ N. Bohr, *Zeitschrift fur Physik*, 9, 1-2, (1922).
- ²⁷ E. Schrodinger, *Annalen der Physik* (4) 79 361 and 489 (1923); 80, 437 (1926); 81,109 (1926).Schrodinger's protests about prevailing quantum mechanical interpretations are well circulated. So far we have not located more solid references.
- ²⁸ Ken Ford, *Building the H Bomb: A personal history*, World Scientific (2015) p. 70
- ²⁹ Ken Ford, *loc. cit.*, p. 92
- ³⁰ C. Sykes, *No Ordinary Genius: The Illustrated Richard Feynman* , W. Norton (1994) p. 84 (Meets Dirac in July 1964)
- ³¹ P. A. M. Dirac, "Forms of Relativistic Dynamics" *Rev. Mod. Physics*, 21: 392 (1949).
- ³² Feynman's Thesis: *A New approach to Quantum Theory*, Edited by Laurie M. Brown, World Scientific (2005) has edited copy of 1941 thesis and discussion of RPF *Space-time approach to non-relativistic quantum mechanics*, *Rev. Mod. Phys.* 20 (1948) pp. 367-387; and R. P. Feynman and A. R. Hibbs, *Quantum Mechanics and Path Integrals* (McGraw-Hill 1965)
- ³³ A. Einstein, "I shall never believe that god plays dice with the universe" Albert Einstein Archives, The Jewish National & University Library, The Hebrew University of Jerusalem (www.albert-einstein.org), Einstein Archives Online, Volume 15, #294, Letter to Cornelius Lanczos, March 21, 1942,<http://www.alberteinstein.info/db/ViewDetails.do?DocumentID=30893>.